TECHNICAL REPORT N-73-1

BEHAVIOR OF STIFF CYLINDERS BURIED IN SAND UNDER STATIC LOADING

by

C. D. Norman, J. D. Prendergast

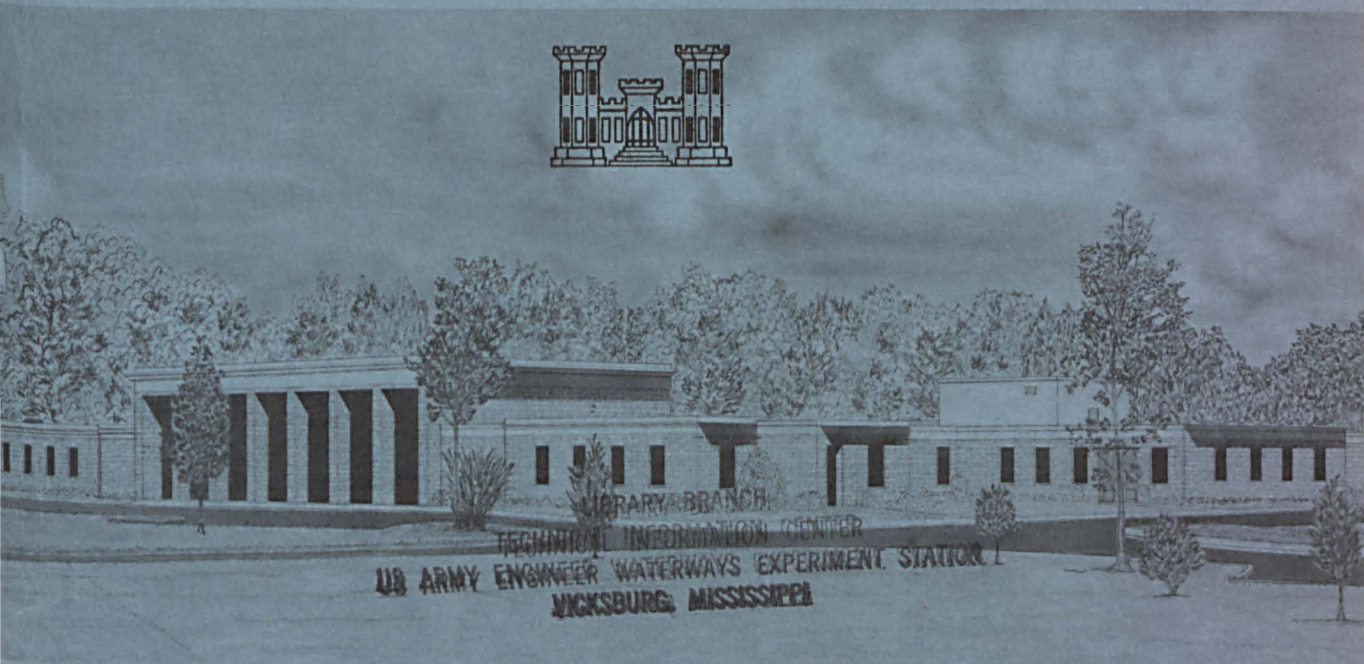

April 1973

Sponsored by Defense Nuclear Agency

Conducted by U. S. Army Engineer Waterways Experiment Station
Weapons Effects Laboratory
Vicksburg, Mississippi

TECHNICAL REPORT N-73-1

BEHAVIOR OF STIFF CYLINDERS BURIED IN SAND UNDER STATIC LOADING

by

C. D. Norman, J. D. Prendergast

April 1973

Sponsored by Defense Nuclear Agency
NWED Subtask SC210

Conducted by U. S. Army Engineer Waterways Experiment Station
Weapons Effects Laboratory
Vicksburg, Mississippi

ARMY-MRC VICKSBURG, MISS.

THE CONTENTS OF THIS REPORT ARE NOT TO BE USED FOR ADVERTISING, PUBLICATION, OR PROMOTIONAL PURPOSES. CITATION OF TRADE NAMES DOES NOT CONSTITUTE AN OFFICIAL ENDORSEMENT OR APPROVAL OF THE USE OF SUCH COMMERCIAL PRODUCTS.

ABSTRACT

The objective of this investigation was to study experimentally the elastic behavior of horizontally oriented, stiff cylinders buried at shallow depths in dense, dry sand and subjected to static surface overpressures.

Static tests were conducted on nine different cylinders in the U. S. Army Engineer Waterways Experiment Station's Small (4-foot-diameter) Blast Load Generator (SBLG). The cylinders were fabricated from steel mechanical tubing having a 6-inch outside diameter and a specially isolated 12-inch-long test section. The nine test specimens comprised three groups of cylinders with wall thicknesses of 1/8, 1/4, and 3/8 inch that corresponded to stiffnesses (EI/R^3) of 170, 1,644, and 5,926 psi, respectively. In order to study the effects of burial depth, the first, second, and third cylinders of each group were tested at depths of 3, 6, and 9 inches, respectively. A total of 14 static tests were conducted, 9 on virgin soil samples and 5 on samples that had been previously loaded. The peak surface overpressure attained for all tests was approximately 1,000 psi. Measurements were made of cylinder hoop strain, vertical diameter change, soil stress, and surface overpressure.

The test results indicated that cylinder stiffness significantly affected the overall response of the soil-structure system. Normalized moment (M/PR^2) data obtained from these tests were determined to be much greater than such values for less stiff cylinders. However, the maximum values of the normalized moments from the test data were in close agreement with the analytically predicted upper-bound values for a rigid cylinder. The experimental information for the 1/4- and 3/8-inch-thick cylinders was used to provide data in the low normalized pressure (PR^3/EI) region, for which very little data previously existed. For the range of cylinder stiffnesses tested, normalized thrust values (T/PR) indicated that both active and passive arching occurred and were dependent on cylinder stiffness.

A description of the properties of the steel used in fabricating

the test cylinders is given in Appendix A, and a description of the confining soil properties is given in Appendix B.

PREFACE

The study reported herein was conducted in the Small Blast Load Generator facility at the U. S. Army Engineer Waterways Experiment Station (WES) under the sponsorship of the Defense Nuclear Agency (DNA) as part of Nuclear Weapons Effects Development (NWED) Subtask SC210, "Response of Buried Structures to Ground Shock."

This work was accomplished during the period April 1969 through February 1972 under the general supervision of Mr. G. L. Arbuthnot, Jr., Chief of the Weapons Effects Laboratory (WEL), WES, and under the direct supervision of Mr. W. J. Flathau, Chief of the Protective Structures Branch, WEL, and Mr. G. E. Albritton, Project Manager. This report was prepared by Mr. C. D. Norman and CPT J. D. Prendergast, both of the Research Projects Group. The review and suggestions by Mr. R. E. Walker and Drs. J. L. Kirkland and J. P. Balsara, WEL, are appreciated.

COL Levi A. Brown, CE, and COL Ernest D. Peixotto, CE, were Directors of WES during the conduct of this study and the preparation of this report. Mr. J. B. Tiffany and Mr. F. R. Brown were Technical Directors.

•

CONTENTS

NOTATION

C_u	Soil coefficient of uniformity
d	Mean cylinder diameter, inches
D	Outside diameter of the cylinder, inches
E	Modulus of elasticity of test cylinders, psi
I	Moment of inertia per unit length of the cylinder cross section, in^4/in
K	Coefficient of lateral earth pressure
M	Circumferential bending moment per unit length of the cylinder, lb-in/in
M_c	Circumferential bending moment measured at the crown, lb-in/in
M_s	Circumferential bending moment measured at the springline, lb-in/in
P	Pressure, psi
R	Outside radius of the cylinder, inches
t	Cylinder wall thickness, inches
T	Circumferential thrust per unit length of the cylinder, lb/in
Z	Burial depth, measured from soil surface to top of cylinder crown, inches
ϵ_e	Exterior cylinder strain in the circumferential direction, in/in
ϵ_i	Interior cylinder strain in the circumferential direction, in/in
θ	Angle measured at the center of the cylinder cross section positive clockwise from the crown, degrees
λ_d	Dry unit weight of the sand, pcf
ϕ	Angle of internal friction, degrees

CONVERSION FACTORS, BRITISH TO METRIC UNITS OF MEASUREMENT

British units of measurement used in this report can be converted to metric units as follows.

Multiply	By	To Obtain
inches	2.54	centimeters
feet	0.3048	meters
pounds	0.45359237	kilograms
pounds (force) per square inch	0.6894757	newtons per square centimeter
kips (force) per square inch	0.6894757	kilonewtons per square centimeter
pounds per cubic foot	16.0185	kilograms per cubic meter
inches per second	2.54	centimeters per second
inch-pounds per inch	4.448222	newton-meters per meter

CHAPTER 1

INTRODUCTION

1.1 BACKGROUND

Many strategic underground systems incorporate horizontally oriented cylindrical structures of various stiffnesses. Thus, in the design or analysis of any strategic structure, whether it be located above or below ground, the applied loading must first be defined and then procedures developed to describe how the structure in its particular environment will respond to the loading. Under attack conditions, it is reasonable to expect that shallow buried strategic facilities could be located in regions in which the airblast pressure could be as great as 1,000 psi[1]. For this reason, buried stiff cylindrical metal and/or reinforced concrete structures that have greater structural resistance than flexible cylindrical elements are considered necessary for such systems.

The information that has become available within the past few years from both analytical and laboratory studies conducted by the U. S. Army Engineer Waterways Experiment Station (WES) (Reference 1) and other agencies has verified that flexible cylindrical structures buried in soil can effectively maintain structural integrity under the loading resulting from a nuclear ground-shock environment by utilizing the resistance provided by the confining media. Therefore, elements of underground protective systems that consist of flexible cylindrical structures such as ventilation conduits, entrances, and escape routes can be designed to remain functional during a proposed threat. However, the same is not true for elements of shallow underground protective systems that consist of stiff horizontally oriented cylindrical structures such as command capsules and, if vertically oriented, missile

---

[1] A table of factors for converting British units of measurement to metric units is presented on page 10.

silos. There is a lack of well documented experimental data for buried stiff cylindrical structures, and the structure-medium interaction (SMI) phenomenon associated with stiff cylinders is not fully understood. Currently, the design practice of extrapolating the existing knowledge to such cylinders surrounded by a soil medium is highly conservative.

1.2 OBJECTIVES

The general objective of this program was to determine the response of cylindrical protective structures for shallow and deeply buried installations subjected to ground surface airblast loading resulting from nuclear detonations. Results of this study will be used to develop rational procedures for analyzing the vulnerability of this class of structures and to improve design procedures.

Specifically, the objectives were to study:

1. Thrust and moment at various sections of the cylinder.
2. Changes in vertical diameter of the cylinder as a function of static overpressure.
3. Arching action of the soil as it affects the total vertical load on the structure.
4. Static behavior of the cylinders as a function of the structural stiffness.
5. Effect of depth of burial on the behavior of the cylinders.

From the test results, it was expected that guidelines could be verified and/or extended in current design procedures for protective structures in order to secure maximum protection at minimum cost.

1.3 PROBLEM UNDER STUDY

Because of the uncertainties associated with the response of shallow buried stiff cylindrical configurations, primarily those constructed of reinforced concrete, the current design procedures for such structures have not been verified. Previously, most experimental research on buried cylindrical structures has utilized metal material for fabrication of the cylinder models, and such structures had stiffnesses (EI/R^3)

of approximately 50 psi or less. However, buried reinforced concrete cylindrical structures designed to resist ground surface airblast pressures ranging from 200 to 1,000 psi may require stiffness values of approximately 100 to 7,500 psi. Consequently, there is virtually no experimental validation for current design criteria for such stiff structures. In addition, as noted in Reference 2, the problems of designing shallow buried protective structures to withstand overpressure-induced loadings from large-yield weapons differ from those associated with other underground cylindrical structures in at least two major ways: (1) the live load is large compared with the dead load, and the structure must be designed primarily for the live load; and (2) the criteria for design, together with the factor of safety, must lead to the least expensive structure that will fulfill requirements.

The approach taken in this study was to test small, stiff, steel cylindrical models under static loading and to use the results as guidelines for designing large-scale reinforced concrete cylindrical structures. There are numerous advantages to this approach: (1) steel is a homogeneous linear elastic material that can be readily analyzed to compute the circumferential thrusts and bending moments, (2) testing devices having specimen chambers and static and dynamic loading capabilities compatible with the size of the models are available, (3) the effect of stiffness of the models can be included in the parameter study, (4) steel cylinders are commercially available in various diameters and wall thicknesses, and (5) because it is less expensive to fabricate and test such models, more tests can be conducted for statistical verification.

1.4 SCOPE

To accomplish the objectives of the study, static tests were conducted on nine different 6-inch-O.D. steel cylinders that had a specially isolated 1-foot-long test section and were horizontally buried in a dense, dry sand. The tests were conducted in the Small Blast Load Generator (SBLG) facility at WES. Three cylindrical structures each had wall thicknesses of 1/8, 1/4, and 3/8 inch, which corresponded

to cylinder stiffnesses (EI/R^3) of 170, 1,644, and 5,926 psi, respectively. Such stiff cylinders were chosen to insure that the results obtained would provide sufficient information concerning the structural stiffness relationship; also, maximum strain experienced by any section was kept below yield, thus allowing repeated testing of the same test section. In order to examine the effect of depth of burial, static tests were conducted for each cylinder at depths of cover equal to 3, 6, and 9 inches over the cylinder crown, i.e., at depths of D/2, D, and 1-1/2 D, where D is the cylinder's outside diameter. During the 14 static tests, measurements were made of hoop strain and vertical diameter change in the cylindrical test sections, surface overpressure, and the associated free-field stress. In addition, various elastic analytical solutions and empirical concepts were examined and compared with the test results.

CHAPTER 2

RESPONSE CRITERIA AND CONCEPTS

2.1 GENERAL

Before the bending moment, thrust, and displacement data acquired in this investigation are discussed, it is of value to cite two previous investigations (References 3 and 4) in order to gain insight into the structure-medium interaction problem. These references (page 95) present information that is relevant to this investigation and to the establishment of reasonable theoretical upper bounds for the bending moments and thrusts developed in stiff, shallow buried cylinders in a soil medium. The pertinent aspects of the aforementioned references are summarized in the following paragraphs so that a comparison between these referenced results and the results of this investigation can be made.

2.2 RESULTS PRESENTED IN REFERENCE 3

In Reference 3, the interaction between a linearly elastic, isotropic, homogeneous medium and an embedded, elastic cylinder was analyzed by use of a mathematical formulation satisfying the conditions of deformational compatibility. The free-field stress distributions in the soil medium were assumed to be a uniformly distributed vertical pressure of magnitude P and a uniformly distributed horizontal pressure of magnitude KP, where K is the coefficient of lateral earth pressure. The analytical results indicated that the distribution of stresses and the deformations of the cylinder were dependent upon the relative stiffnesses of the medium and the embedded cylinder. In addition, the analytical results indicated that for a soil with a coefficient of lateral earth pressure of 0.35, a rigid cylinder, and the case with no slippage on the soil-cylinder interface, the upper bound for the normalized springline thrust T/PR is 1.4.

2.3 RESULTS PRESENTED IN REFERENCE 4

In the Reference 4 analysis, the same vertical and horizontal soil pressures used in the Reference 3 study were assumed. However, in the analysis presented in Reference 3, the interaction of the soil and the cylinder was not considered and, in addition, the influence of cylinder deflection on bending moments was neglected. In Reference 4, the equation for the bending moment per unit length of cylinder in terms of the polar coordinates R and θ is expressed as:

$$M = \frac{PR^2}{4} (1 + K - 2 \sin^2 \theta - 2K \cos^2 \theta) \tag{2.1}$$

where θ is measured clockwise from the crown, and positive moments are defined as producing compression in external fibers of the cylinder. Inspection of Equation 2.1 reveals that the crown and springline moments are of equal magnitude but are opposite in sign and can be expressed respectively as:

$$M_c = \frac{PR^2}{4} (1 - K) \tag{2.2}$$

$$M_s = \frac{PR^2}{4} (K - 1) \tag{2.3}$$

Utilizing Reference 5 and Appendix B of this report, the coefficient of lateral earth pressure for Cook's Bayou No. 1 sand (used in this test program) was estimated to be approximately 0.325. By substituting this value in Equations 2.2 and 2.3, the following values for the normalized crown and springline bending moments were determined:

$$\frac{M_c}{PR^2} = 0.167 \tag{2.4}$$

and

$$\frac{M_s}{PR^2} = -0.167 \tag{2.5}$$

As indicated in Reference 4, these values represent an upper bound to the possible bending moment; however, these values are at least five times greater than any previous test data indicate.

CHAPTER 3

EXPERIMENTAL PROCEDURES

3.1 CYLINDRICAL TEST SPECIMENS

3.1.1 Design Considerations. Several practical considerations were influential in the selection of the geometrical dimensions and material for the cylinders. The relative size of the cylinders was governed primarily by three factors: (1) the dimensions of the 4-foot-diameter SBLG, (2) the diameters and thicknesses of commercially available mechanical tubing that would provide the range of stiffnesses desired, and (3) the desirability to have test results from previous investigations with which to compare the test results from the most flexible cylinder considered in this study. The range of overpressures at which this comparison could be made was 0 to 250 psi. Steel was selected as the cylinder material because it has well defined elastic properties, which simplifies the computational procedures for circumferential bending moments and thrusts. Also, steel mechanical tubing was commercially available in sizes and thicknesses that would reduce fabrication time and costs.

3.1.2 Descriptions of Test Specimens. All of the cylindrical test specimens were fabricated from cold-drawn, low-carbon, seamless, steel mechanical tubing. The outside diameter of all specimens was 6 inches, and the wall thicknesses t were 1/8, 1/4, and 3/8 inch (Figure 3.1). The nominal variations in the outside diameter and the wall thickness of the tubing were $\pm 1/2$ and ± 2 percent, respectively. The stress-strain properties of the mechanical tubing were obtained from longitudinal tension test specimens in accordance with the procedures discussed in Appendix A. The modulus of elasticity E was 30.0×10^6 psi ± 4 percent. The proportional limit and the rupture strength were 47,700 psi ± 5 percent and 91,200 psi ± 5 percent, respectively.

The test geometry for the cylinders is illustrated in Figure 3.2. Although the outside diameter of all cylinders was 6 inches, the mean

diameters d for the 1/8-, 1/4-, and 3/8-inch wall thicknesses were 5.880, 5.750, and 5.625 inches, respectively. The corresponding d/t ratios were 49.0, 23.0, and 15.0, and the EI/R^3 values were 170.0, 1,643.8, and 5,925.8 psi, respectively. To minimize the influence of the end conditions and other boundary effects, the length of the central test section of all cylinders was fixed at 12 inches. The closed-end caps were 8 inches long and were constructed in such a way that the cylindrical section of the end cap could be changed when the thickness of the central test section was changed. The closed-end caps were independently supported by four 3/4-inch-diameter, cold-drawn steel rods. The rods were arranged in a circular pattern to provide uniform support for the closed-end cap plates. The four support rods were provided with interior bracing plates to prevent buckling and to add to the rigidity of the assemblage. The ends of the support rods were threaded and provided with nuts in order that the separation between the central test section and the closed-end caps could be adjusted and maintained. The separations between the end caps and the central test section were closed with a pliable gasket fabricated from vulcanized silicone rubber. The purpose of the gasket was to prevent soil from entering the interior of the cylinder test specimens during the test.

The end conditions of the central test section were essentially representative of a free boundary, since the independent support system for the end caps prevented the transfer of any axial load to the central test section. In addition, the possible development of longitudinal bending moments in the central test section resulting from differential settlement of the end caps was eliminated. However, a small nonuniform radial shear load was applied to the central test section as a result of the separation between the end caps and the central test section. Calculations demonstrated that the effects of the radial shear load on the circumferential bending moments and thrusts at the midpoints of the central test section were negligible.

3.2 TESTING FACILITY

All testing was conducted in the WES SBLG facility utilizing the

high-pressure test pit in the 18-foot-deep foundation shown in Figure 3.3.

The SBLG 1,000-psi-capacity cylindrical rings provided the lateral confinement for the soil sample. The rings have an outside diameter and wall thickness of 48 and 9/16 inches, respectively. The ends of the rings are flanged so that they can be bolted together in various combinations to vary the depth of the soil sample. A combination aluminum and neoprene rubber diaphragm was installed over the soil sample surface to prevent the surface overpressure from entering the voids in the soil. During the static tests, the surface overpressure was applied to the soil surface by air acting on the diaphragm. A more complete physical description of the SBLG is given in Reference 6, and the operating procedures are discussed in Reference 7.

Throughout the test program, the depth of the soil sample was maintained at 39 inches. This depth was maintained by the use of 3-, 12-, and 24-inch-high rings. The 12-inch ring served as an adapter to make the bolt circle in the base plate of the high-pressure test pit compatible with the remaining cylindrical rings. The 24-inch ring was bolted to the 12-inch ring, and subsequently, the 3-inch ring was bolted to the 24-inch ring.

3.3 SOIL PROPERTIES AND PLACEMENT

Cook's Bayou No. 1 sand, which has been used extensively in other experimental programs at WES, was used throughout the test program. This sand is a uniform fine sand and is classified as SP according to the Unified Soil Classification System. Additional information on this sand is presented in Appendix B.

A WES-designed box sprinkling device, shown in Figure 3.4a and described in Reference 2, was used to place the sand. The sprinkling device was maintained at a height of 24 inches above the sand surface and rotated at a rate of approximately 21 rpm to provide a uniform and average repeatable density of 109.6 $\pm$1 pcf. During the process of backfilling around the cylindrical test specimens, it was necessary to use a can sprinkler (Figure 3.4b) to insure a uniform density adjacent

to the test specimen. This device consisted of a sprinkling apparatus similar to that of the box sprinkler; however, the can sprinkler could be manually controlled, thus permitting the sprinkling of sand to be confined to a small area. This device was also capable of placing the sand at an average repeatable density of 109.1 ±1 pcf.

3.4 INSTRUMENTATION

3.4.1 Strain Measurements. Circumferential strains at the central test sections' midpoints were measured with Micro-Measurements Type EA-06-250BG-120 strain gages. These strain gages are 120-ohm, resistance-type foil gages with a 0.25-inch gage length and were temperature-compensated for steel. The strain gages were affixed to the interior and exterior surfaces of the central test sections at the 0-, 30-, 60-, 90-, 120-, 150-, 180-, and 270-degree locations (Figure 3.5) and were oriented to measure circumferential strains. In order to form a wheatstone bridge and insure temperature compensation, each of the circumferential strain gages and the primary sensing elements of the bridge were connected to three dummy strain gages. The dummy strain gages were mounted on a 1-1/4-inch-square steel bar, which was axially supported between the bracing plates for the four rods supporting the closed-end caps. Since the central test section had essentially free boundary conditions and was not subjected to axial loads, longitudinal strain gages were not provided.

Each of the four rods supporting the closed-end caps was instrumented with four strain gages that were identical with those used on the central test section. Two strain gages had their axes parallel to the axis of the rod and were positioned diametrically opposite each other. Two other strain gages were placed perpendicular to the axis of the rod to provide automatic temperature compensation. Because of the manner in which the strain gages were arranged to form the wheatstone bridge, there was no imbalance in the bridge as a result of loads that were not tension or compression loads.

3.4.2 Deflection Measurement. A deflection gage to measure the relative displacement between the crown and invert of the central test

section was constructed from a Bourns Linipot, 5,000-ohm, 7/16-inch potentiometer; a 402-ohm wheatstone bridge; and a 51,000-ohm limit resistor, as shown in Figure 3.6. The deflection gage, which was mounted 0.75 inch from the end of the central test section, had a resolution of 0.002 inch. It was desirable to place the deflection gage adjacent to the circumferential strain gages at the midpoint of the central test section. However, the dummy gage block within the framework of the end-cap support rods prevented the placement of the gage at this location.

3.4.3 Pressure Measurements. Free-field soil pressures were measured with WES SE wafer-type diaphragm transducers. A detailed description of this gage is presented in Reference 8. Free-field soil pressures were measured at eight locations around the central test section, as illustrated in Figure 3.7. Four of the gages were oriented to measure vertical soil pressure, and four were oriented to measure horizontal soil pressure.

The static surface overpressure was measured with two 5,000-psi Norwood diaphragm-type pressure transducers. The Norwood pressure transducers were actually located outside the bonnet, monitoring the surface overpressure through a 6-inch-long, 3/8-inch-I.D. tube.

A Consolidated Electrodynamics Corporation (CEC) Type 4-313 pressure transducer was used to monitor the soil pore pressure. The pore pressure was measured to determine if the diaphragm covering the soil sample's surface developed a leak or rupture. The gage was located in an instrumentation access port in the 12-inch-high ring section. A porous bronze plate, which allowed the gage to sense pore pressure changes and yet not be affected by horizontal soil pressure, was used.

3.4.4 Recording and Reduction Equipment. Sensor Analog Module (SAM) amplifiers and B and F transducer conditioning modules coupled with DANA amplifiers were employed to condition the resistance-type bridge circuits. Both the systems provided dc variable-excitation voltage, automatic double-shunt calibration of the bridge circuit, and amplifiers to meet the input requirements of the recording equipment.

Three Sangamo magnetic-tape recorders were employed to record and

play back the analog voltage signals from the static tests. Each tape recorder has 14 recording channels and an edge voice track for addressing purposes. In addition, each tape recorder has multiple-speed record and playback capabilities; however, for this test program, a recording speed of 7-1/2 in/sec was selected. The playback speed was determined by the duration of the static test.

3.5 TEST PREPARATIONS

Prior to testing, it was necessary to assemble the components of the cylindrical test specimen (Figure 3.8) and connect the circumferential strain gages to the dummy gages, as illustrated in Figure 3.9a. All cable connections associated with the interior and exterior strain gages were located at terminal strips at opposite ends of the support rods. After all connections had been completed and the remaining end cap attached, the pliable gaskets were placed in the separation joints as illustrated in Figure 3.9b. The cylindrical test specimen was then firmly strapped to the wooden cradle. The cradle was used to position the various components in the proper orientation and also to assist in the placement of the specimen in the soil sample.

Prior to placement of the soil sample, a sidewall friction reducing liner was taped to the inner surface of the SBLG cylindrical rings. The liner consisted of thin layers of automotive and artillery grease spread between two 0.008-inch-thick layers of polyethylene sheeting. This particular liner has been used extensively in the SBLG and is discussed in more detail in Reference 9.

Each soil sample was constructed utilizing the procedures discussed in Section 3.3. When the sand reached the approximate level at which a free-field soil pressure gage was to be installed, sprinkling was stopped and the surface leveled at the proper depth. The gage was carefully placed, and any excess cable was placed in an area where no measurements were being taken or along the inner surface of the cylindrical rings.

Likewise, when construction of the soil sample reached the proper level for placement of the cylindrical test specimen, the sprinkling

was stopped and the sand surface leveled. However, before placement of the cylindrical test specimen, it was necessary to excavate a bedding surface with a 70-degree bedding angle for the invert of the cylinder. The guide and template used to excavate the bedding surface are shown in Figure 3.10a. The cylindrical test specimen was then placed in the bedding surface (Figure 3.10b), and the bedding surface was carefully backfilled. Figure 3.11 shows the cylindrical test specimen in the half-buried configuration. Also shown in the figure are four of the free-field soil pressure gages.

When construction of the soil sample was completed, a 1/16-inch-thick neoprene rubber diaphragm was placed over the surface of the soil. During the first test, however, this diaphragm ruptured at the inner edge of the cylindrical rings. The rupture was attributed to the high localized strains at the ring edge and also to abrasion from the sand. Subsequently, a combination aluminum and neoprene rubber diaphragm was fabricated and placed over the sample. This combination diaphragm satisfactorily reduced the diaphragm rupture problems.

The static bonnet was then bolted to the cylindrical rings, and the Norwood and CEC pressure transducers were installed. Air lines for pressure input and exhaust were connected to the bonnet, and all resistive gages were connected to conditioning modules. Calibration voltages were applied to the respective tape channels, and deviation of each channel was adjusted to the proper level.

3.6 TEST PROCEDURES

Immediately preceding a test, calibration voltages were applied to all channels and recorded on magnetic tape. When the calibration sequence was completed, the loading of the surface of the soil sample was initiated. During the loading cycle, compressed air was permitted to fill the bonnet until the peak surface overpressure was attained. The loading rate was controlled by monitoring the output from one of the Norwood pressure transducers on an X-Y plotter. The typical loading rate was approximately 130 psi/min, and the typical unloading rate was approximately 110 psi/min until a surface overpressure of 200 psi was

reached. Thereafter, the unloading rate was approximately 25 psi/min. The output from all transducers was monitored throughout both the loading and unloading cycles.

After the test, the data were played back and recorded on an oscillograph. Then a preliminary analysis of the data was conducted. If the data were satisfactory, the cylindrical test specimen was removed and buried at a new depth or the stiffness of the cylinder was changed. If the data were not satisfactory, the test was repeated without replacing the cylindrical test specimen, i.e., the cylindrical test specimen was reloaded.

Figure 3.1 Seamless mechanical tubing.

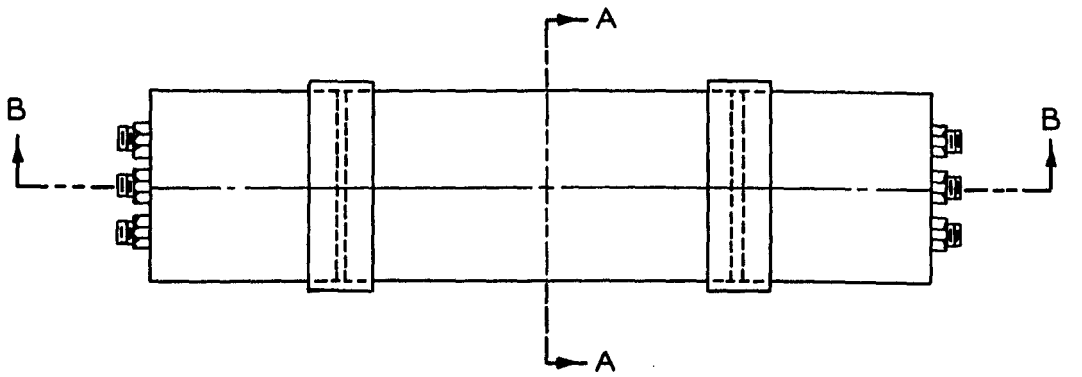

PLAN VIEW

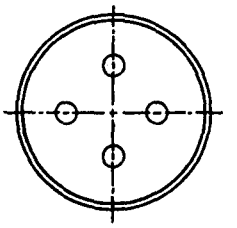

SECTION A-A

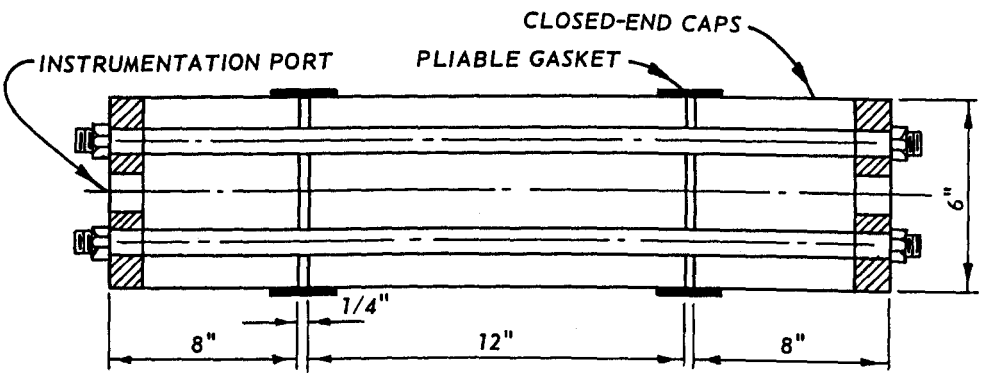

SECTION B-B

Figure 3.2 Geometry of cylindrical test specimen.

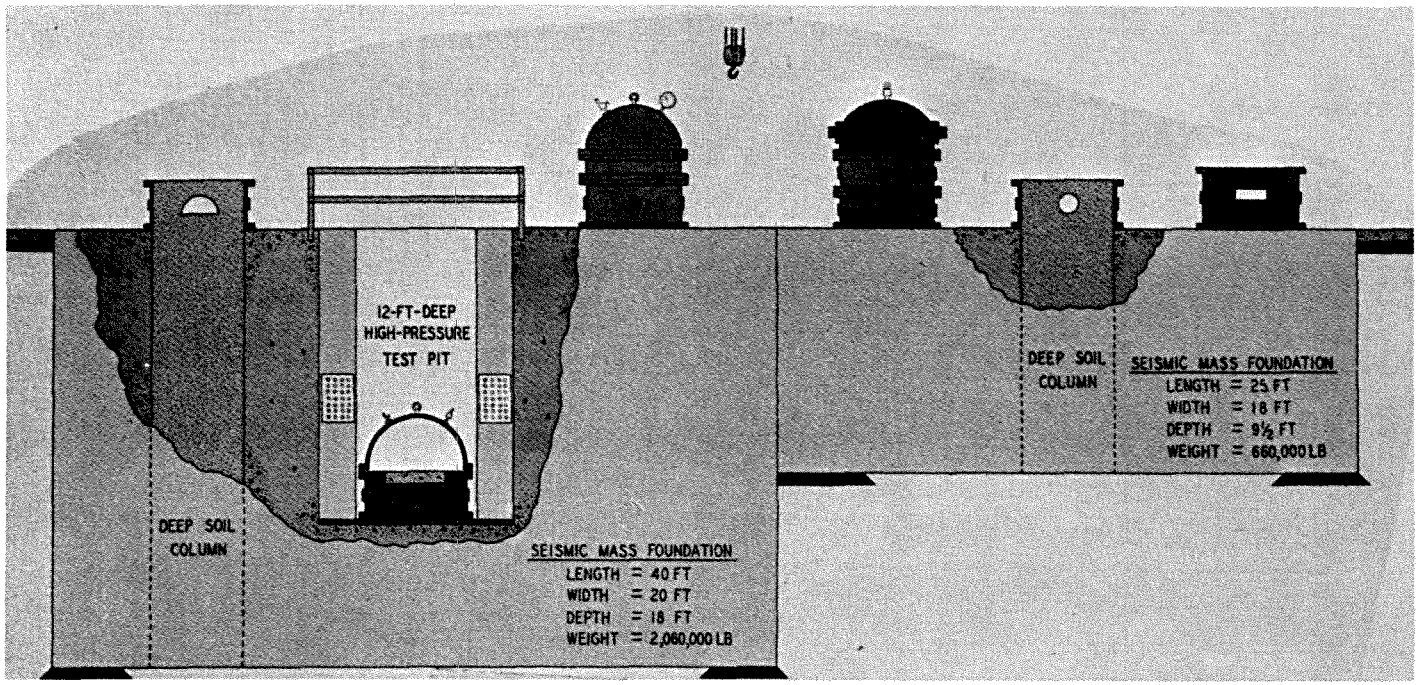

Figure 3.3 SBLG facility.

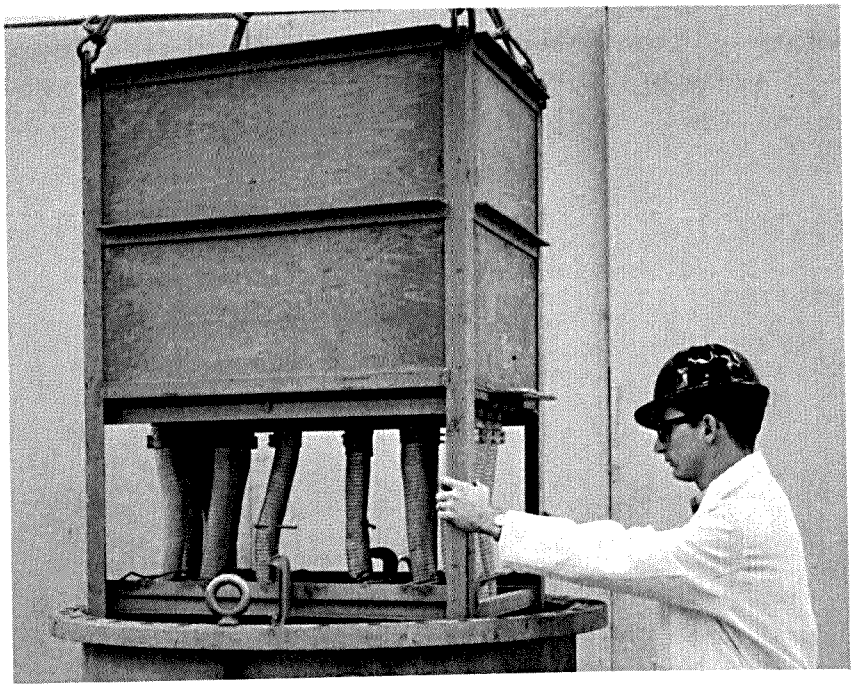

a. Initial sand placement using box sprinkler.

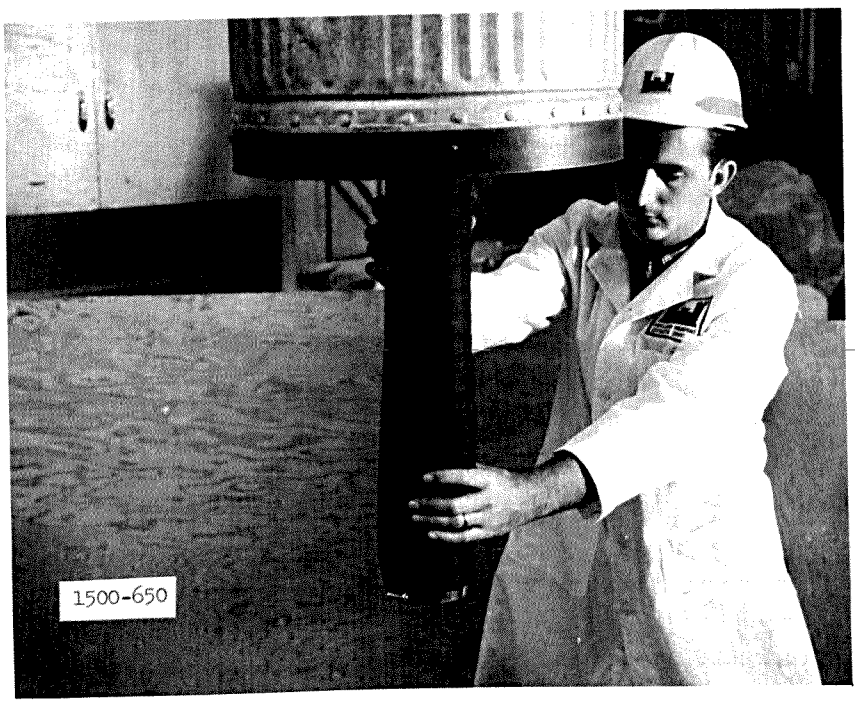

b. Backfilling with can sprinkler.

Figure 3.4 WES soil placement devices.

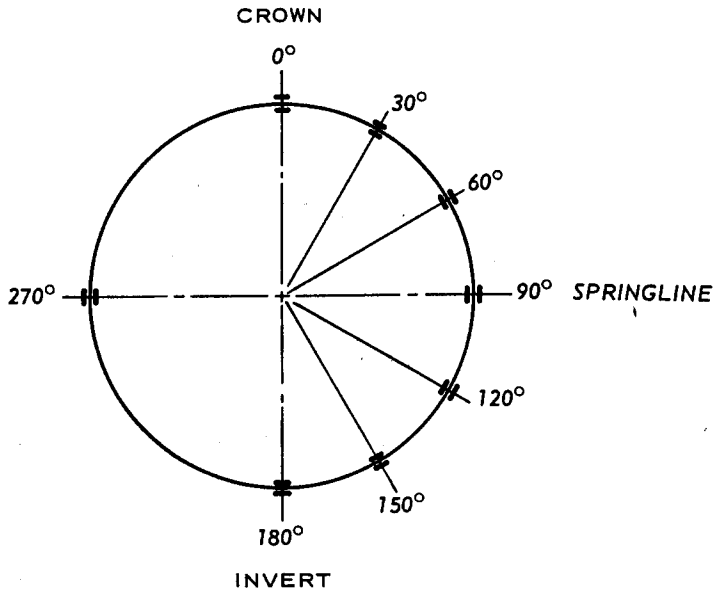

a. END VIEW OF CENTRAL TEST SECTION

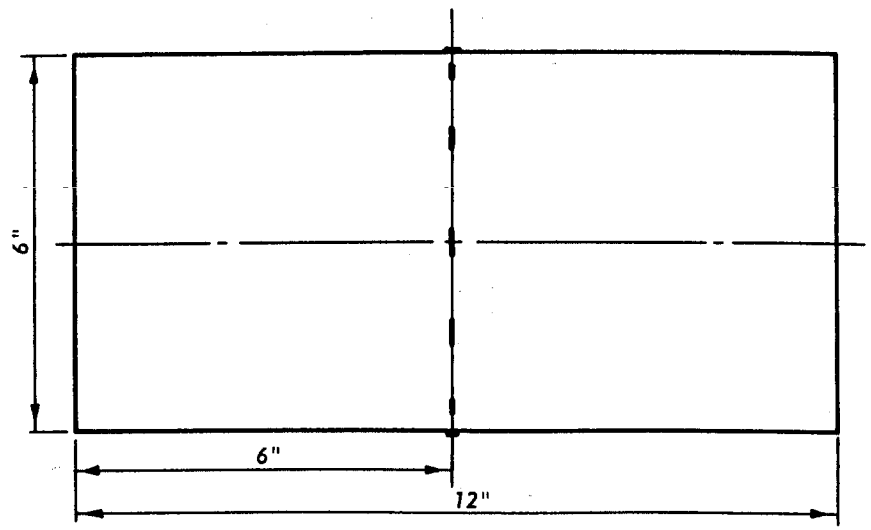

b. ELEVATION VIEW OF CENTRAL TEST SECTION

Figure 3.5 Locations of cylindrical test specimen strain gages.

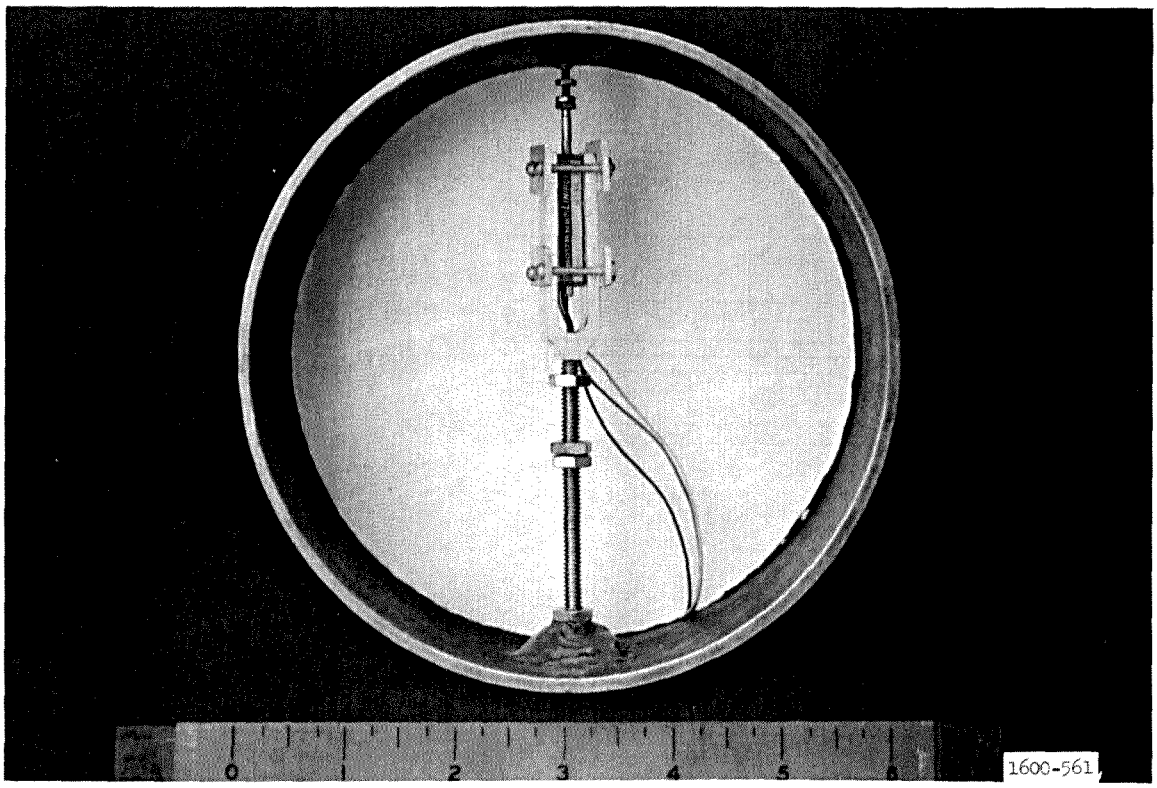

a. Deflection gage in place.

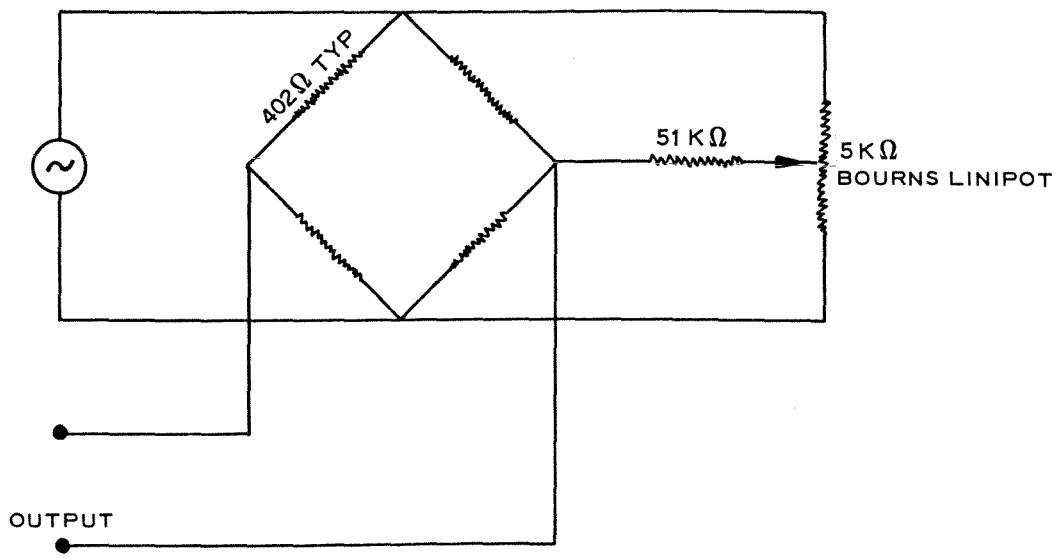

b. Electrical diagram of deflection gage.

Figure 3.6 Deflection gage.

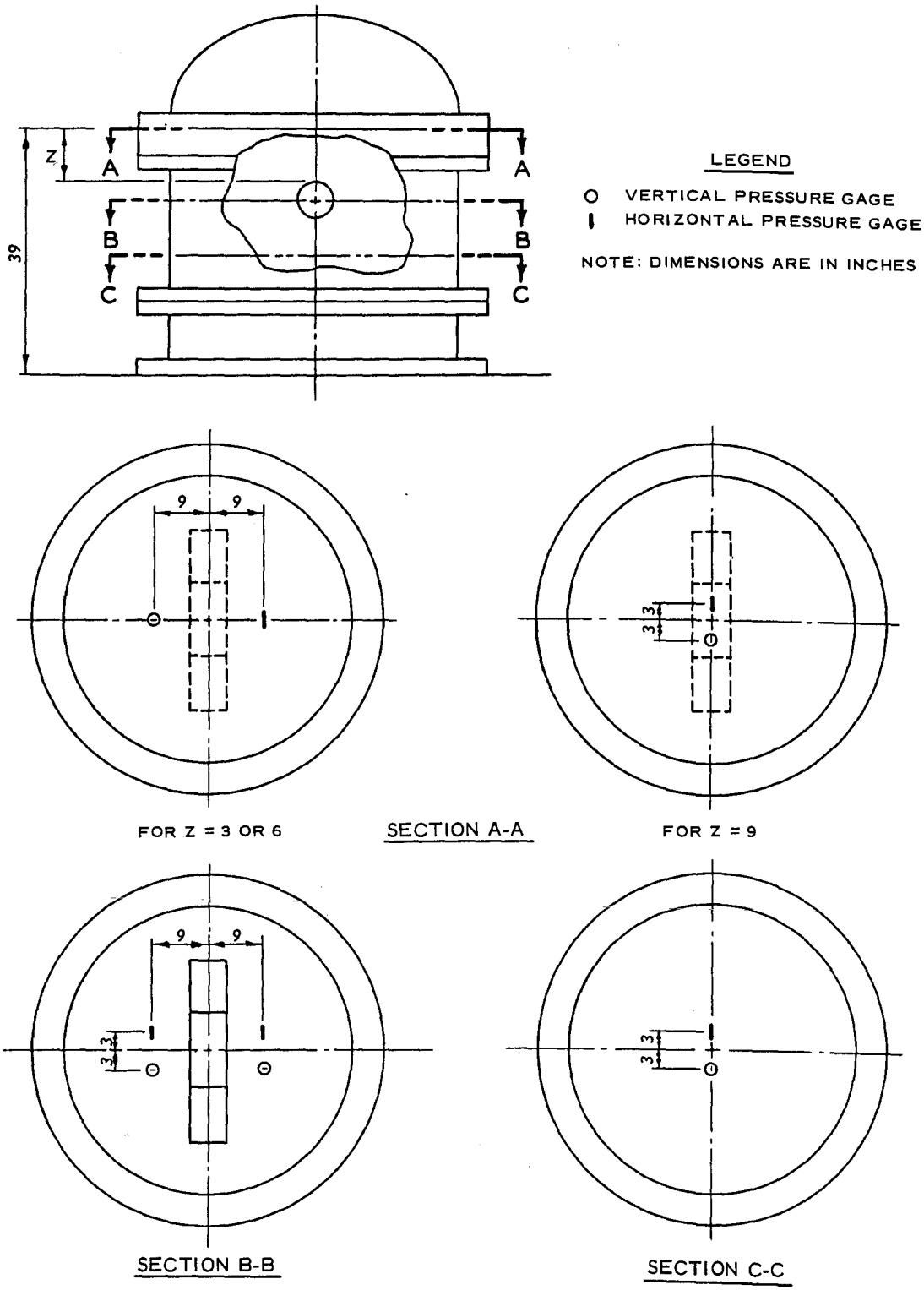

Figure 3.7 Locations of soil pressure gages.

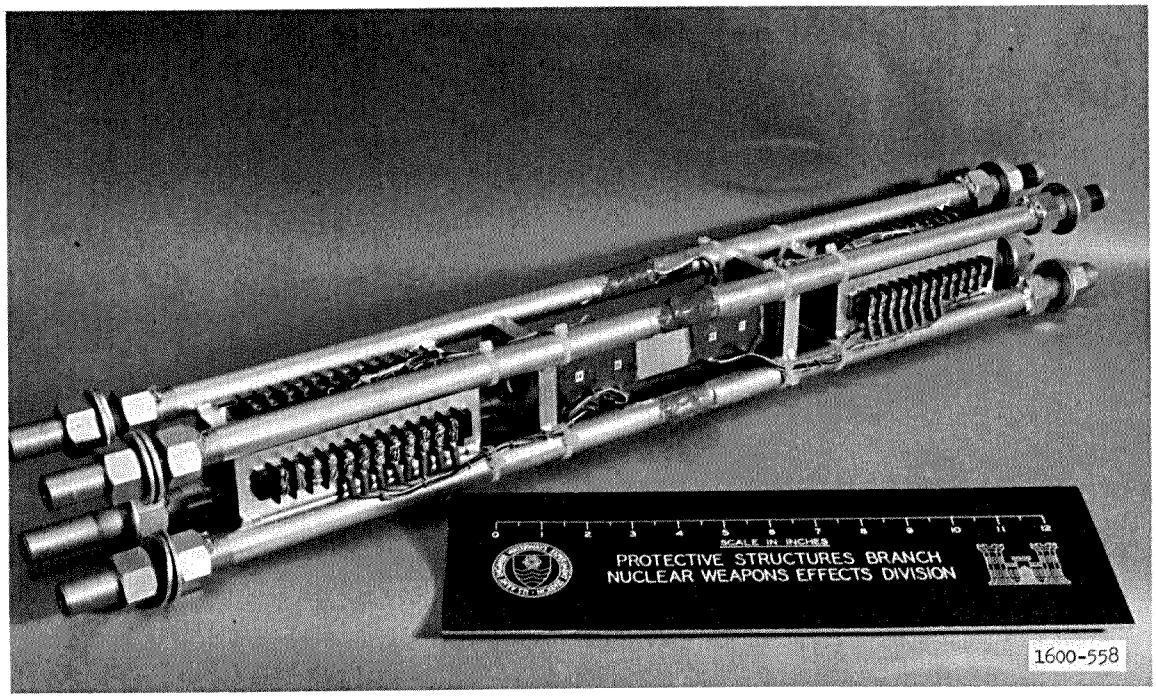

a. End-cap support assemblage.

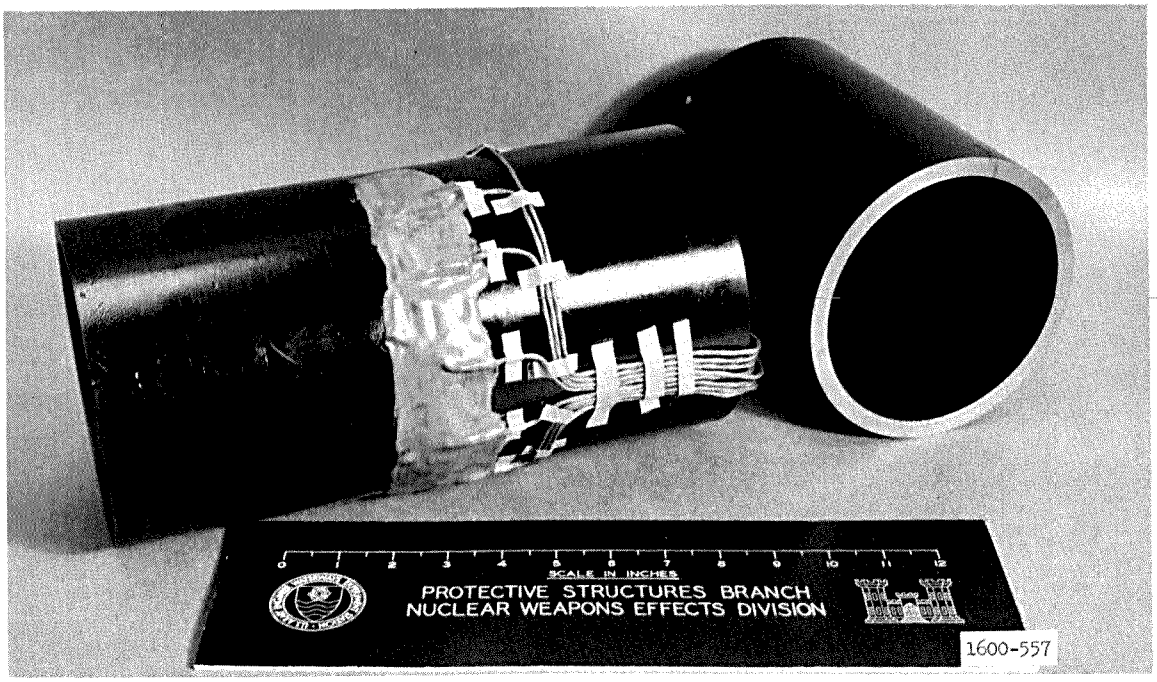

b. Central test section and end cap.

Figure 3.8 Components of the cylindrical test specimens.

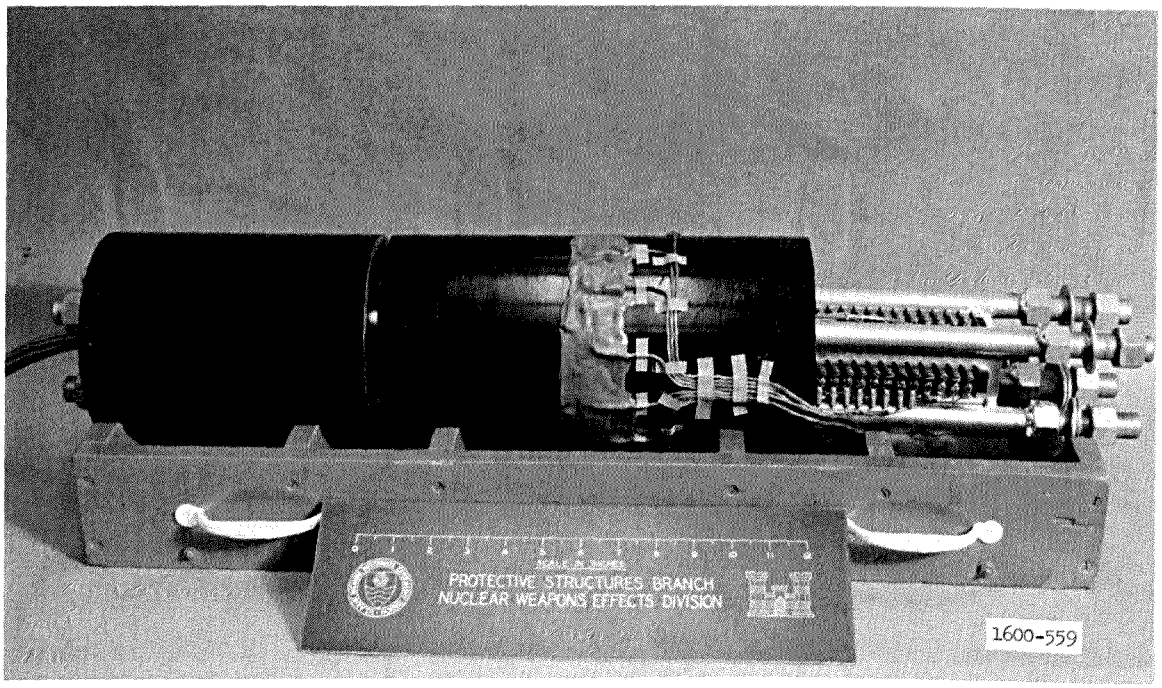

a. Connection of strain gage leads.

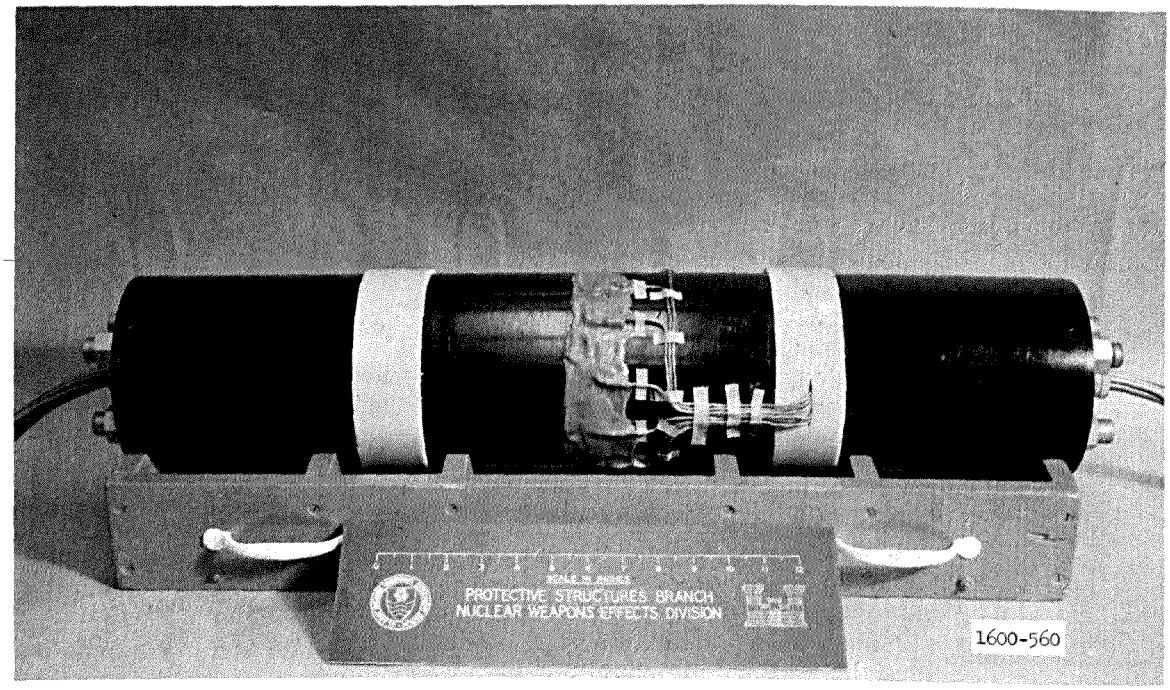

b. Pliable gaskets in separation joints.

Figure 3.9 Assemblage of cylindrical test specimen.

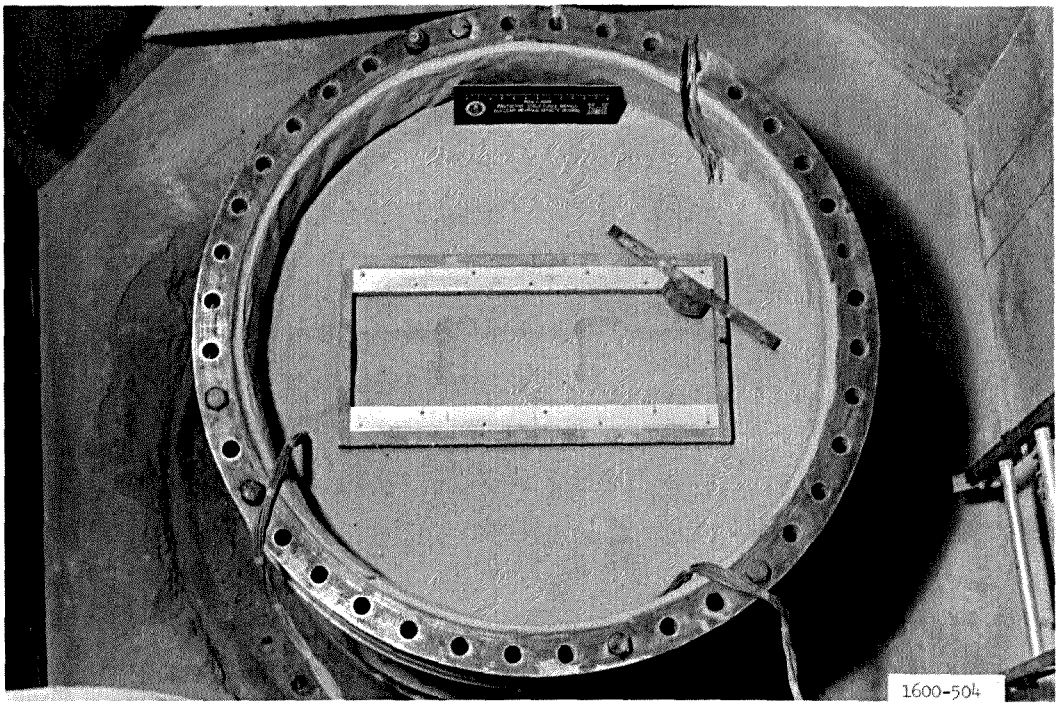

a. Guide and template used to excavate bedding surface.

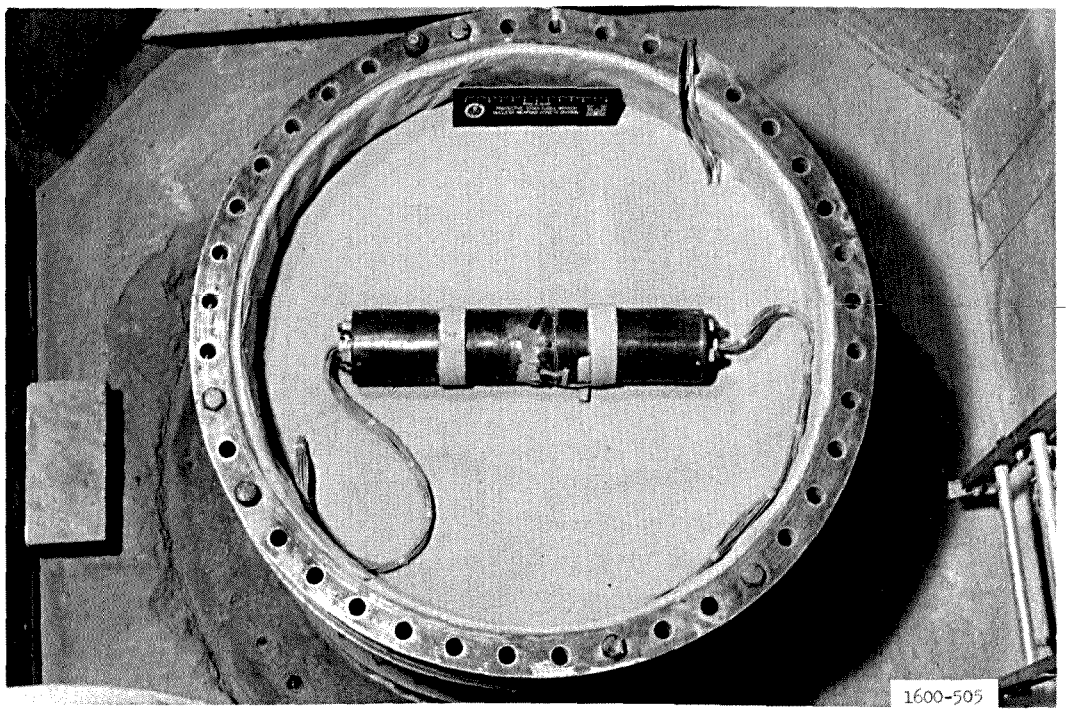

b. Installed cylindrical test specimen.

Figure 3.10 Placement of cylindrical test specimen in soil.

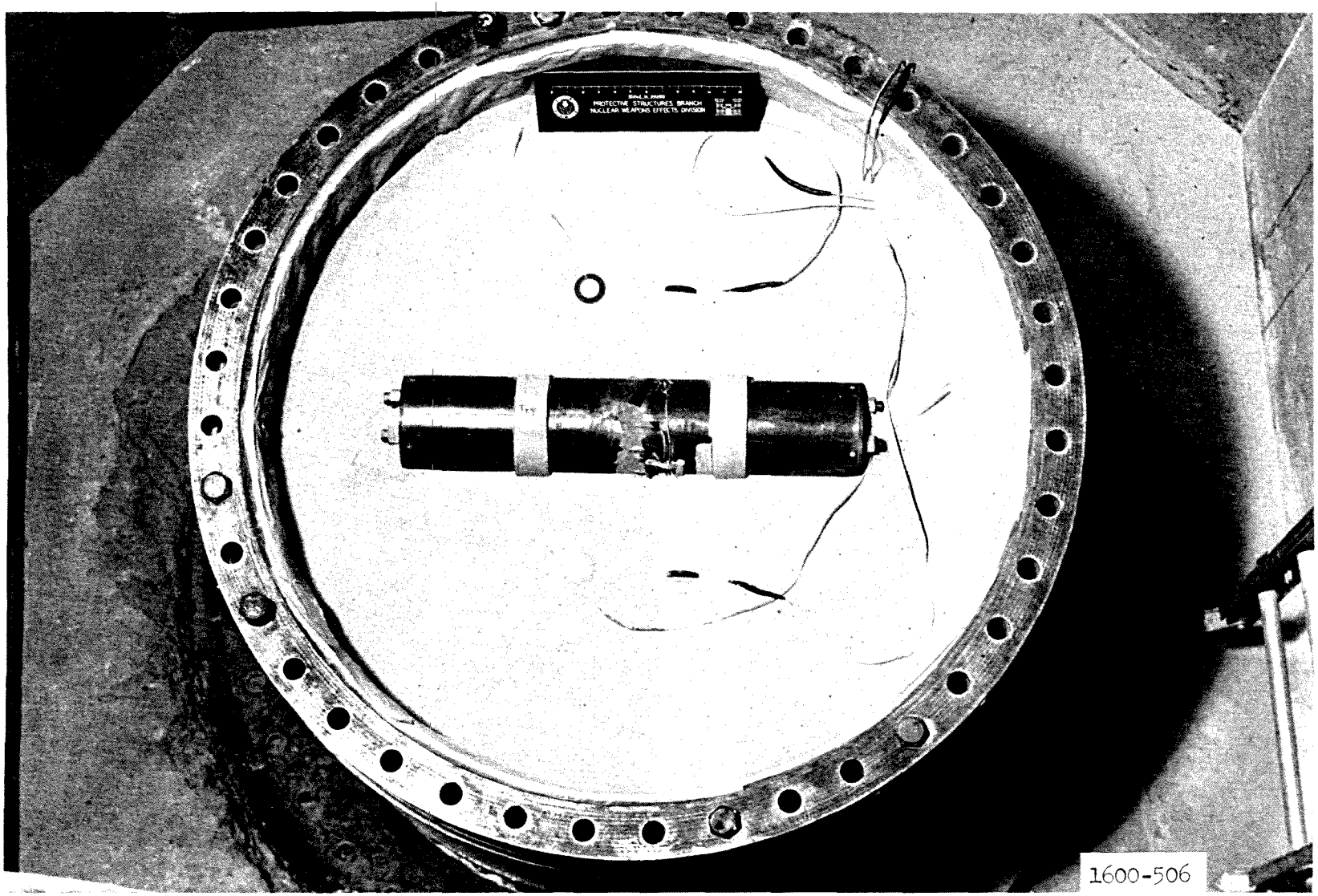

Figure 3.11 Cylindrical test specimen buried to middepth.

CHAPTER 4

SUMMARY OF TESTS AND DISCUSSION OF RESULTS

4.1 SUMMARY OF TESTS

A summary of the tests conducted during this experimental investigation is presented in Table 4.1. A total of 14 static tests were conducted, 9 of which were conducted on virgin soil samples and 5 of which were conducted on soil samples that had previously been loaded. In general, the reloading was conducted because a major data channel was either saturated or because it malfunctioned during the previous test. The time and economic advantages in reloading are considerable and, in addition, reloading provides an opportunity to assess the effects that cyclic loading has on test specimens.

During the test program, all tests relating to one cylinder stiffness (EI/R^3) were conducted prior to changing to another cylinder stiffness. The test program commenced with testing of the least stiff specimen and concluded with testing of the stiffest specimen. While testing a particular cylinder stiffness, the depth of burial was varied in the following order: 9, 6, and 3 inches. This format of testing was adopted mainly because previous test results at low pressures could be used to predict the response of the 1/8-inch-thick cylinder at high overpressures. A typical SBLG static surface overpressure versus time curve is presented in Figure 4.1.

4.2 DISCUSSION OF RESULTS

Values for the measured bending moments and thrusts presented in this chapter were calculated as follows:

$$M = \frac{Et^2}{12} (\epsilon_e - \epsilon_i) \tag{4.1}$$

$$T = \frac{Et}{2} (\epsilon_e + \epsilon_i) \tag{4.2}$$

Where: M = circumferential bending moment, in-lb/in

E = elastic modulus of the material, psi

t = thickness of the cylinder wall, inches

ϵ_e = exterior strain in the circumferential direction, in/in

ϵ_i = interior strain in the circumferential direction, in/in

T = circumferential thrust, lb/in

The use of Equations 4.1 and 4.2 for calculation purposes implies the assumption of linear elastic material behavior. This assumption is justified since no permanent set in the material was noticed when the strain gages were read before and after all tests. Compressive strains and thrusts are considered positive. Also, moment causing compression in the external cylinder fibers is considered positive.

Figures 4.2 through 4.8 present plots of moment versus surface overpressure for each cylinder at three different depths of burial. The bending moments were determined at the crown and at 30-degree intervals (going clockwise) to the invert. Figures 4.2 through 4.8 also present composite plots showing the variation of moment with cylinder stiffness. Each composite plot was made by drawing a weighted line through the test data for each cylinder and then superimposing these curves on a common set of coordinate axes. Obviously, the composite plots mask, to some extent, the effects of depth of burial. However, the figures are arranged in such a manner that the reader can judge the validity of the composite plot curves by observing the scatter due to depth of burial in the accompanying plots of a particular figure. The influence on bending moment caused by recycling a typical test is shown in Figure 4.9.

Thrust versus surface overpressure plots are presented in Figures 4.10 through 4.16. For each cylinder, the thrusts were determined at the same locations as the moments; also, the format for the thrust figures is the same as that for the moment figures. The only difference in the presentation of the thrust and moment data is that the thrust data were banded because of scatter.

Dimensionless plots of M/PR^2 versus PR^3/EI at the crown and

springline are shown in Figures 4.17 and 4.18, respectively. Three plots, one for each depth of burial, are presented in each of these figures. Plots of M/PR^2 versus PR^3/EI at the crown for the range $0 < PR^3/EI < 1.0$ are shown in Figure 4.19. Also, in each of Figures 4.17 through 4.19, the recommended design envelope for buried cylinders, as established in Reference 1, is presented as a solid line. The relative displacement between the crown and invert is plotted as a function of surface overpressure in Figure 4.20.

Physical properties of the steel tubing and the confining soil media are given in Appendixes A and B, respectively.

4.2.1 Bending Moment. Examination and comparison of the moment data reveal that the cylinder stiffness EI/R^3 is the single most important variable influencing the bending moment. The bending moment response of the cylinders was, in general, nonlinear, particularly for the 1/8- and 1/4-inch-thick cylinders in the low surface overpressure range. The significant effect of the cylinder stiffness is attributable to soil arching, which is a function of the relative stiffnesses of the cylinder and soil.

Since the 1/8-inch-thick cylinder was more flexible (less stiff) than the surrounding soil environment, active soil arching developed as the overpressure was applied to the soil-structure system. However, the 3/8-inch-thick cylinder was generally stiffer than the surrounding soil; consequently, passive soil arching developed.

The effect of cylinder stiffness on the interface pressure distribution can also be observed by comparing the composite bending moment versus surface overpressure plots. At peak surface overpressure, the differences between the crown and invert bending moments for the 1/8-, 1/4-, and 3/8-inch-thick cylinders as percentages of their mean values are $\pm$10.0, $\pm$3.8, and $\pm$0.5 percent, respectively. Comparison of the average crown and invert bending moments with the average springline bending moments shows another transition. At peak surface overpressures, the average springline bending moments for the 1/8-, 1/4-, and 3/8-inch-thick cylinders are approximately 55, 90, and 100 percent,

respectively, of the average values of the crown and invert bending moments. Thus, as the cylinder stiffness increased, the crown, springline, and invert bending moments approached a common value.

The crown bending moments at high surface overpressures for the 1/8- and 1/4-inch-thick cylinders at the 3-inch depth of burial are approximately 15 percent greater than the corresponding bending moments for the 6- and 9-inch depths of burial. The reverse situation occurs in the bending moment data for the 3/8-inch-thick cylinder, i.e., the bending moments for the 3-inch depth of burial are less than the corresponding bending moments for the 6- and 9-inch depths of burial. From Reference 3, experimental measurements of the interface pressure at the crown of a shallow buried cylinder with a D/t ratio similar to that of the 1/8-inch-thick cylinder indicated that the crown interface pressure decreased with an increase in depth of burial. However, for a virtually rigid cylinder, the crown interface pressure increased with an increase in depth of burial. Except for the relative arrangement of the bending moments for the 6- and 9-inch burial depths, the bending moment data obtained in this study agree with the experimental measurements given in Reference 3.

The effects that recycling had on the bending moment response of the cylinders were most prevalent for the 1/8-inch-thick cylinder. Recycling resulted in the bending moments of the second and following cycles being greater than those produced in the initial loading cycle, particularly in the low surface overpressure range.

4.2.2 Thrust. As stated earlier, the plots of thrust versus surface overpressure are banded in Figures 4.10 through 4.16 due to the scatter in the data. The thrust data for the stiffer cylinders display considerably more scatter than the corresponding bending moment data, primarily as a result of the respective calculation procedures. The interior and exterior circumferential strains, which were of opposite signs at all times during a test, were algebraically subtracted in Equation 4.2 and algebraically added in Equation 4.1. Since the strains were generally large and of the same order of magnitude, the thrust

calculations were very sensitive to the accuracy of the data. The bending moment calculations were not as significantly affected. As cylinder stiffness increases, the effects of density irregularities on bending moments decrease, and the scatter in test data becomes primarily dependent on calculation procedures.

Except for the scatter and the unusually high thrusts for the 1/8-inch-thick cylinder at the 30-degree location, the thrust data are relatively consistent. All of the thrusts are positive, i.e., compressive, although the thrust for the 3/8-inch-thick cylinder at the crown is positive by only a small amount.

The normalized springline thrust T/PR is a measure of the amount and type of arching created in the soil-structure system. A normalized thrust value of 1.0 is the bifurcation point for soil arching, i.e., passive arching occurs above 1.0 and active arching occurs below 1.0. Since at peak overpressure the normalized springline thrust values were 0.95, 1.05, and 1.30 for the 1/8-, 1/4-, and 3/8-inch-thick cylinders, respectively, active arching was present during the loading of the 1/8-inch-thick cylinder, and passive arching was present during the loading of the 1/4- and 3/8-inch-thick cylinders. The latter normalized springline thrust value is also in relatively good agreement with the theoretical reasonable upper bound for thrust reported in Chapter 2.

The average of the normalized crown and invert thrusts serves as a measure of the lateral earth pressures applied to the buried cylinder. Ideally, the crown and invert thrusts would have equal magnitude; however, this was only approximated in the case of the 1/8-inch-thick cylinder. In this instance, the average of the normalized crown and invert thrusts at the peak surface overpressure was approximately 0.52, an increase of about 65 percent over the coefficient of earth pressure at rest for this soil. In the case of the 3/8-inch-thick cylinder, the average of the normalized crown and invert thrusts at peak surface overpressure was about 0.21, a decrease of about 35 percent relative to the coefficient of earth pressure at rest. Again, this is to be expected because there is a decrease in the vertical soil stress laterally adjacent to the cylinder due to the passive soil arching. Also, in this

instance, the extension of the horizontal diameter of the cylinder is only about 20 percent of the corresponding extension for the 1/8-inch-thick cylinder. Thus, the mobilization of the passive resistance of the soil is not expected to be as great.

4.2.3 Dimensionless Plots. The dimensionless plots in Figures 4.17 and 4.18 can be most effectively used in studying the response of the 1/8-inch-thick cylinder. The responses of the 1/4- and 3/8-inch-thick cylinders can best be seen in Figure 4.19, in which the PR^3/EI axis has been expanded in the interval of 0 to 1.

It can be seen in Figures 4.17 and 4.18 that normalized moment M/PR^2 data for tests of the 1/8-inch-thick cylinder consistently fall outside the recommended design envelope presented in Reference 1. The normalized moment decreases rapidly for low values of PR^3/EI, particularly in the interval $0 < PR^3/EI < 1$. For values of $PR^3/EI > 1$, the normalized moment tends to decrease more slowly, as an almost constant slope is approached at high values of PR^3/EI, i.e., $PR^3/EI \simeq 5$. It is interesting to note that the differences in the crown and springline normalized bending moments for the 1/8-inch-thick cylinder at each burial depth remain practically constant for all pressures throughout the test.

The influence of burial depth on the data presented in Figures 4.17 and 4.18 is relatively small. However, in each figure the lowest normalized moment values occur at the $Z = 3D/2$ depth. M/PR^2 data at the crown are approximately equal for the $Z = D$ and $Z = 3D/2$ depths. At the springline, however, normalized moment data are approximately equal for the $Z = D/2$ and $Z = D$ depths.

Only the crown normalized moment data are shown in Figure 4.19 for the 1/4- and 3/8-inch-thick cylinders. Because the normalized springline moments for these stiffer cylinders were approximately equal to those values at the crown, they are not presented.

Examination of Figure 4.19 reveals that the normalized bending moment for the stiffer cylinders approaches a maximum value between 0.16 and 0.185. The theoretical considerations for the bending moment in a rigid cylinder, discussed in Chapter 2, indicated a reasonable

theoretical upper bound for the crown, springline, and invert bending moments of 0.167, which is in close agreement with the test data. The normalized moments decrease with increasing pressure, but remain over twice the value prescribed by the design envelope.

4.2.4 Diameter Change. The vertical diameter change with overpressure for the cylinders, as presented in Figure 4.20, was greatest for the 1/8-inch-thick cylinder. No real trend was observed regarding the effect of burial depth on diameter change, since only the data for the 1/8-inch-thick cylinder reflected any noticeable effects of depth of burial.

TABLE 4.1 SUMMARY OF TESTING

Test Designation	Peak Surface Overpressure	Cylinder Wall Thickness	Depth of Burial	Remarks
	psi	inches	inches	
S 11	984	0.120	3	--
S 12-1	1,021	0.120	6	First loading of specimen
S 12-2	1,034	0.120	6	Second loading of specimen
S 12-3	1,036	0.120	6	Third loading of specimen
S 12-4	940	0.120	6	Fourth loading of specimen
S 13	1,075	0.120	9	--
S 21	968	0.250	3	--
S 22-1	1,086	0.250	6	First loading of specimen
S 22-2	1,086	0.250	6	Second loading of specimen
S 23-1	1,015	0.250	9	First loading of specimen
S 23-2	1,020	0.250	9	Second loading of specimen
S 31	962	0.375	3	--
S 32	1,067	0.375	6	--
S 33	1,061	0.375	9	--

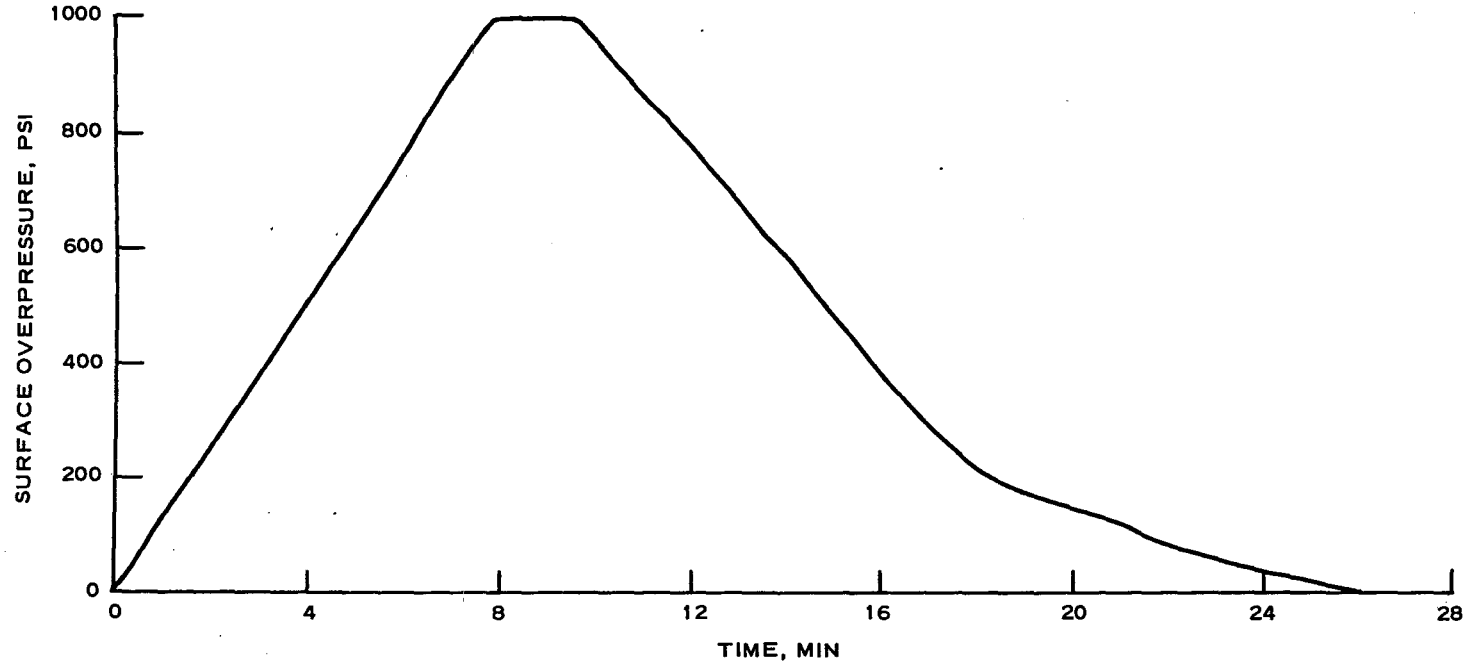

Figure 4.1 Typical SBLG surface overpressure versus time history.

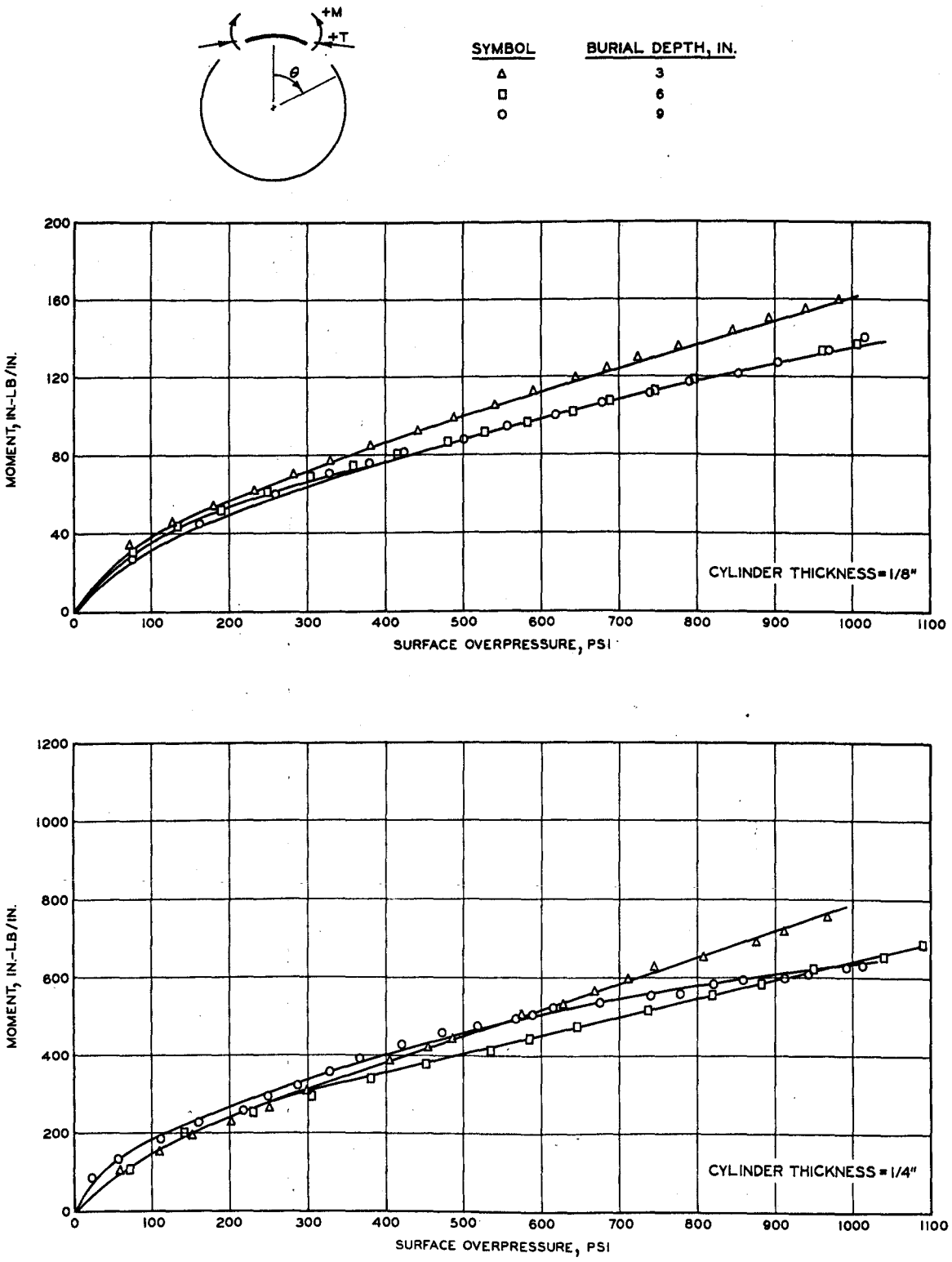

Figure 4.2 Bending moment versus surface overpressure at θ = 0 degrees for 1/8-, 1/4-, and 3/8-inch-thick cylinders (sheet 1 of 2).

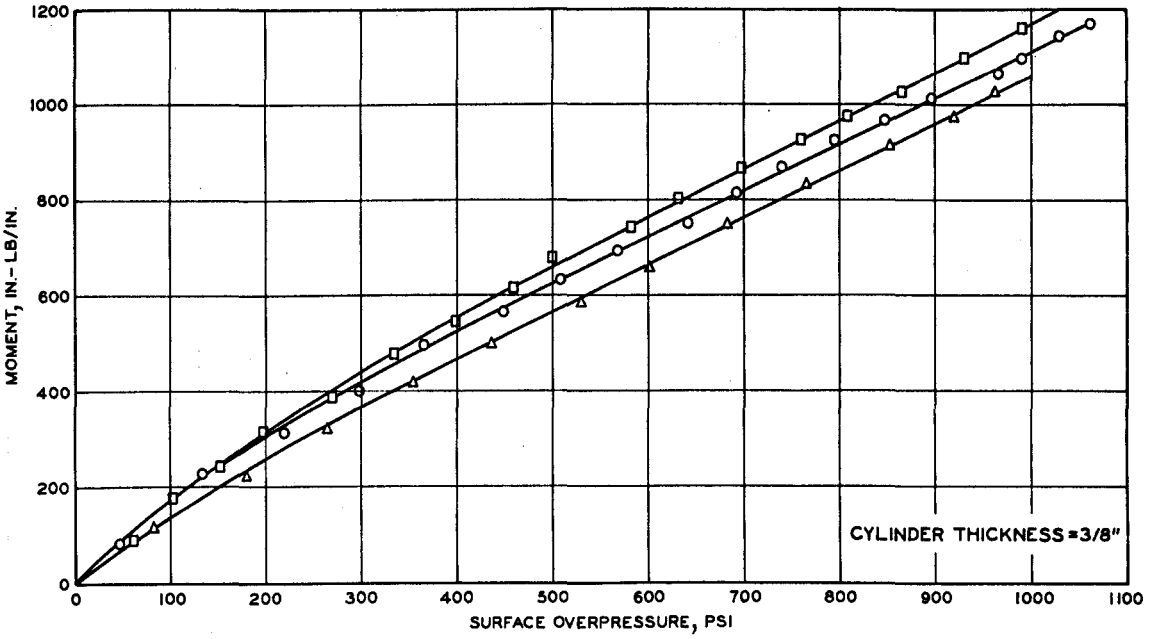

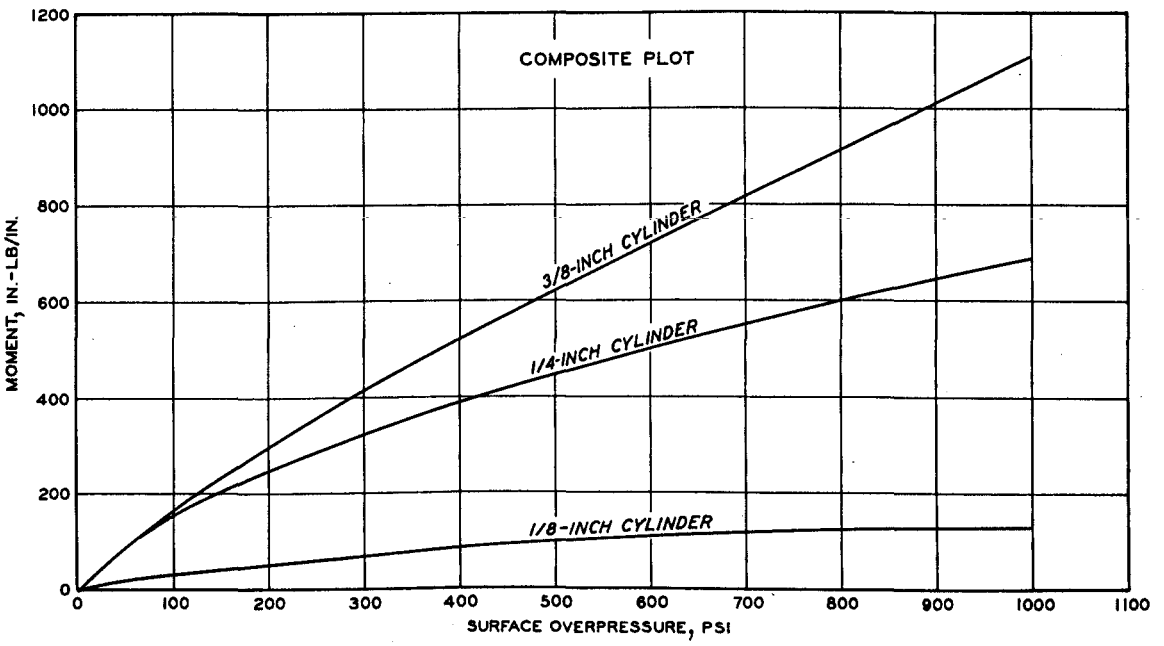

Figure 4.2 (sheet 2 of 2).

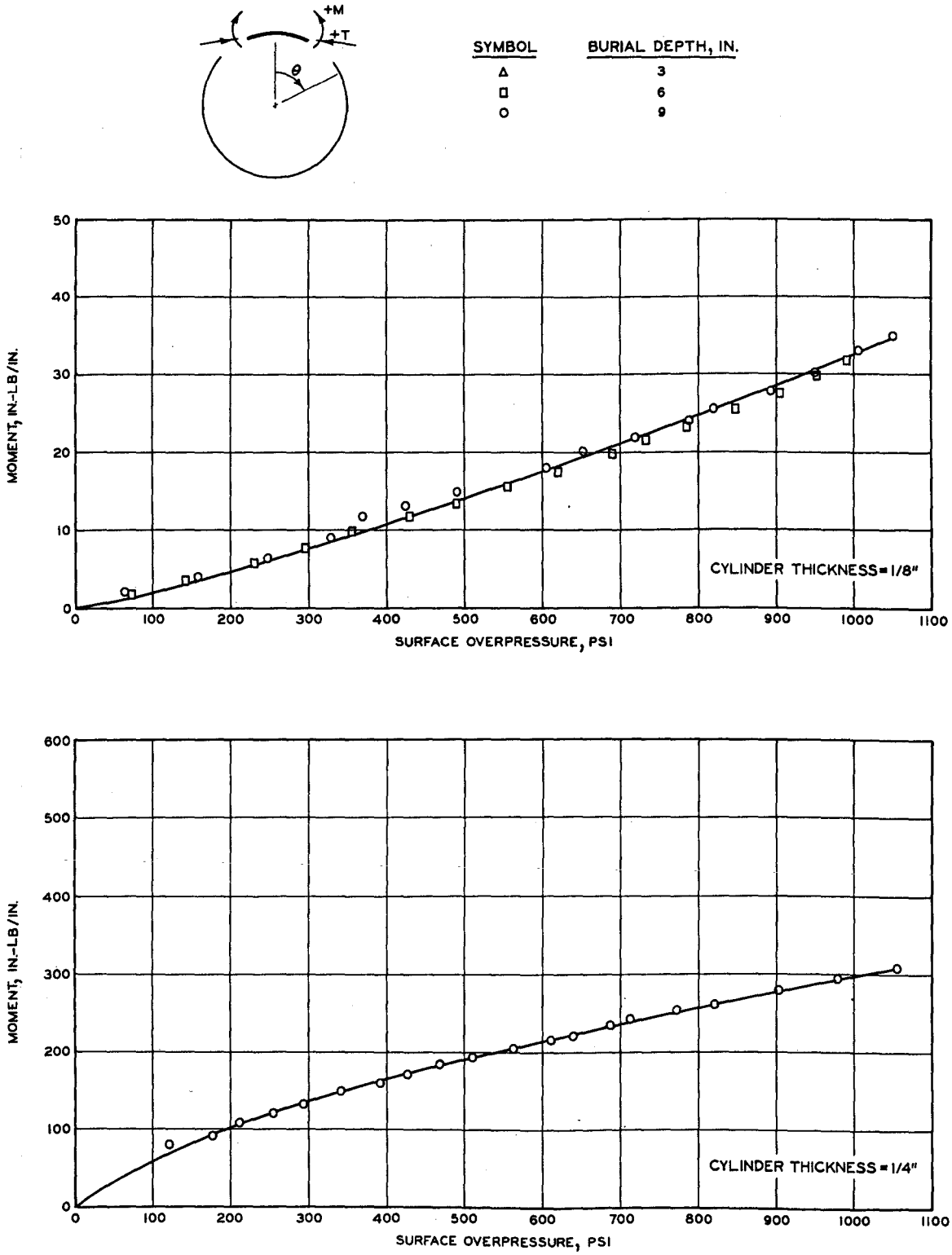

Figure 4.3 Bending moment versus surface overpressure at θ = 30 degrees for 1/8-, 1/4-, and 3/8-inch-thick cylinders (sheet 1 of 2).

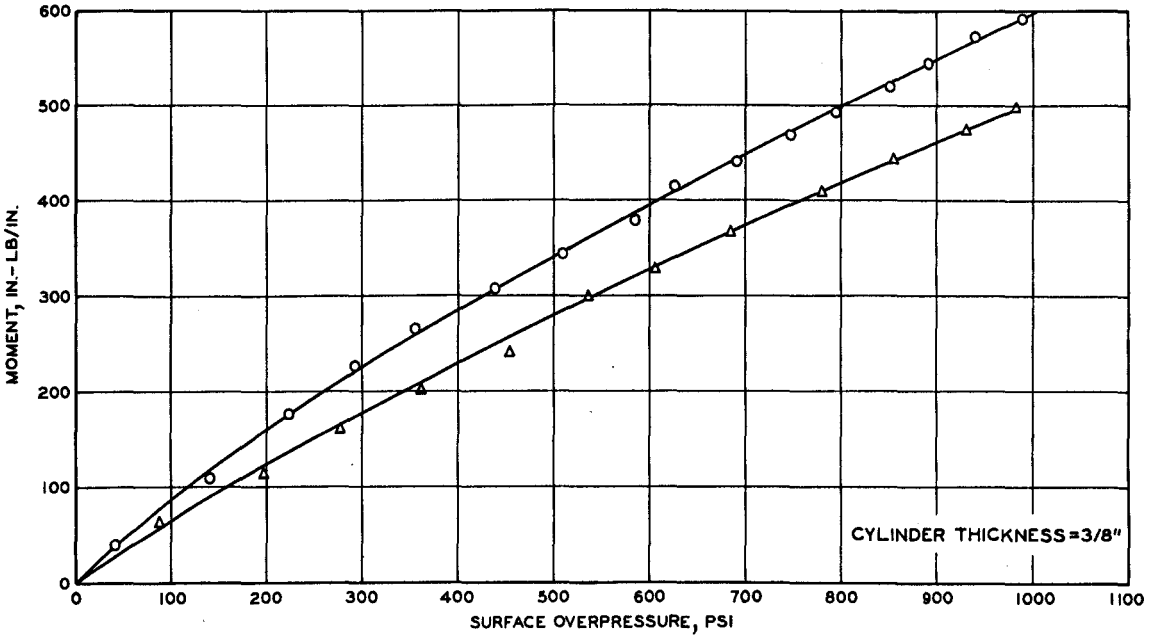

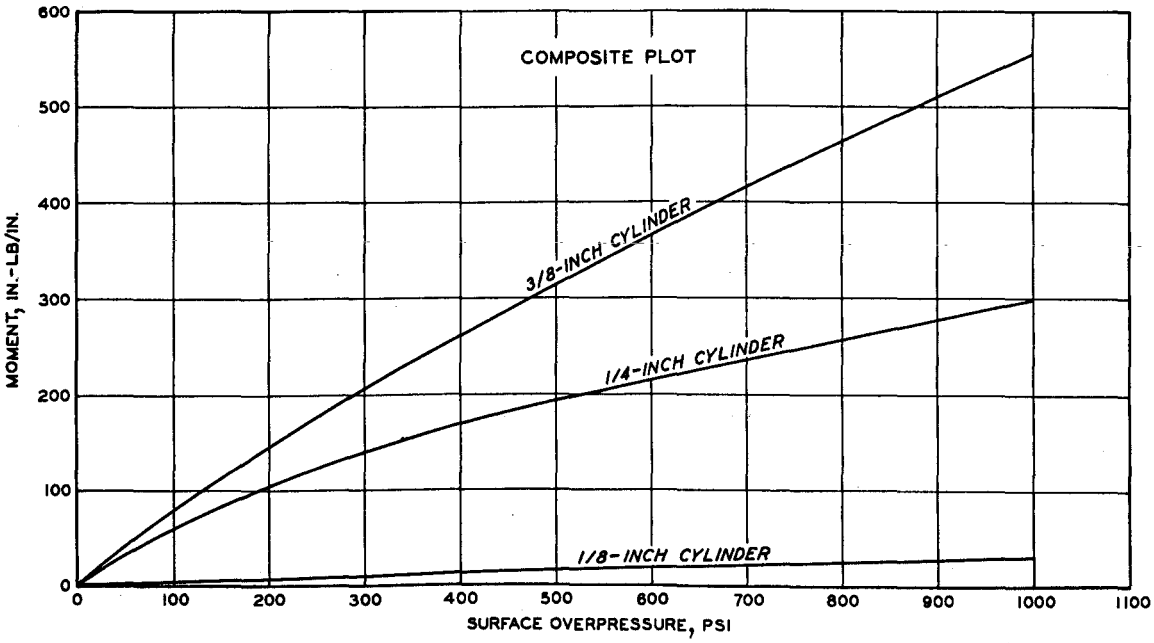

Figure 4.3 (sheet 2 of 2).

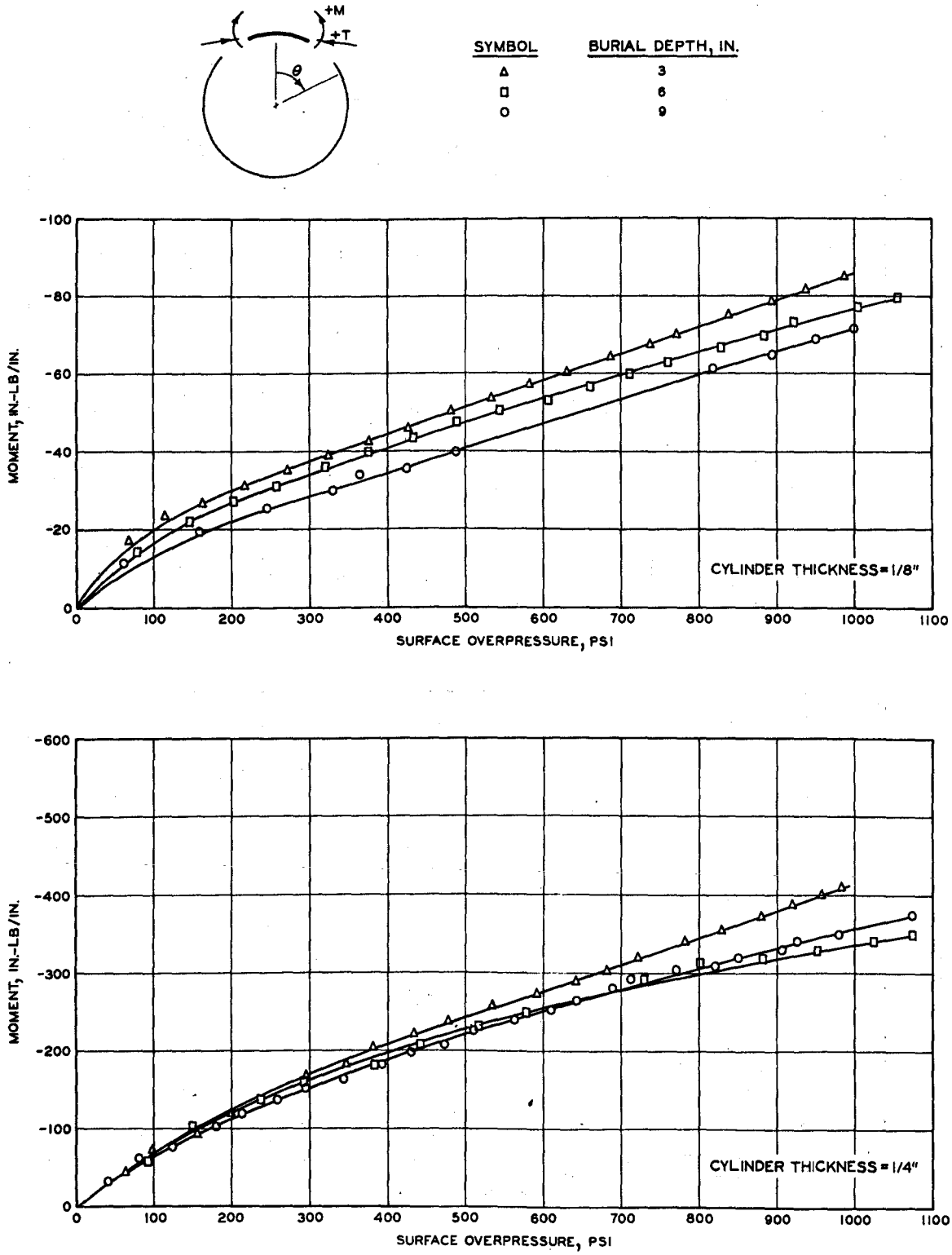

Figure 4.4 Bending moment versus surface overpressure at θ = 60 degrees for 1/8-, 1/4-, and 3/8-inch-thick cylinders (sheet 1 of 2).

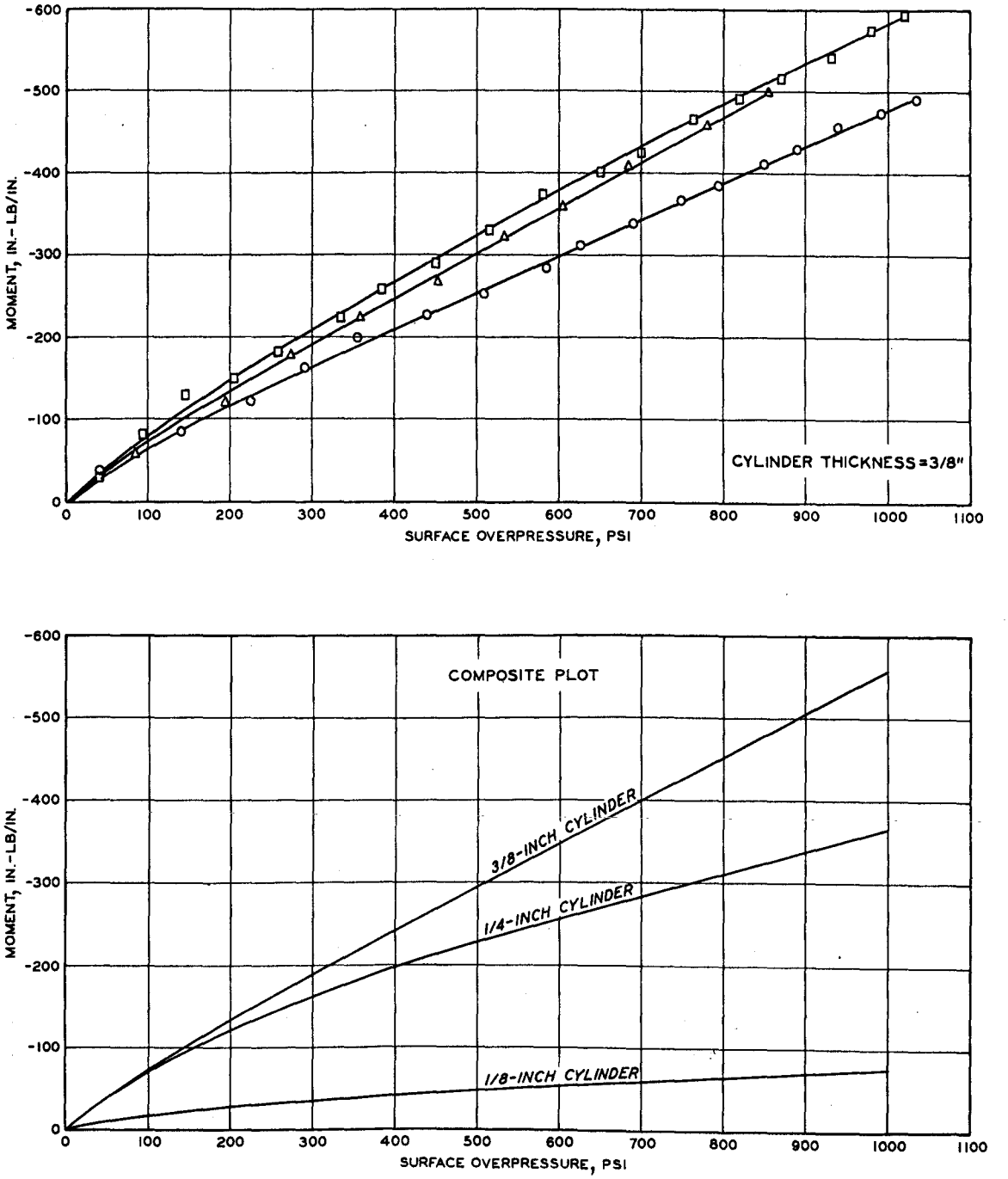

Figure 4.4 (sheet 2 of 2).

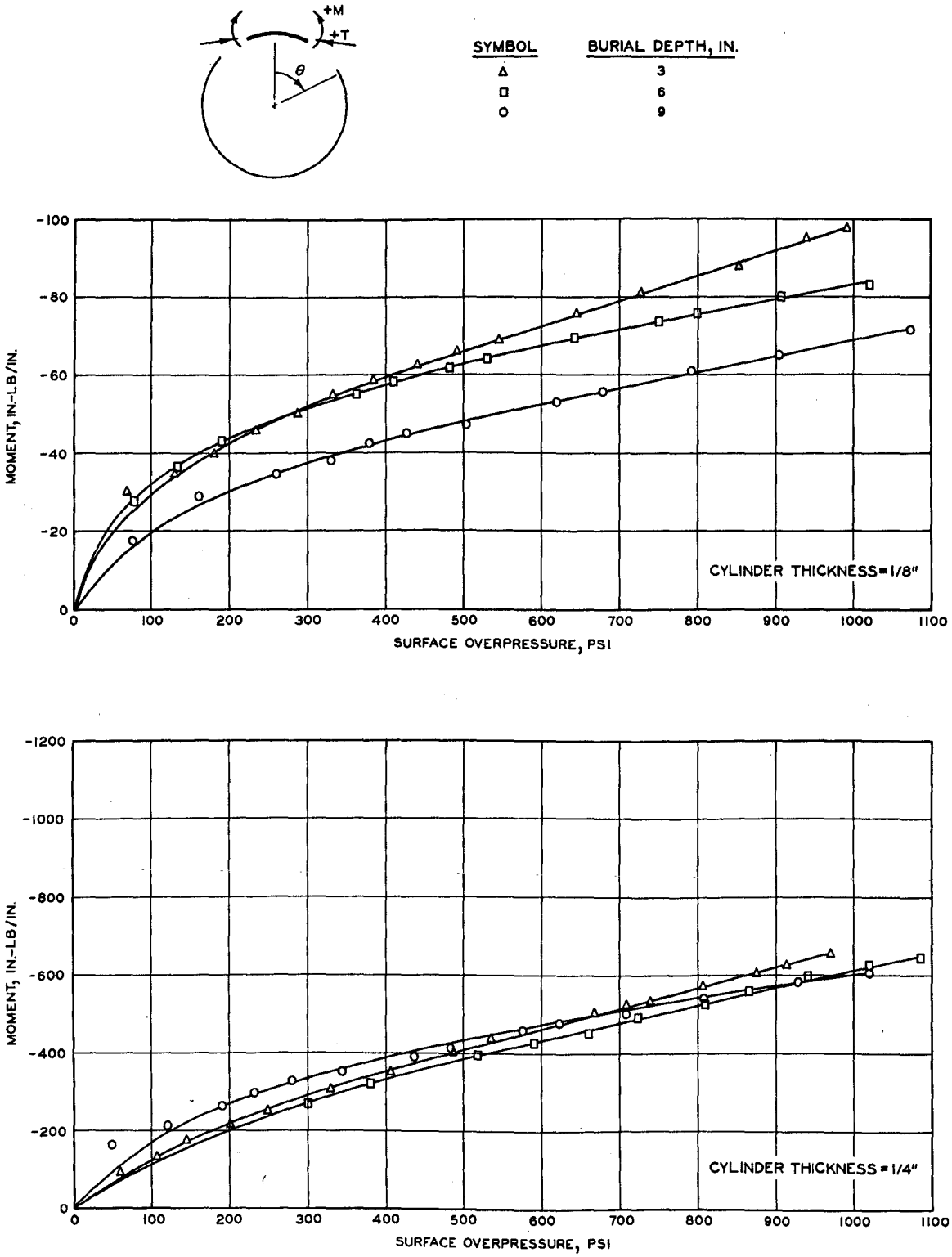

Figure 4.5 Bending moment versus surface overpressure at θ = 90 degrees for 1/8-, 1/4-, and 3/8-inch-thick cylinders (sheet 1 of 2).

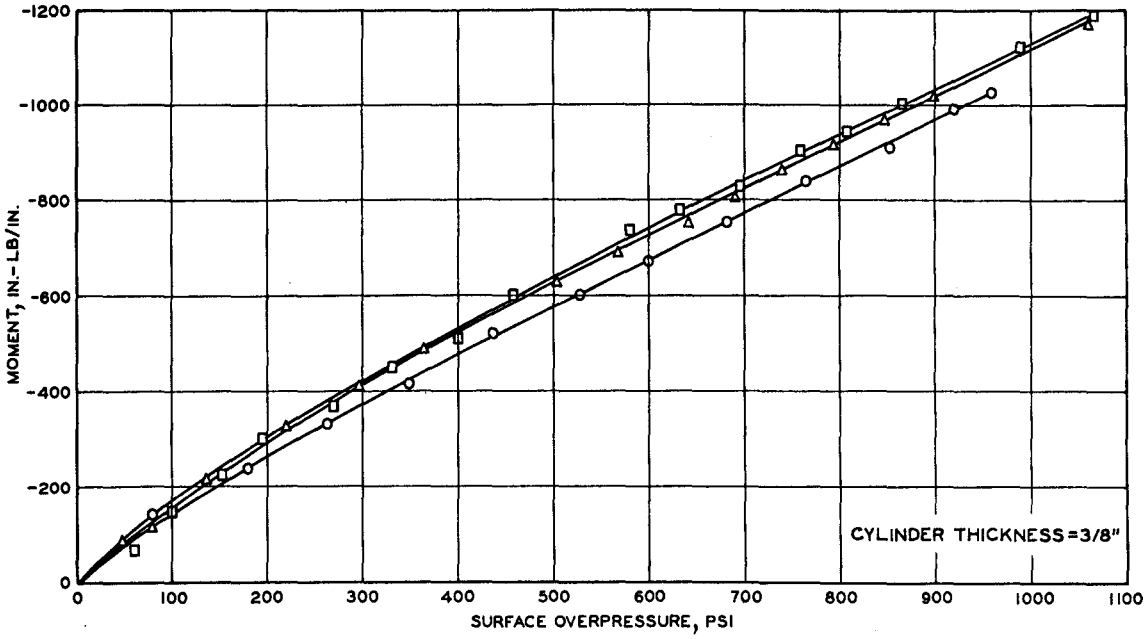

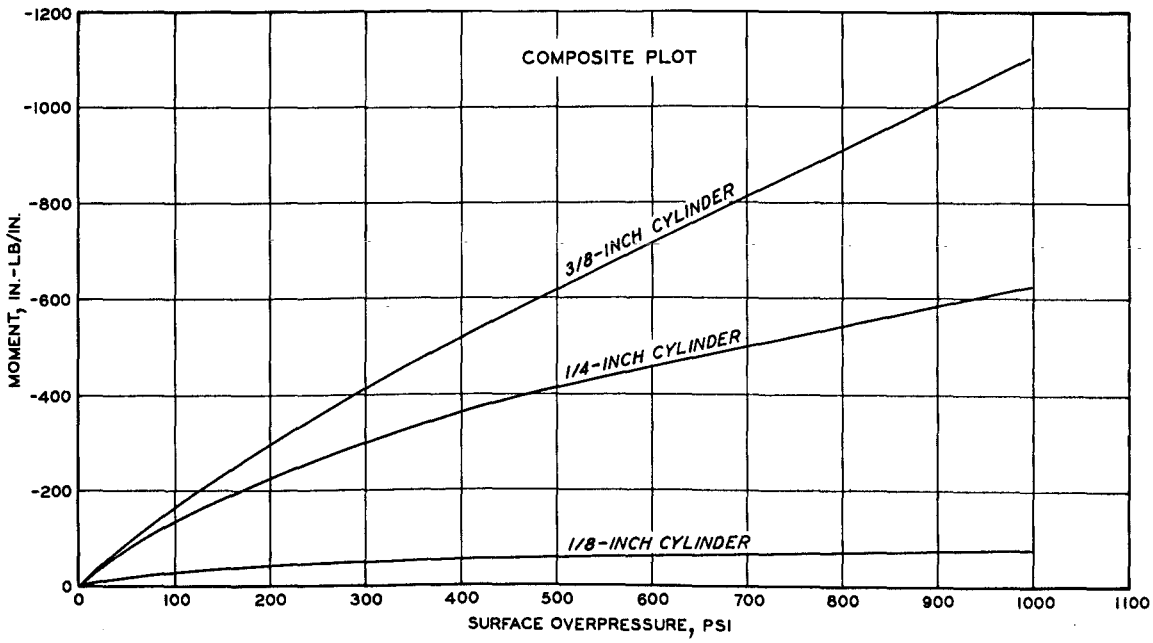

Figure 4.5 (sheet 2 of 2).

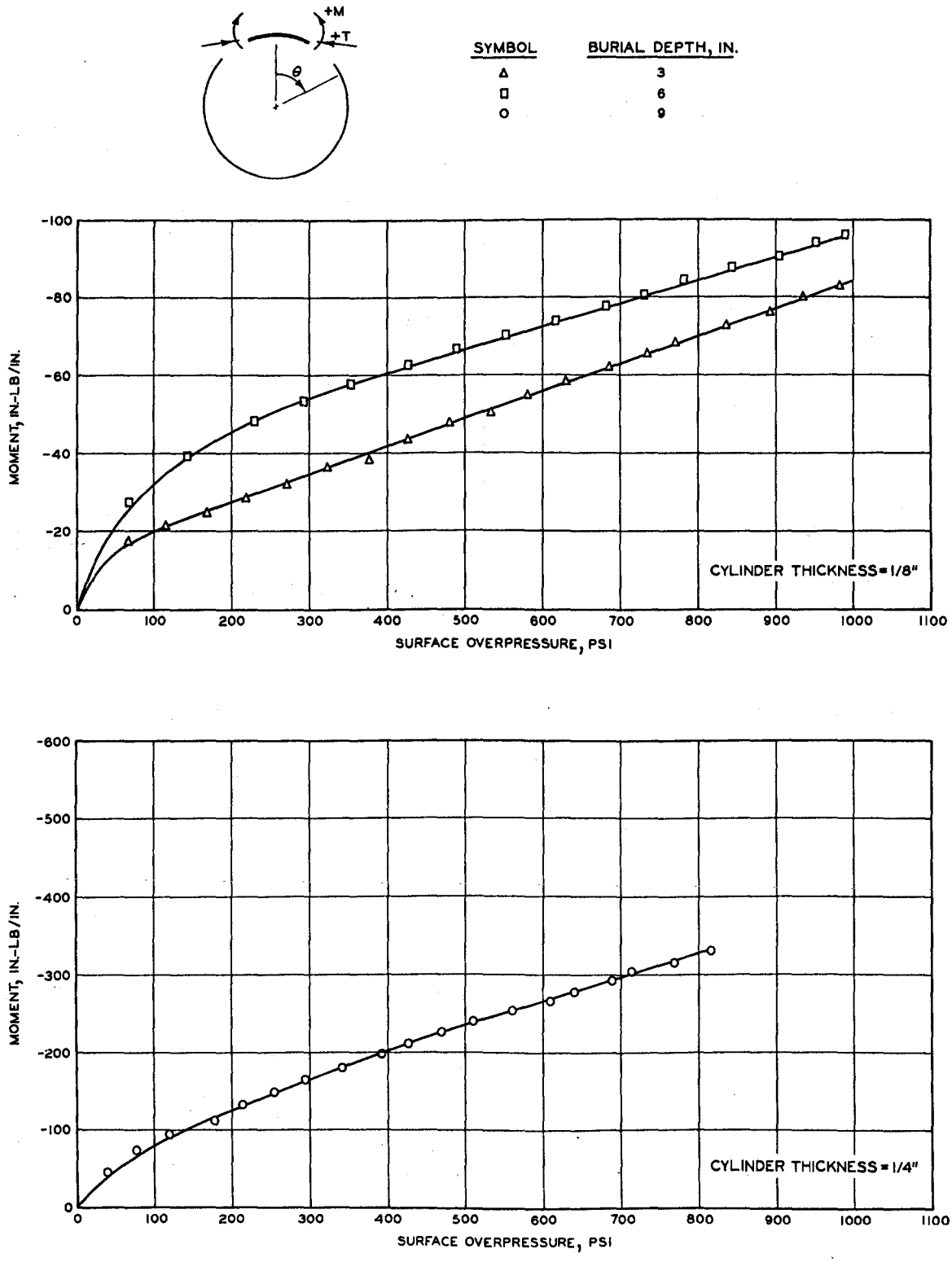

Figure 4.6 Bending moment versus surface overpressure at θ = 120 degrees for 1/8-, 1/4-, and 3/8-inch-thick cylinders (sheet 1 of 2).

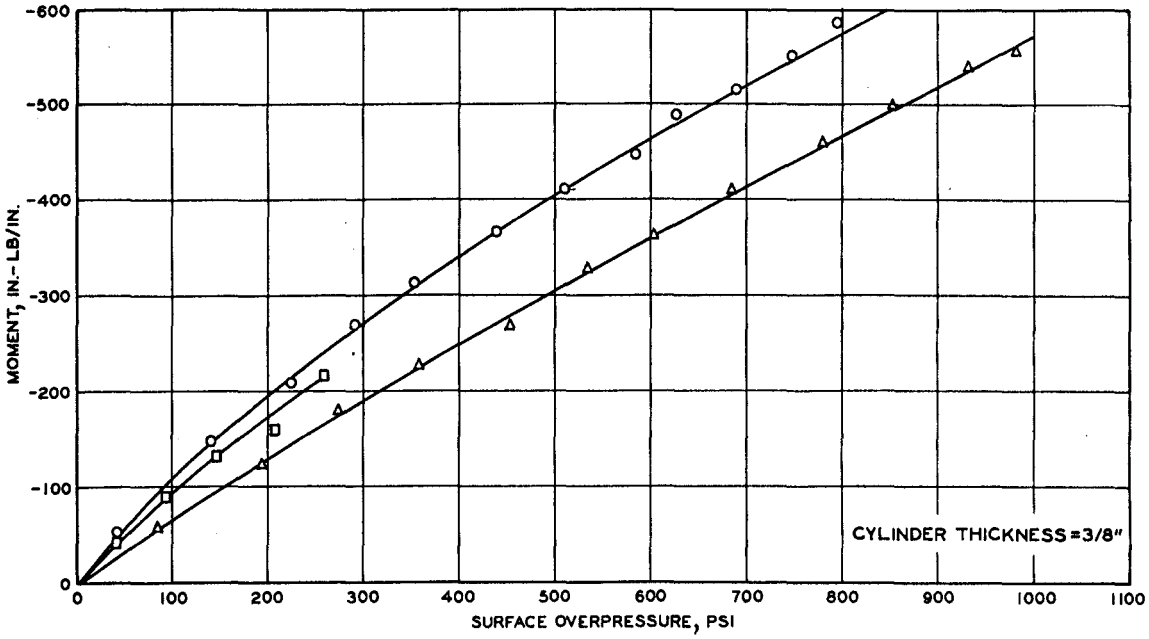

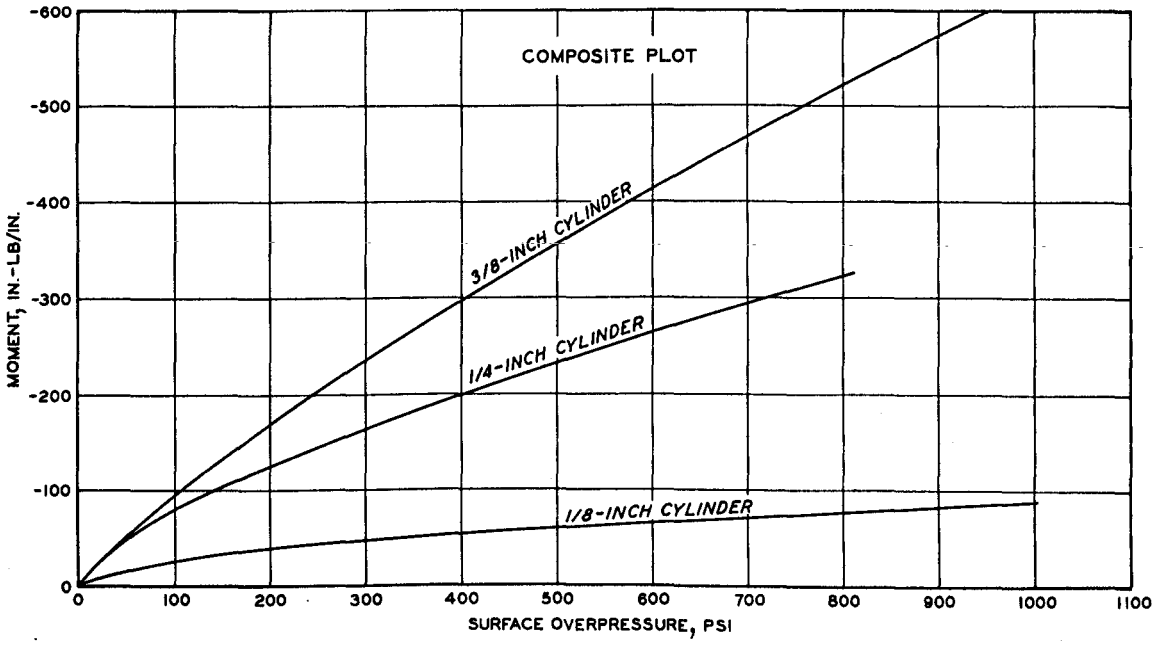

Figure 4.6 (sheet 2 of 2).

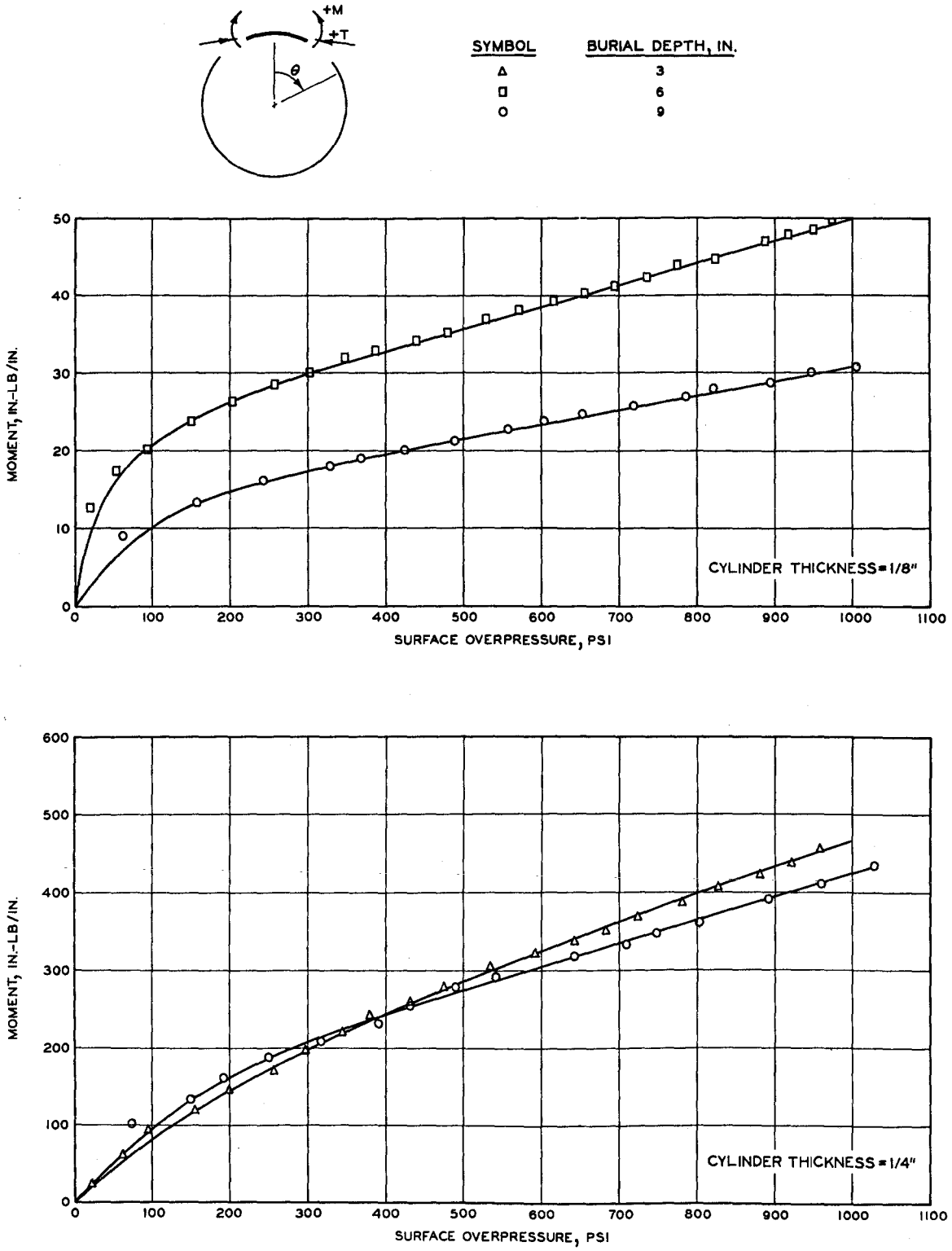

Figure 4.7 Bending moment versus surface overpressure at θ = 150 degrees for 1/8-, 1/4-, and 3/8-inch-thick cylinders (sheet 1 of 2).

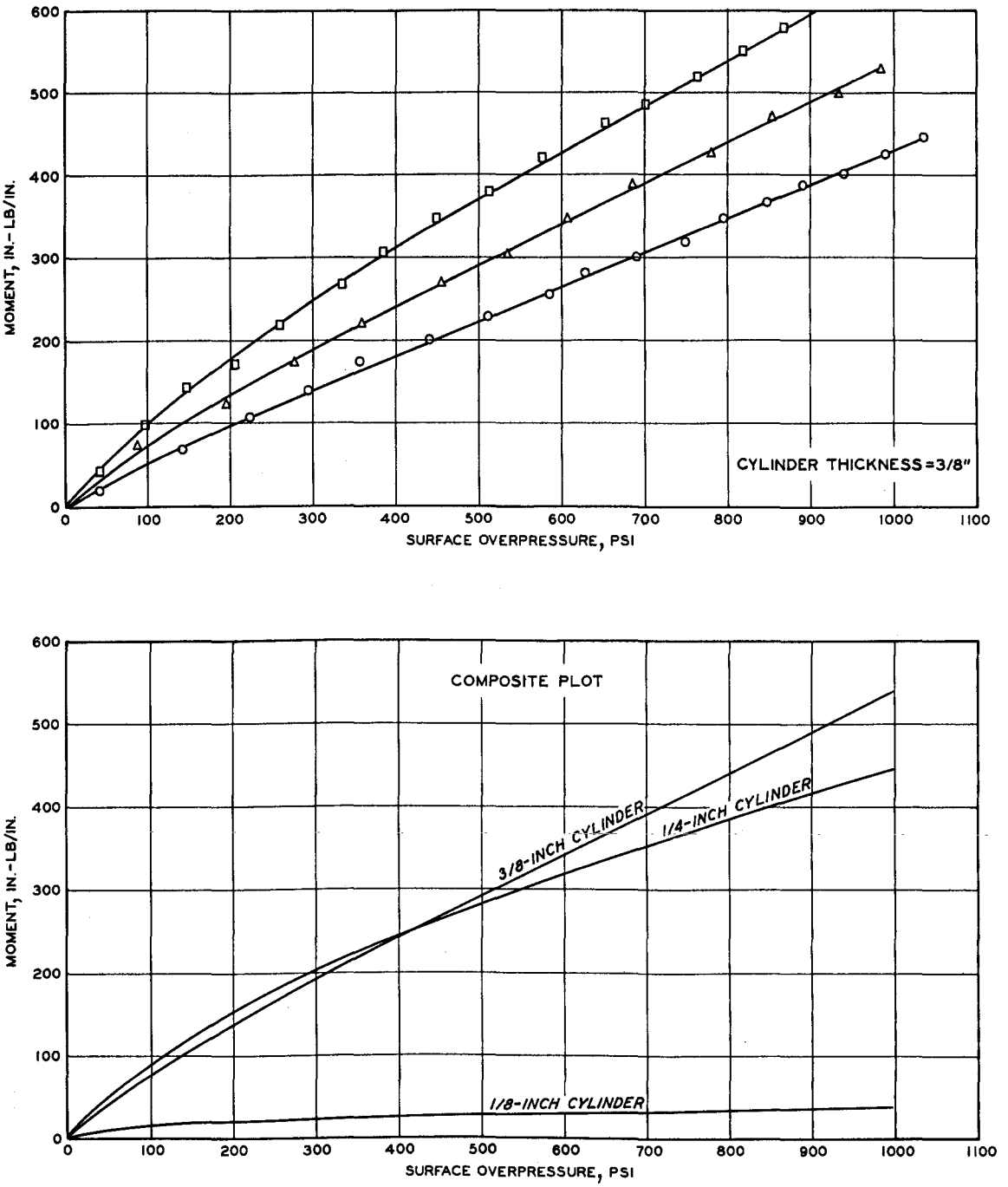

Figure 4.7 (sheet 2 of 2).

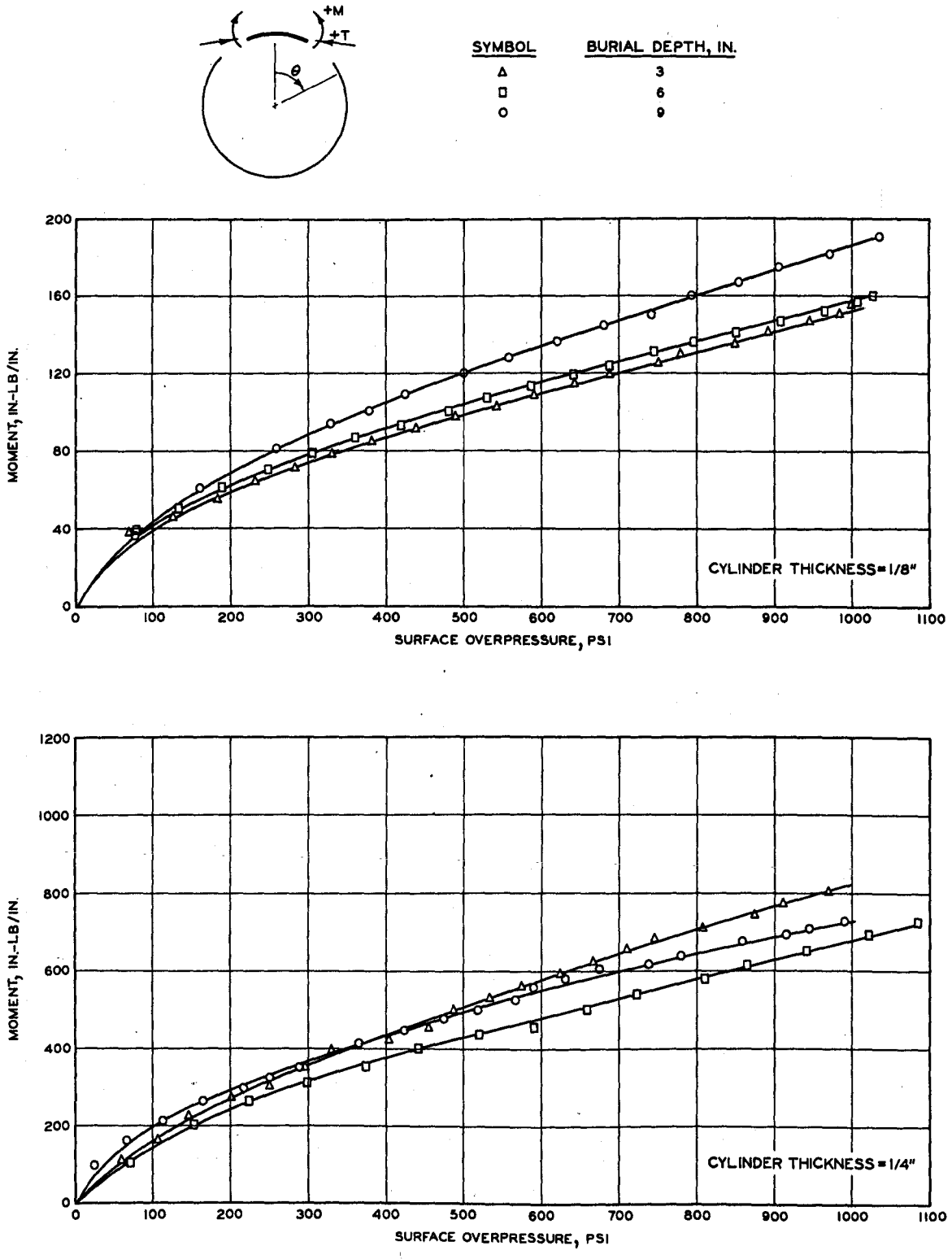

Figure 4.8 Bending moment versus surface overpressure at θ = 180 degrees for 1/8-, 1/4-, and 3/8-inch-thick cylinders (sheet 1 of 2).

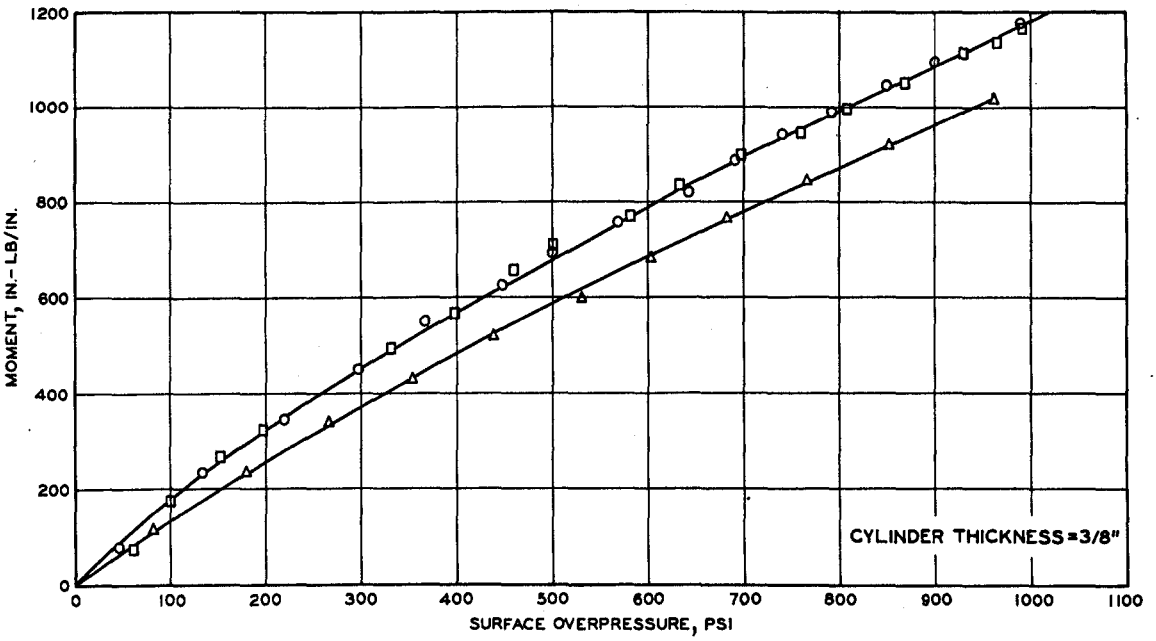

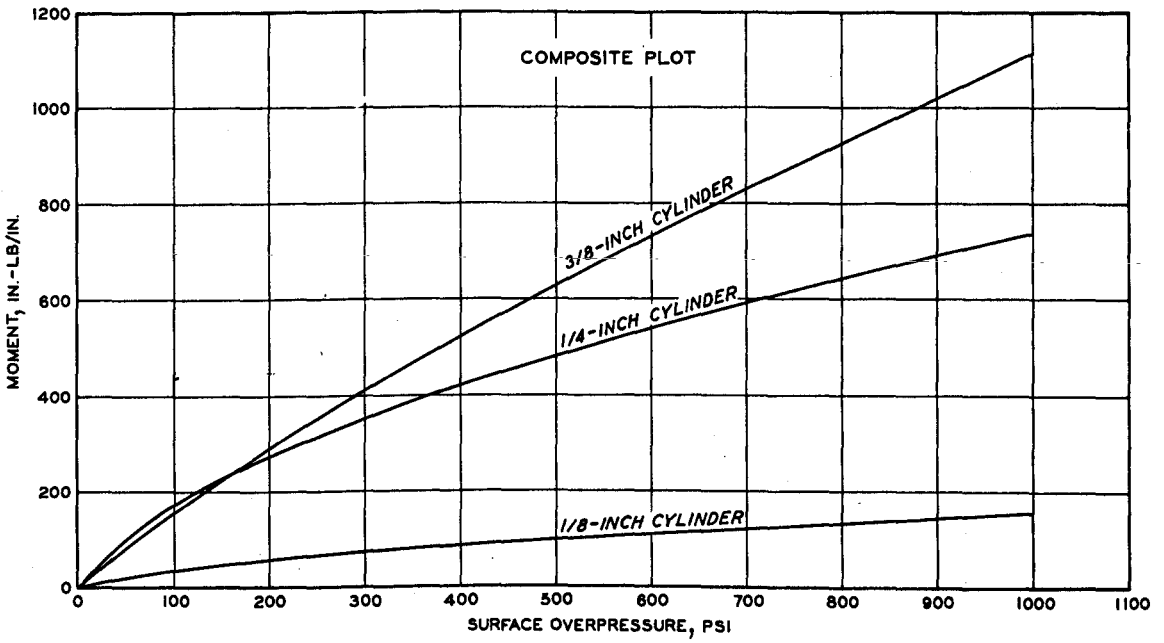

Figure 4.8 (sheet 2 of 2).

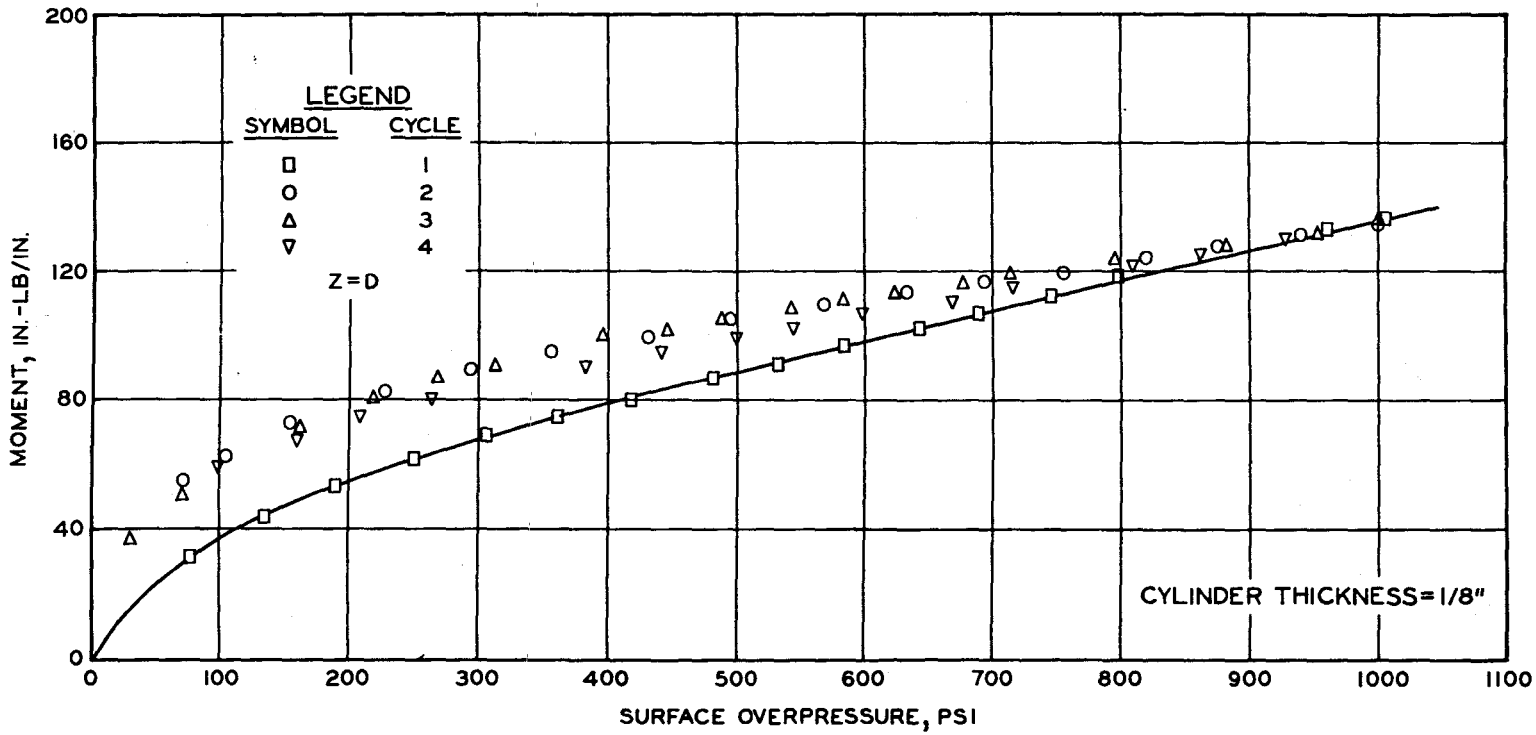

Figure 4.9 Cyclic loading effects on cylinder moment response.

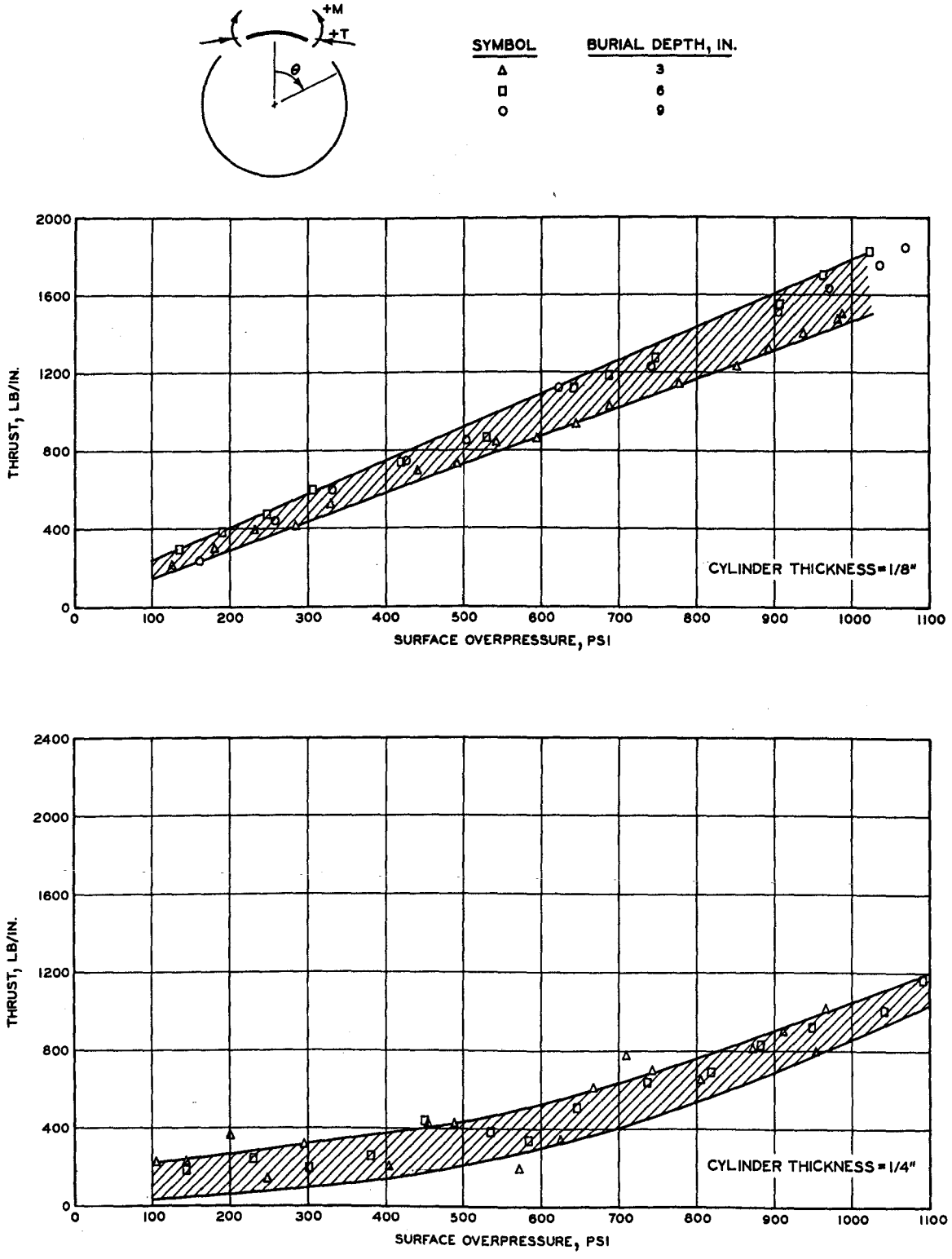

Figure 4.10 Thrust versus surface overpressure at θ = 0 degrees for 1/8-, 1/4-, and 3/8-inch-thick cylinders (sheet 1 of 2).

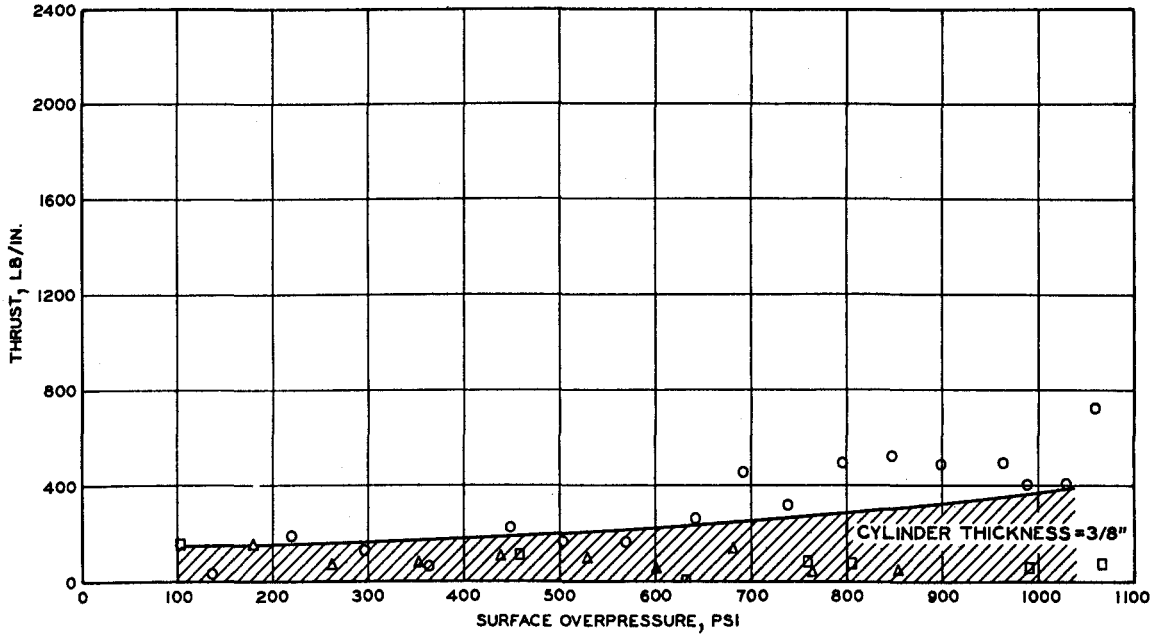

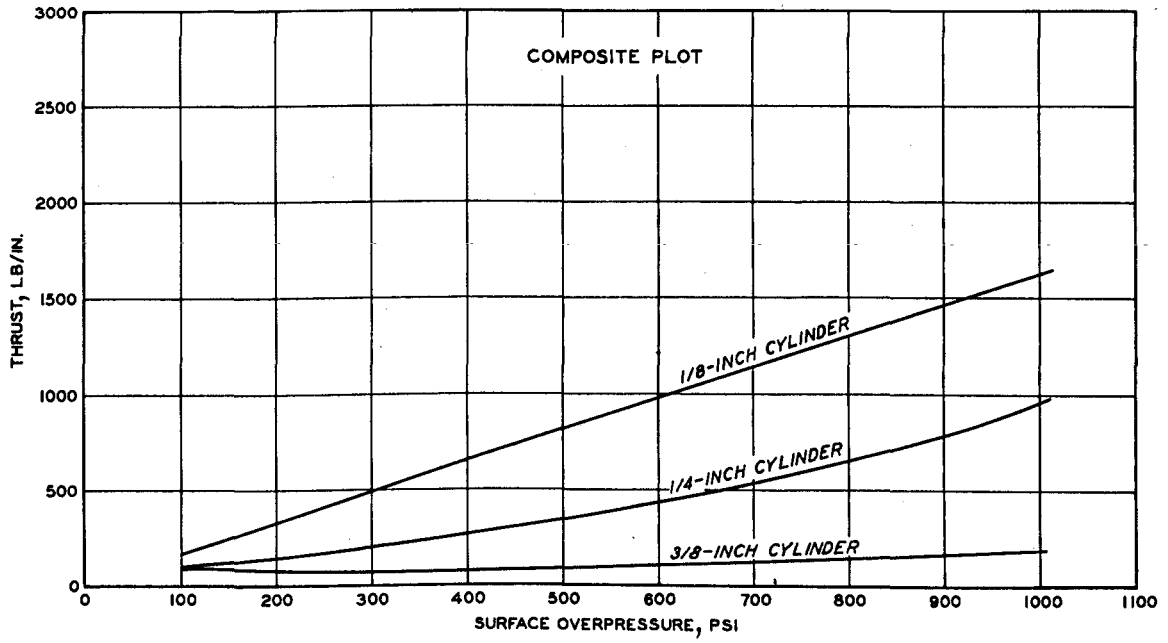

Figure 4.10 (sheet 2 of 2).

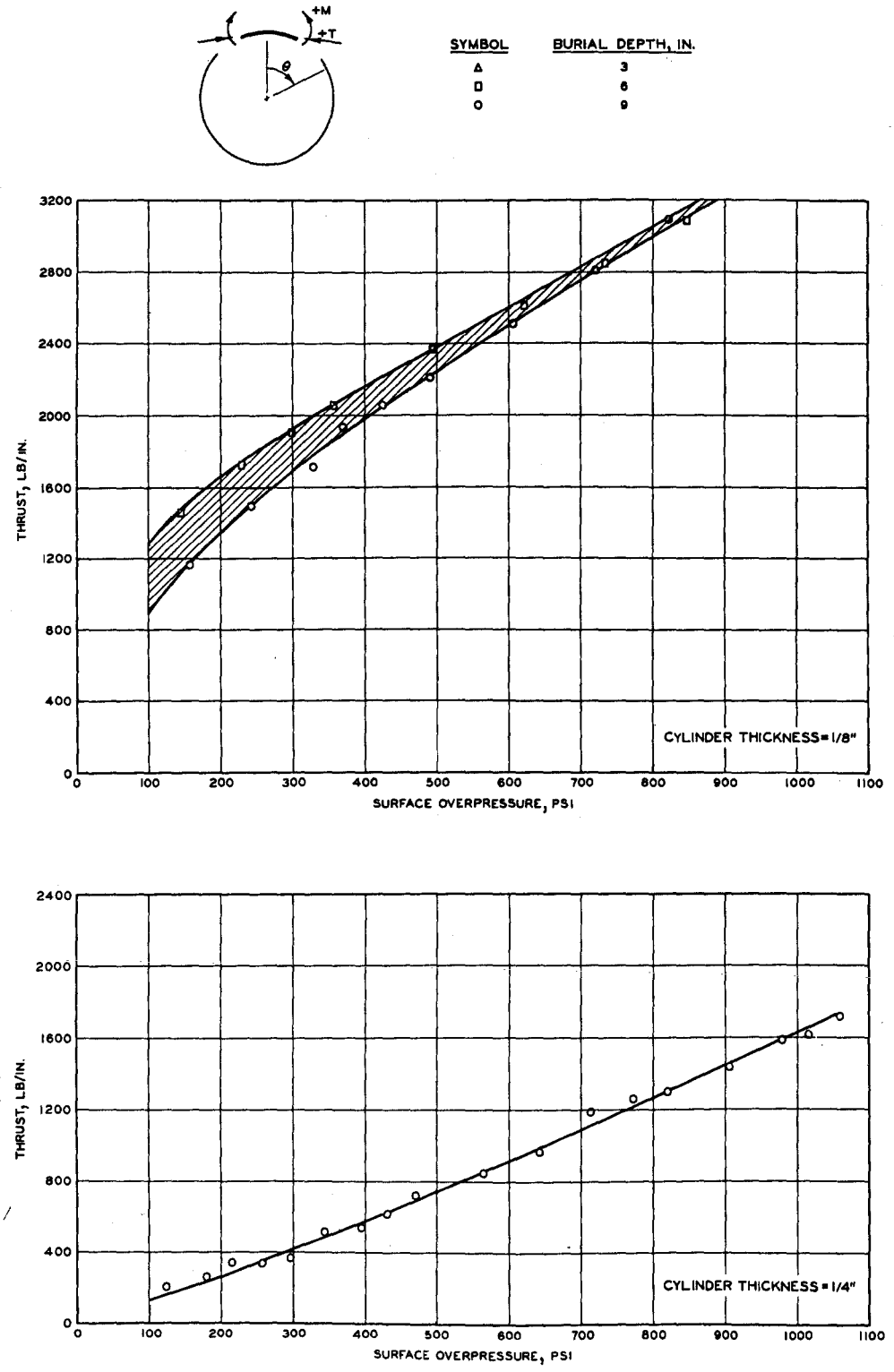

Figure 4.11 Thrust versus surface overpressure at θ = 30 degrees for 1/8-, 1/4-, and 3/8-inch-thick cylinders (sheet 1 of 2).

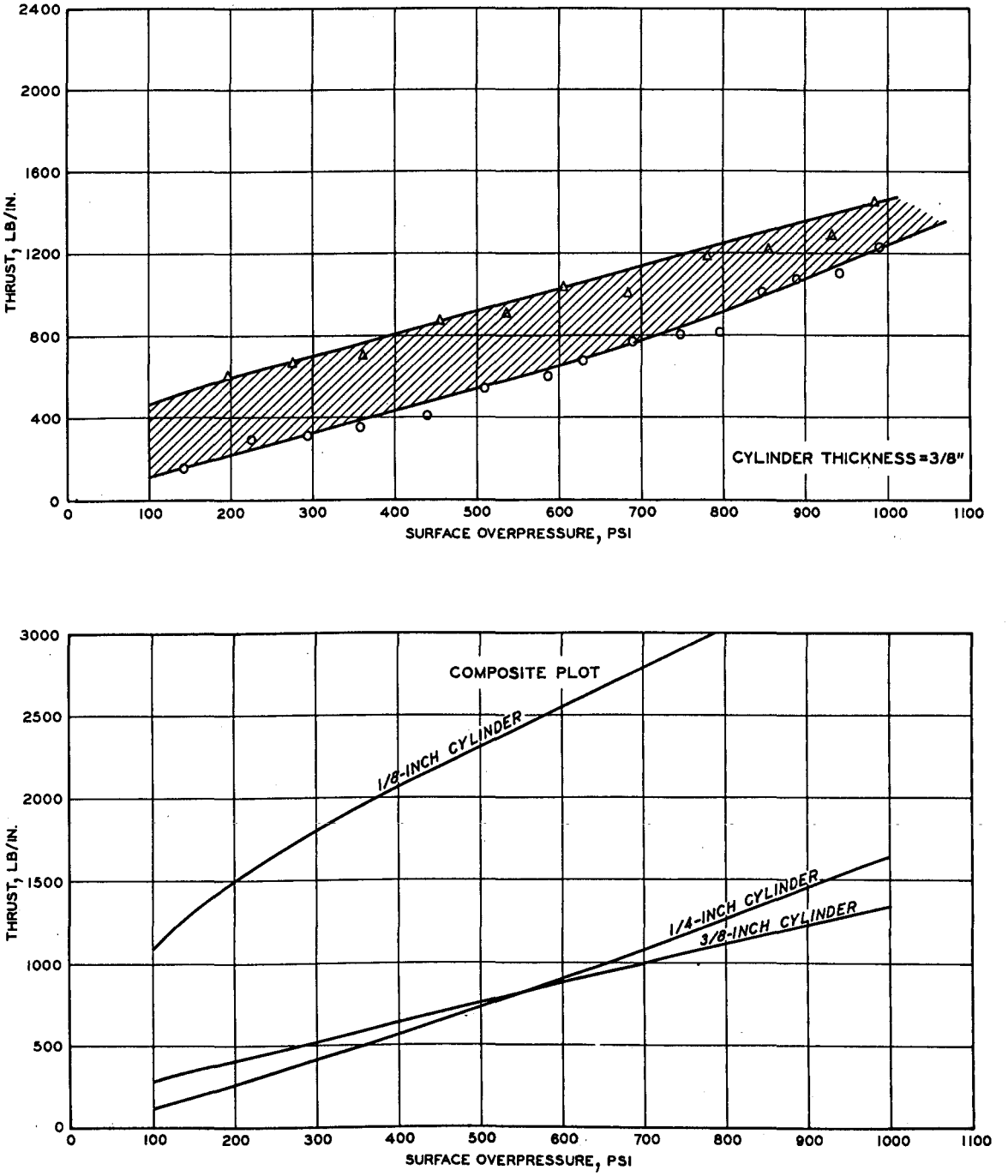

Figure 4.11 (sheet 2 of 2).

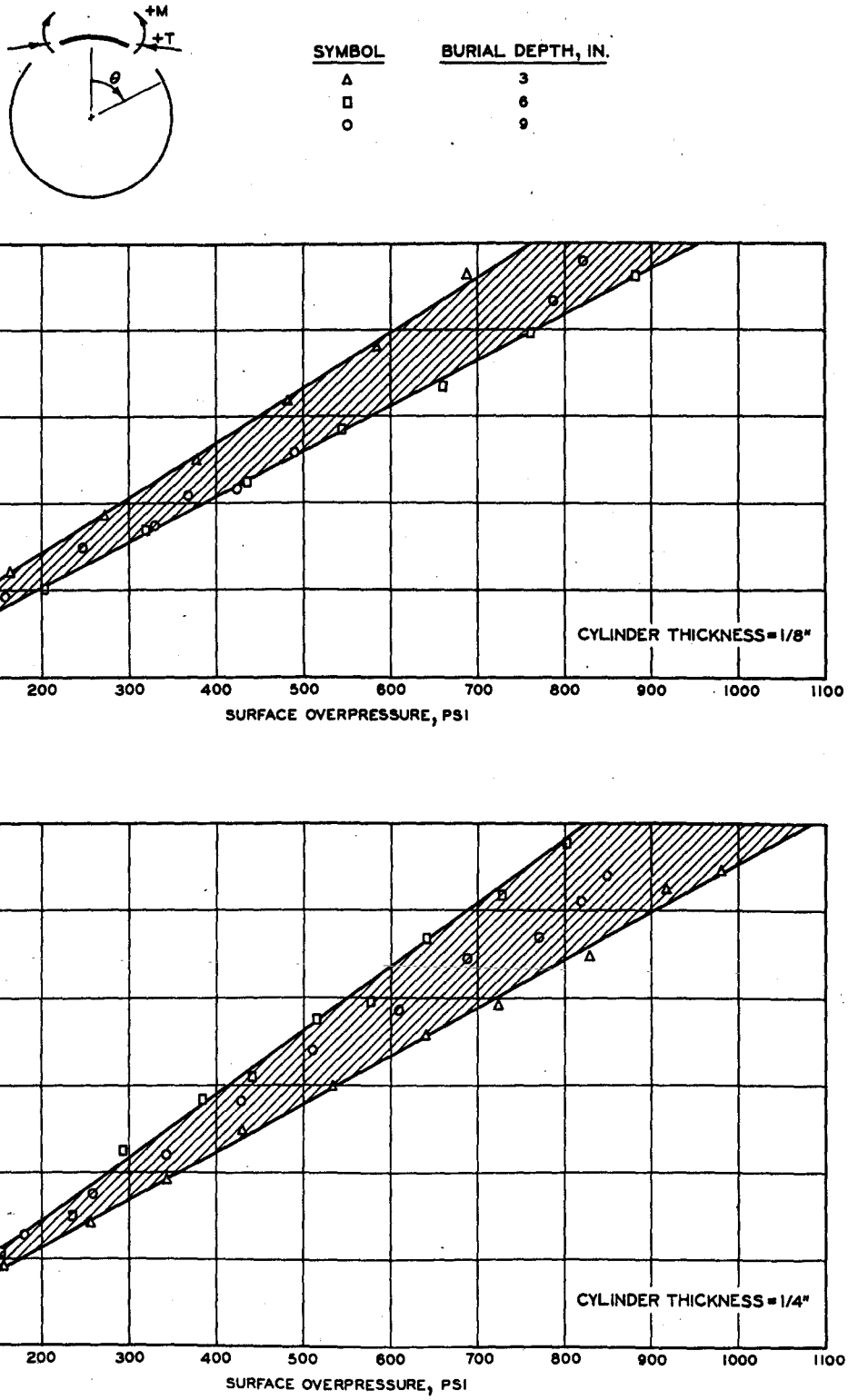

Figure 4.12 Thrust versus surface overpressure at θ = 60 degrees for 1/8-, 1/4-, and 3/8-inch-thick cylinders (sheet 1 of 2).

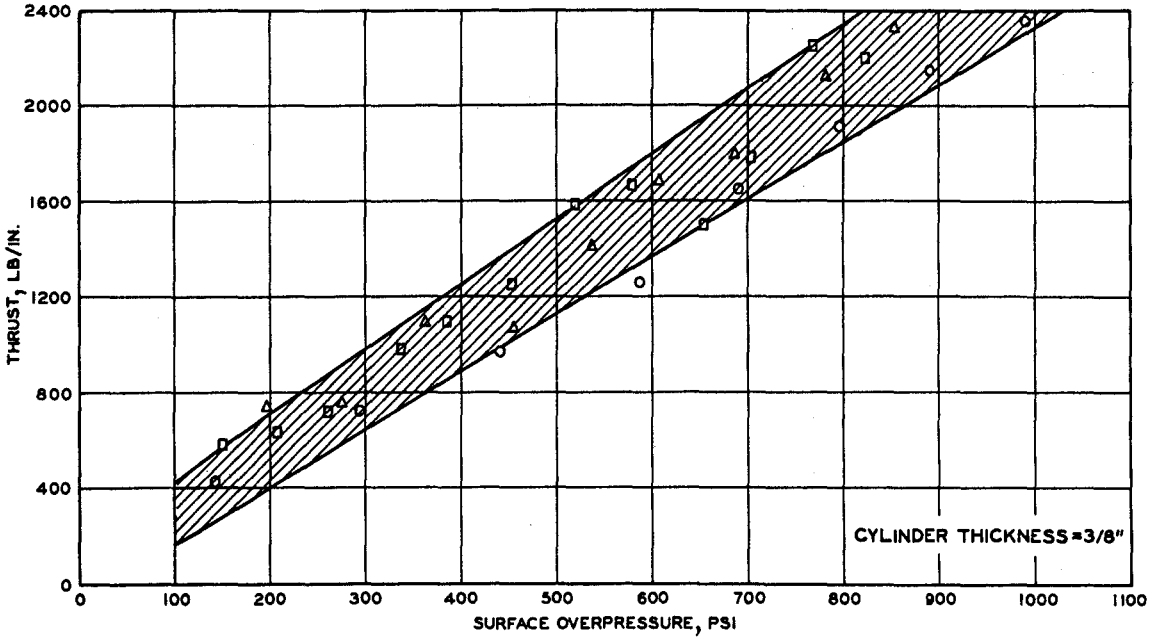

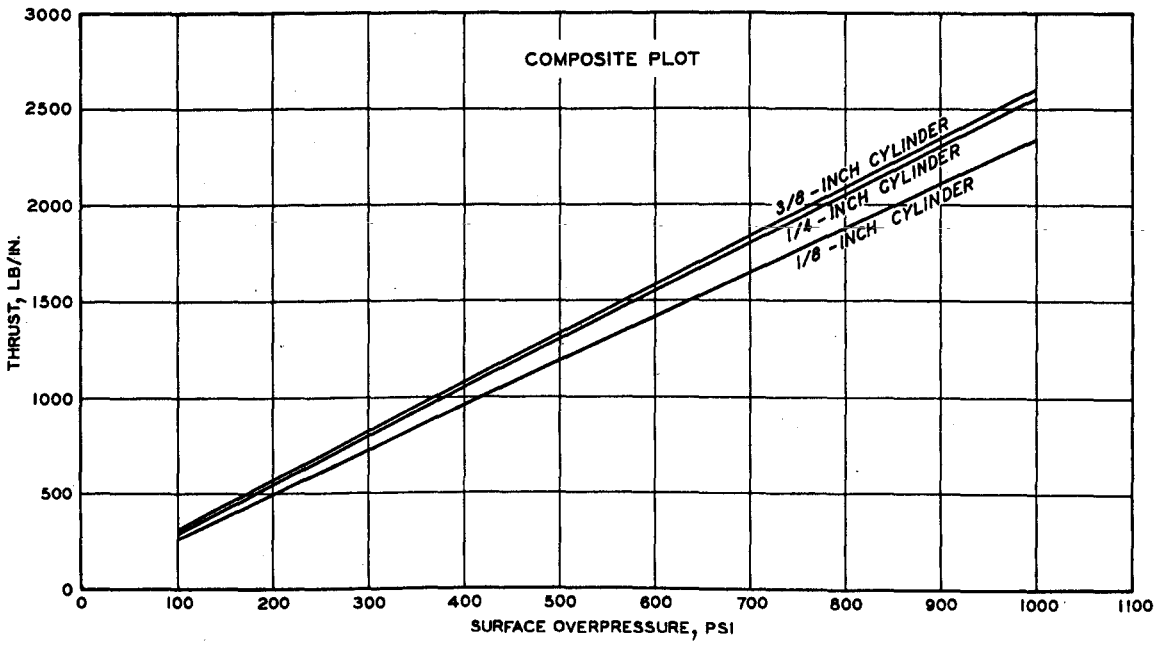

Figure 4.12 (sheet 2 of 2).

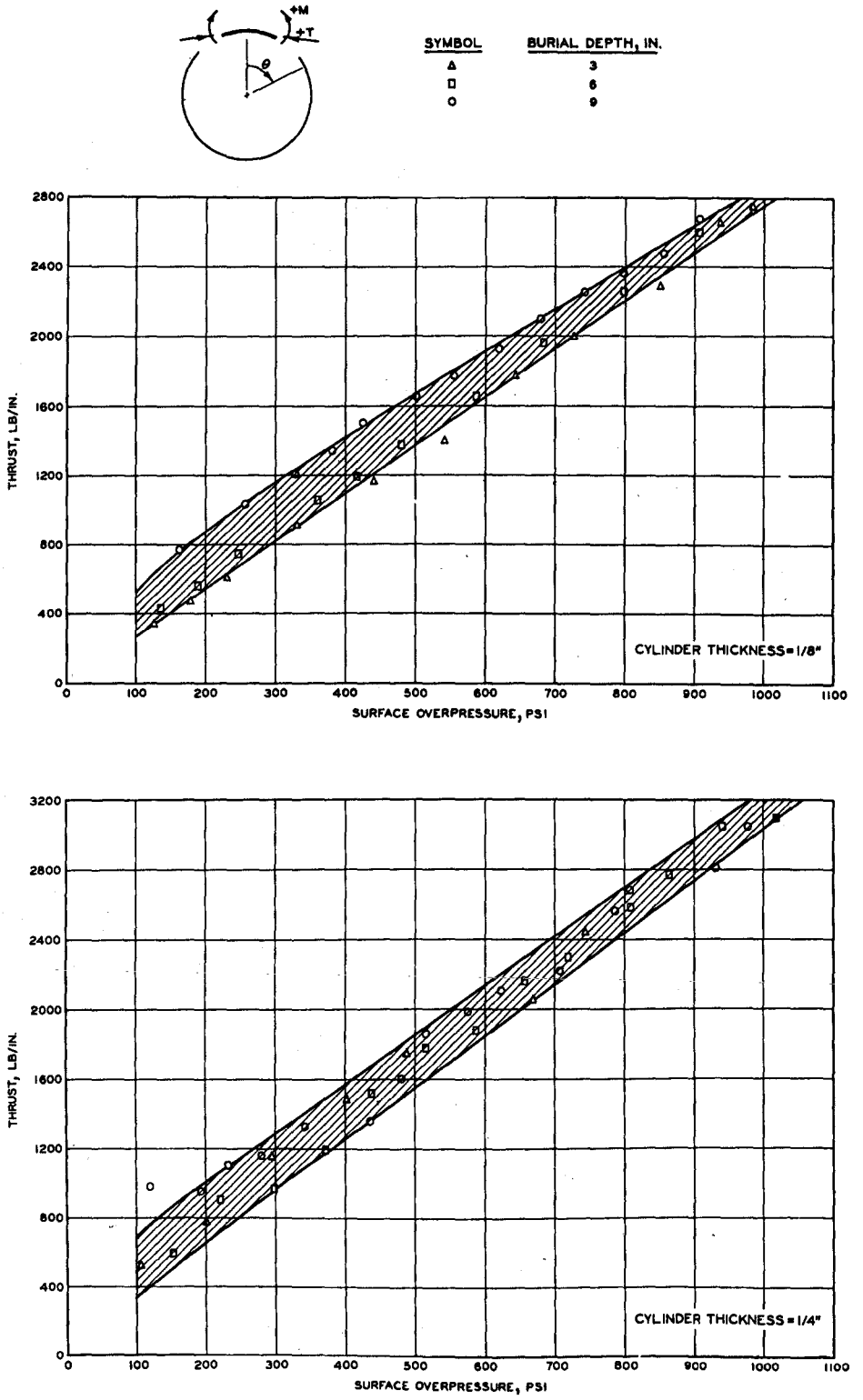

Figure 4.13 Thrust versus surface overpressure at θ = 90 degrees for 1/8-, 1/4-, and 3/8-inch-thick cylinders (sheet 1 of 2).

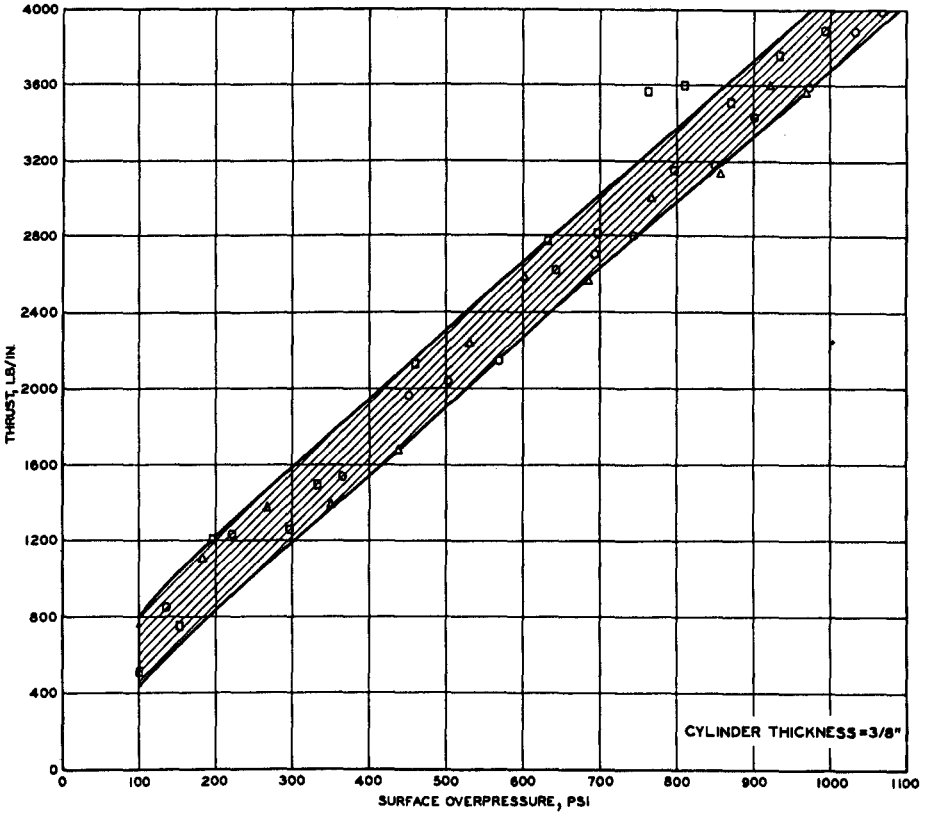

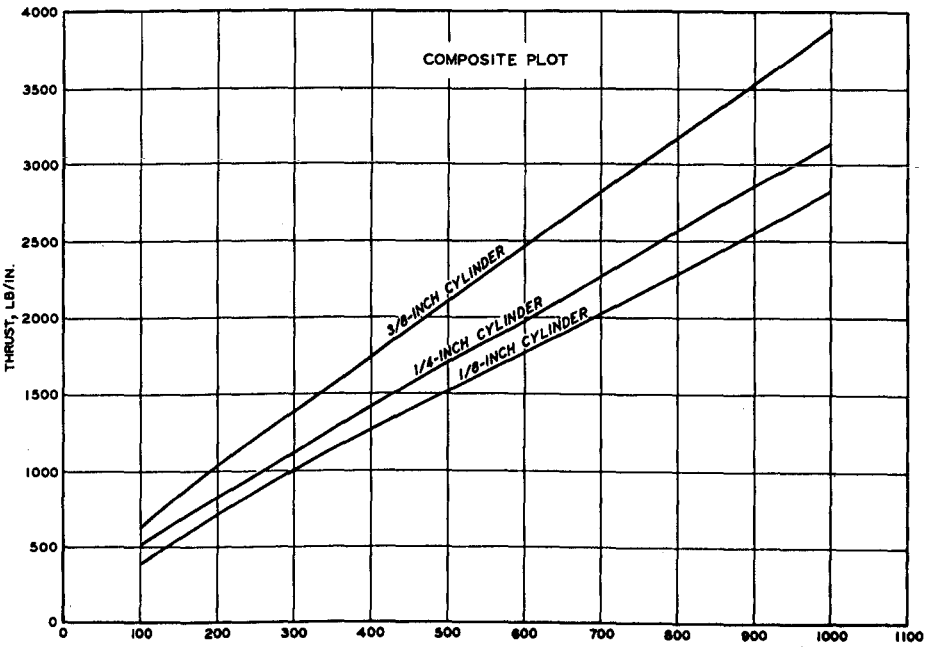

Figure 4.13 (sheet 2 of 2).

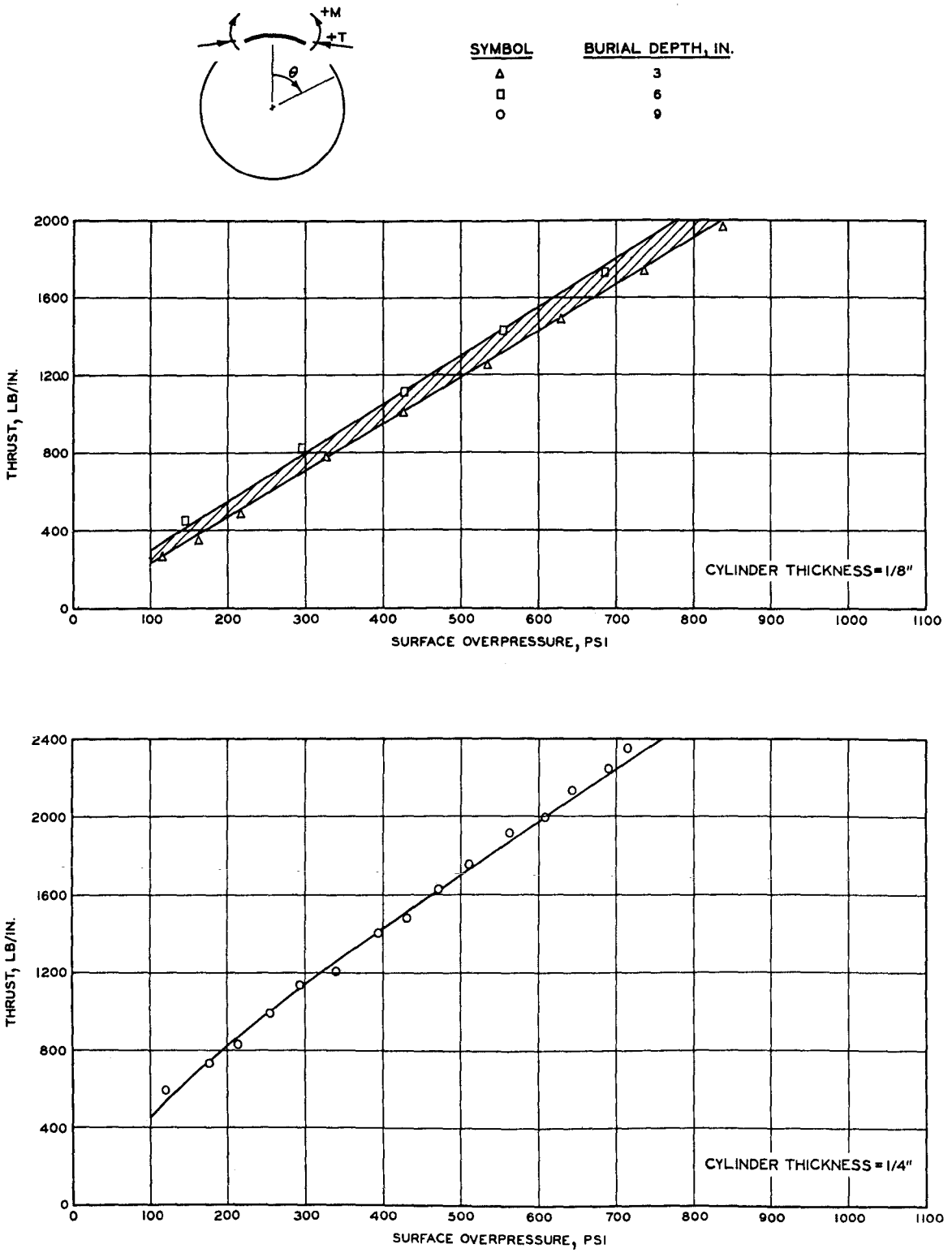

Figure 4.14 Thrust versus surface overpressure at θ = 120 degrees for 1/8-, 1/4-, and 3/8-inch-thick cylinders (sheet 1 of 2).

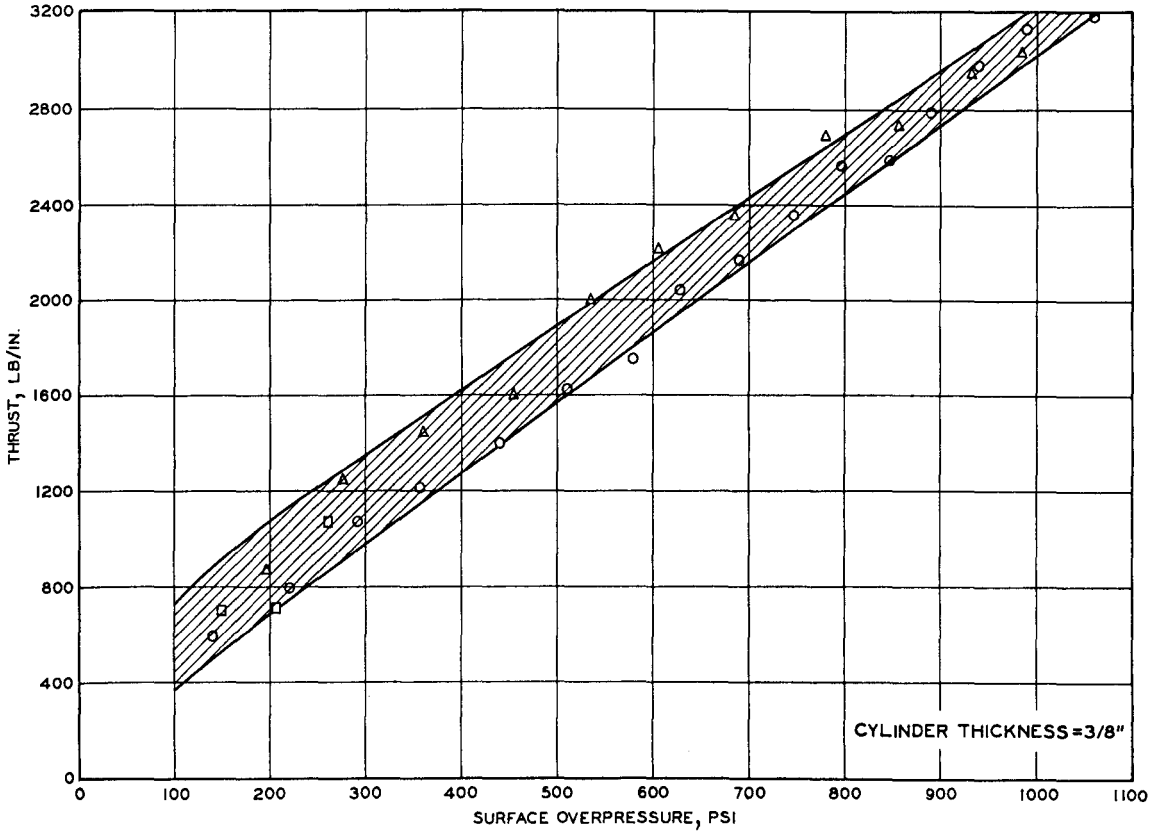

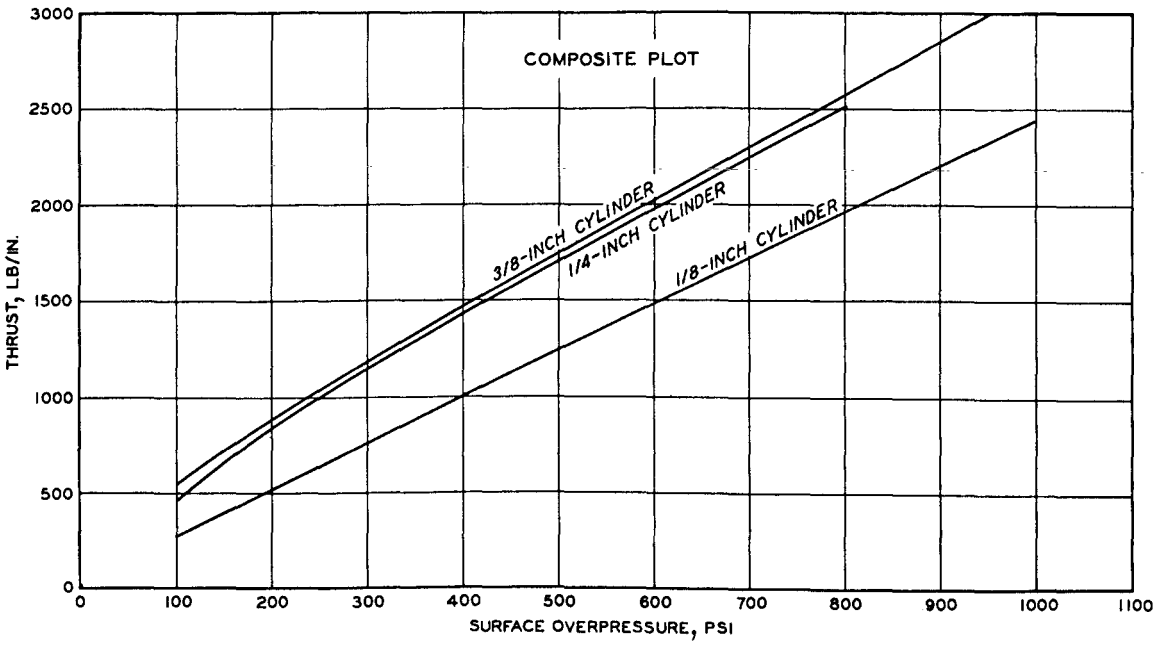

Figure 4.14 (sheet 2 of 2).

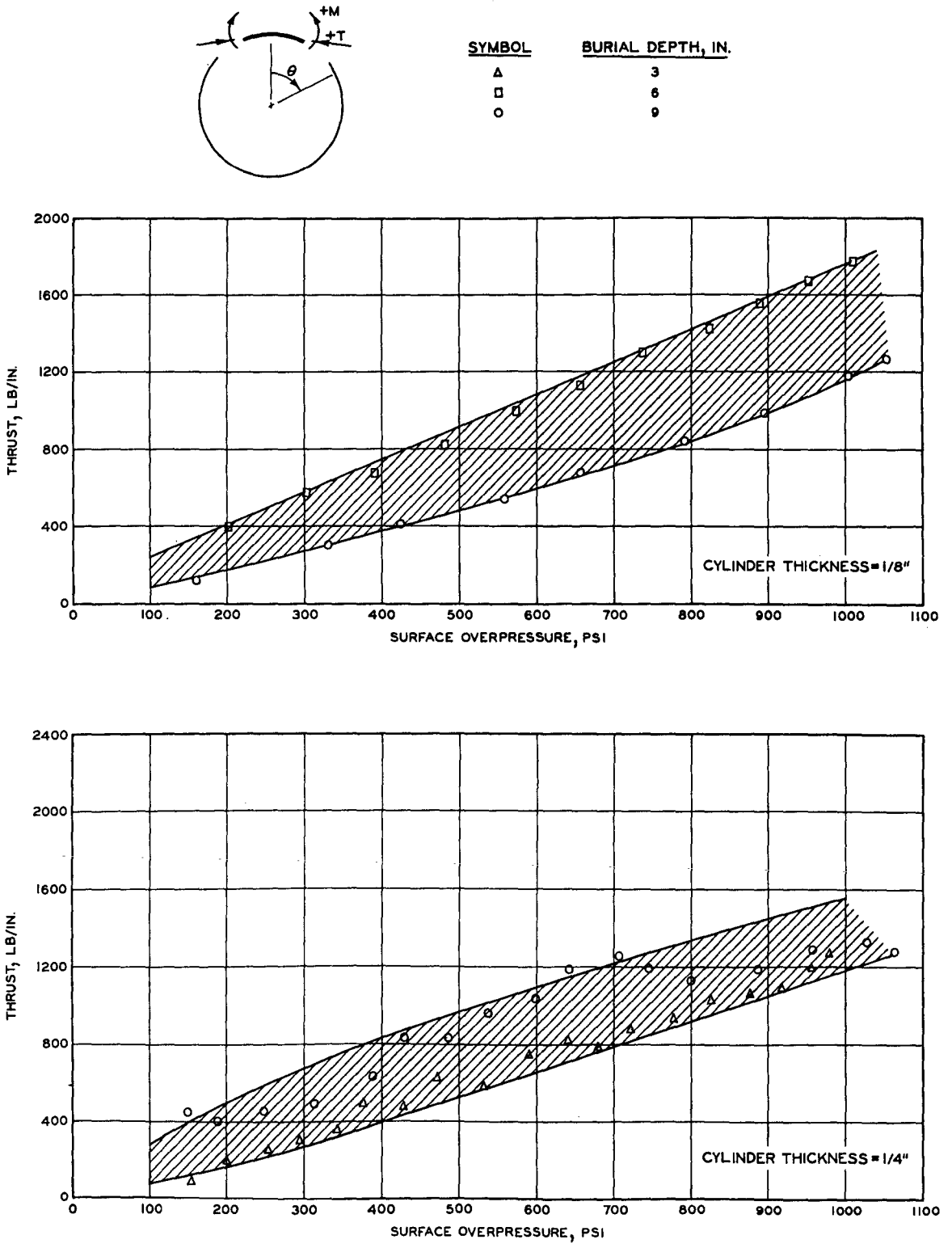

Figure 4.15 Thrust versus surface overpressure at θ = 150 degrees for 1/8-, 1/4-, and 3/8-inch-thick cylinders (sheet 1 of 2).

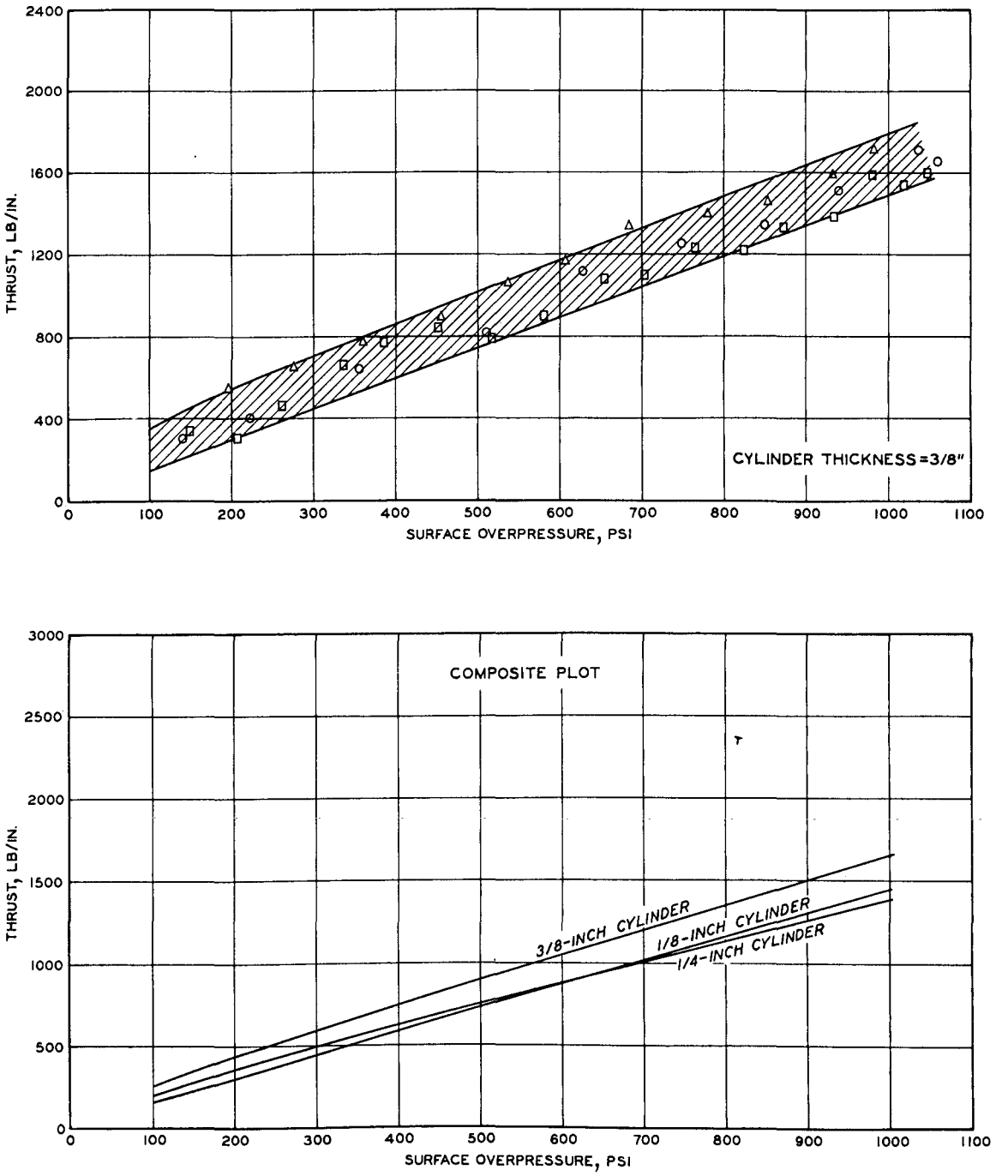

Figure 4.15 (sheet 2 of 2).

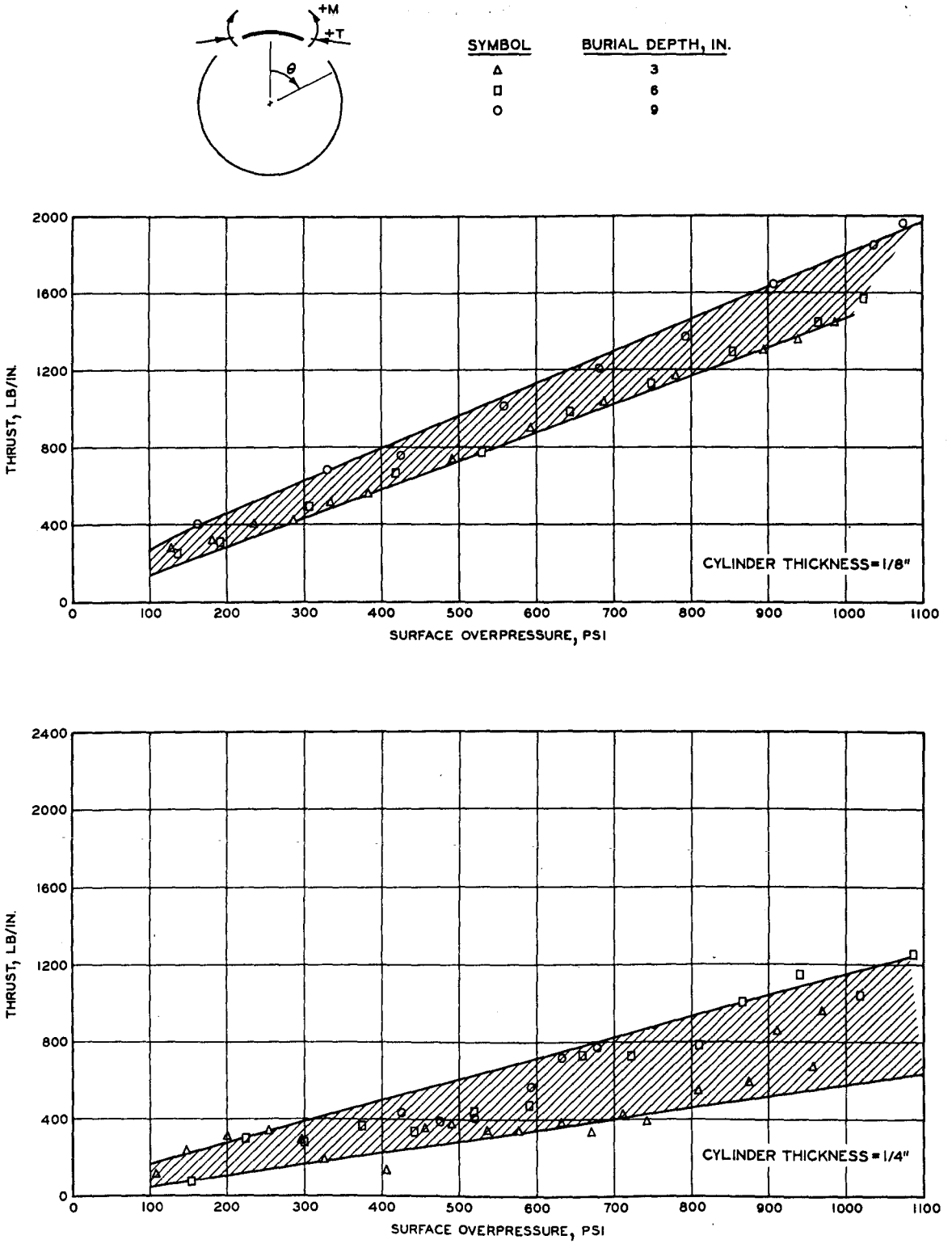

Figure 4.16 Thrust versus surface overpressure at θ = 180 degrees for 1/8-, 1/4-, and 3/8-inch-thick cylinders (sheet 1 of 2).

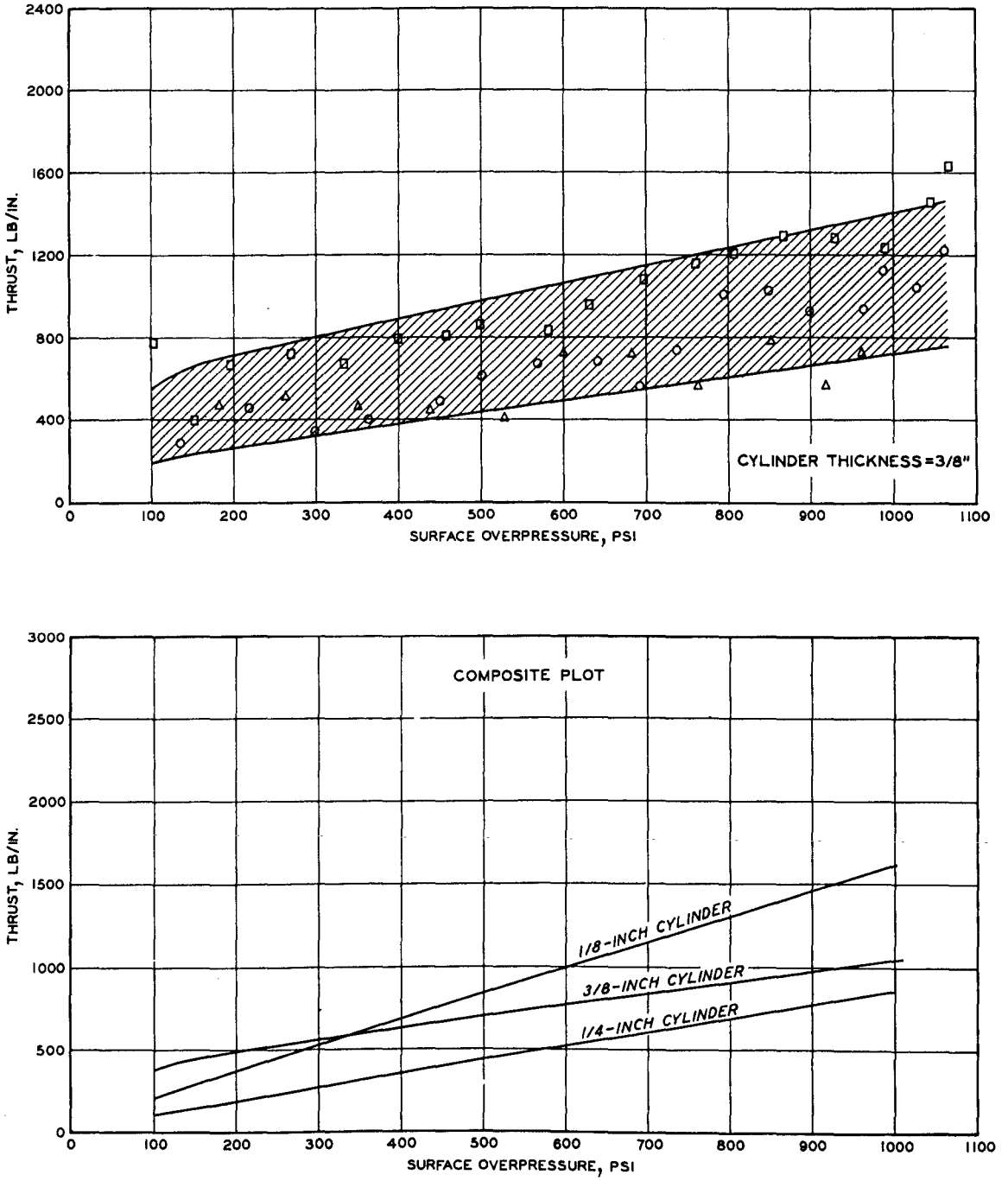

Figure 4.16 (sheet 2 of 2).

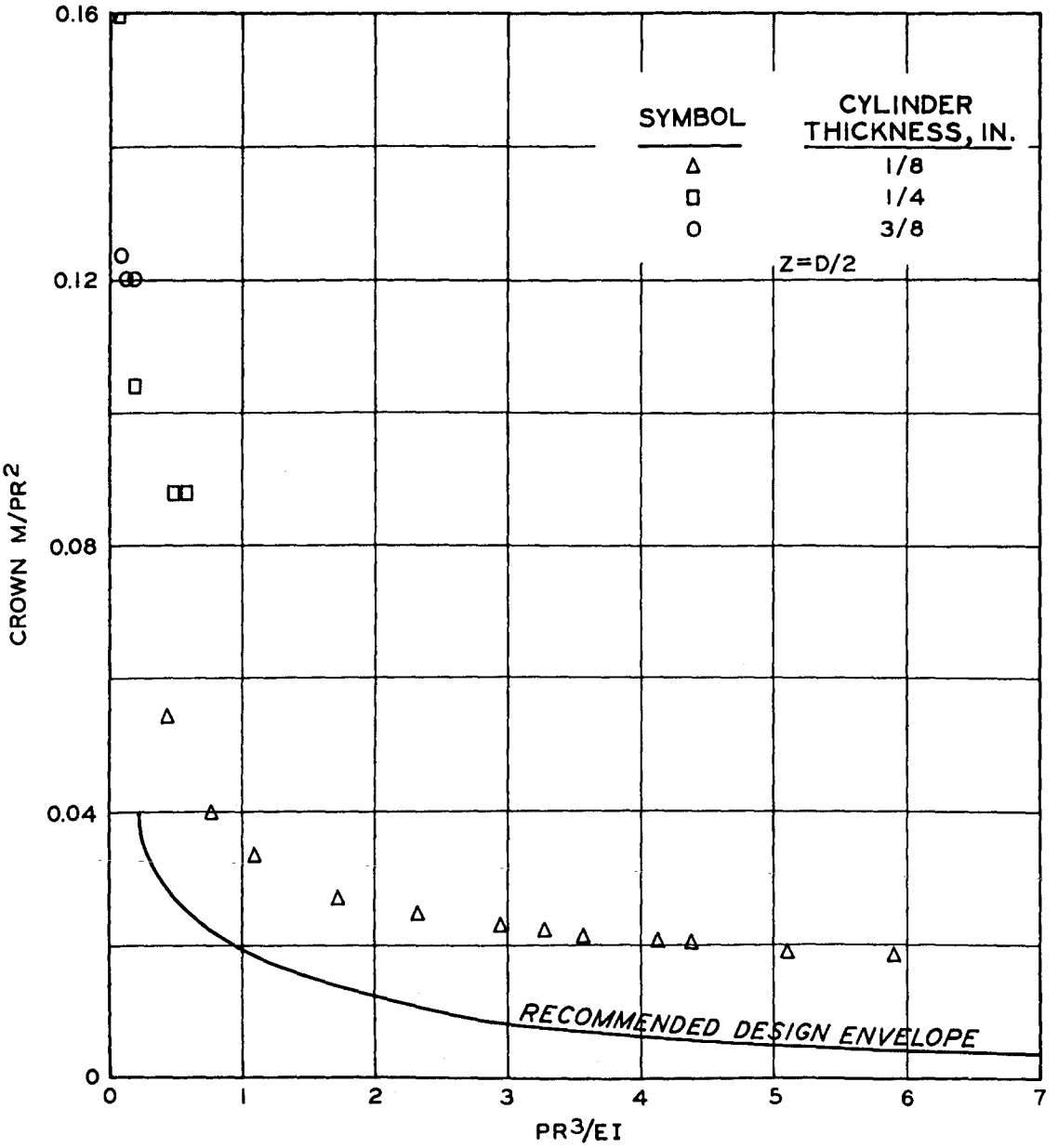

Figure 4.17 Crown normalized moment versus normalized overpressure at Z = D/2, Z = D, and Z = 3D/2 for 1/8-, 1/4-, and 3/8-inch-thick cylinders (sheet 1 of 3).

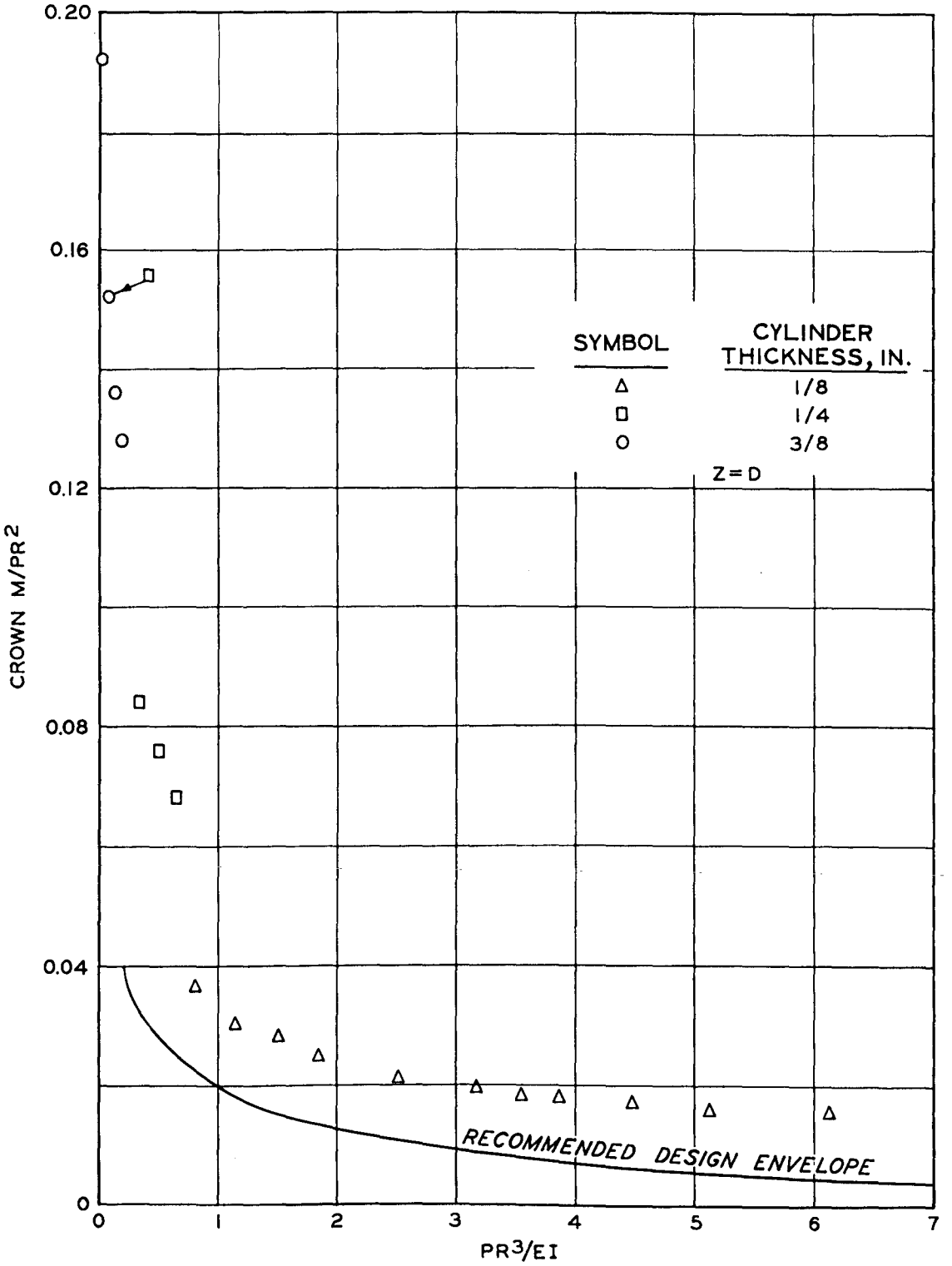

Figure 4.17 (sheet 2 of 3).

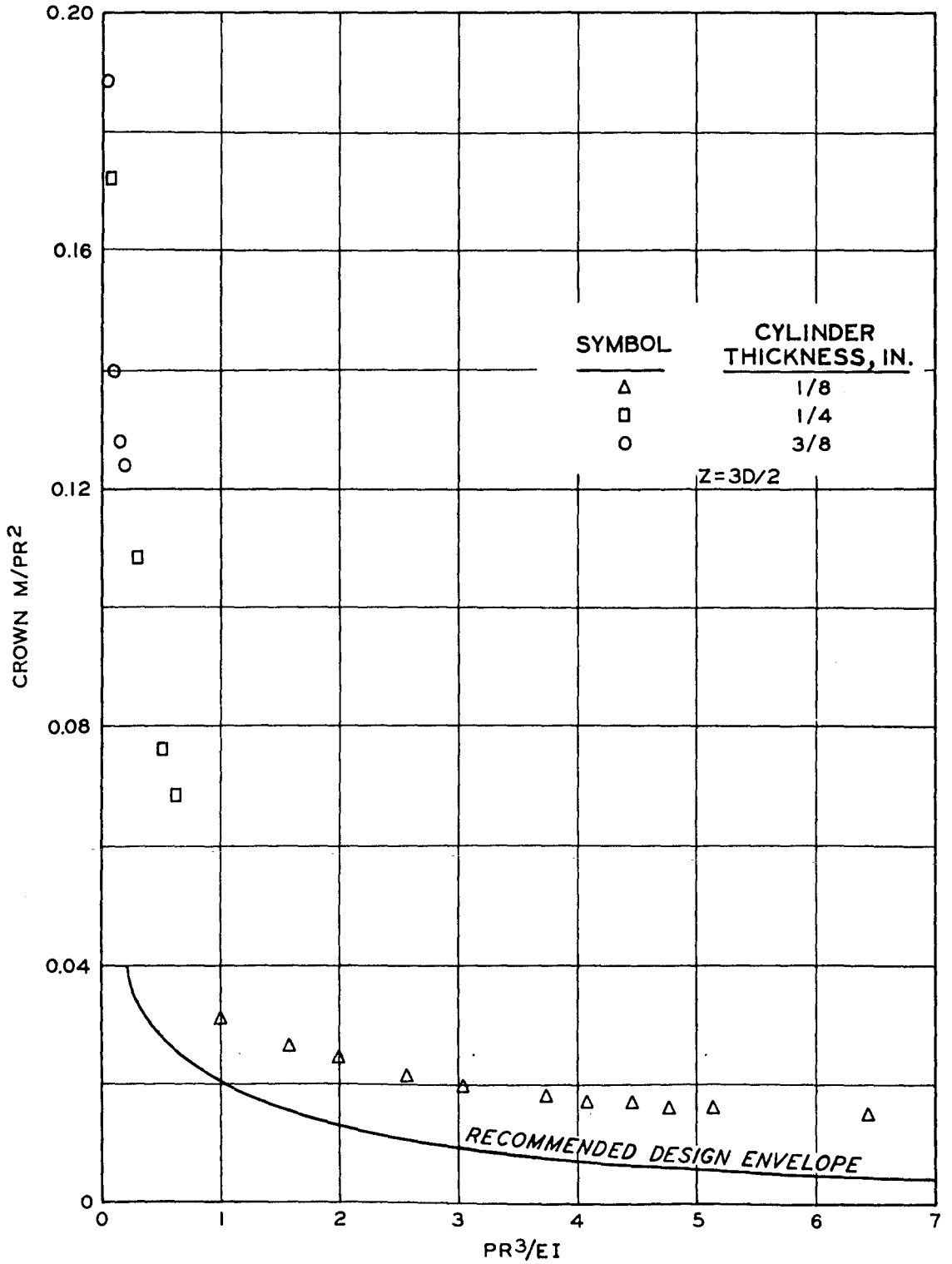

Figure 4.17 (sheet 3 of 3).

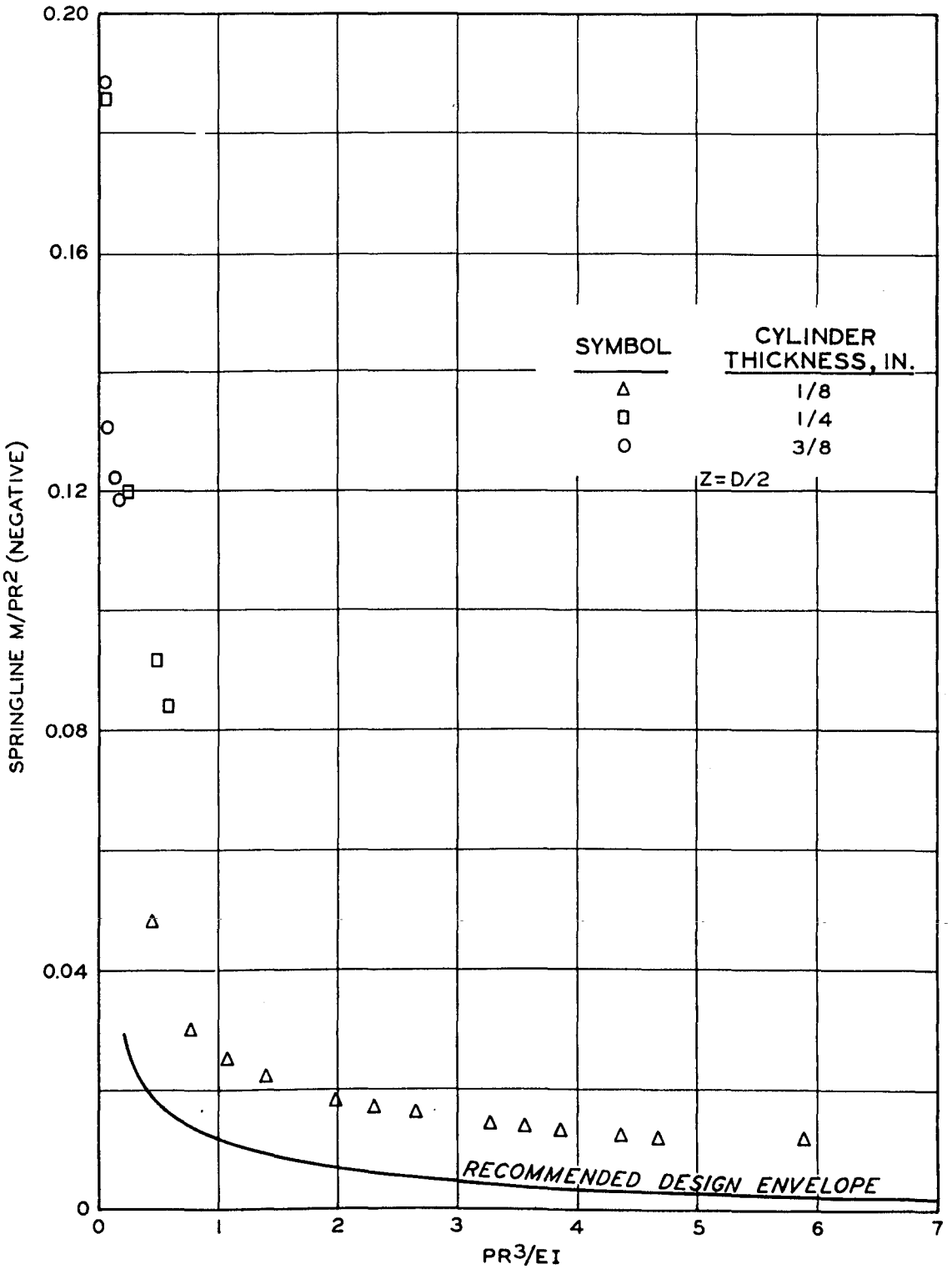

Figure 4.18 Springline normalized moment versus normalized overpressure at Z = D/2, Z = D, and Z = 3D/2 for 1/8-, 1/4-, and 3/8-inch-thick cylinders (sheet 1 of 3).

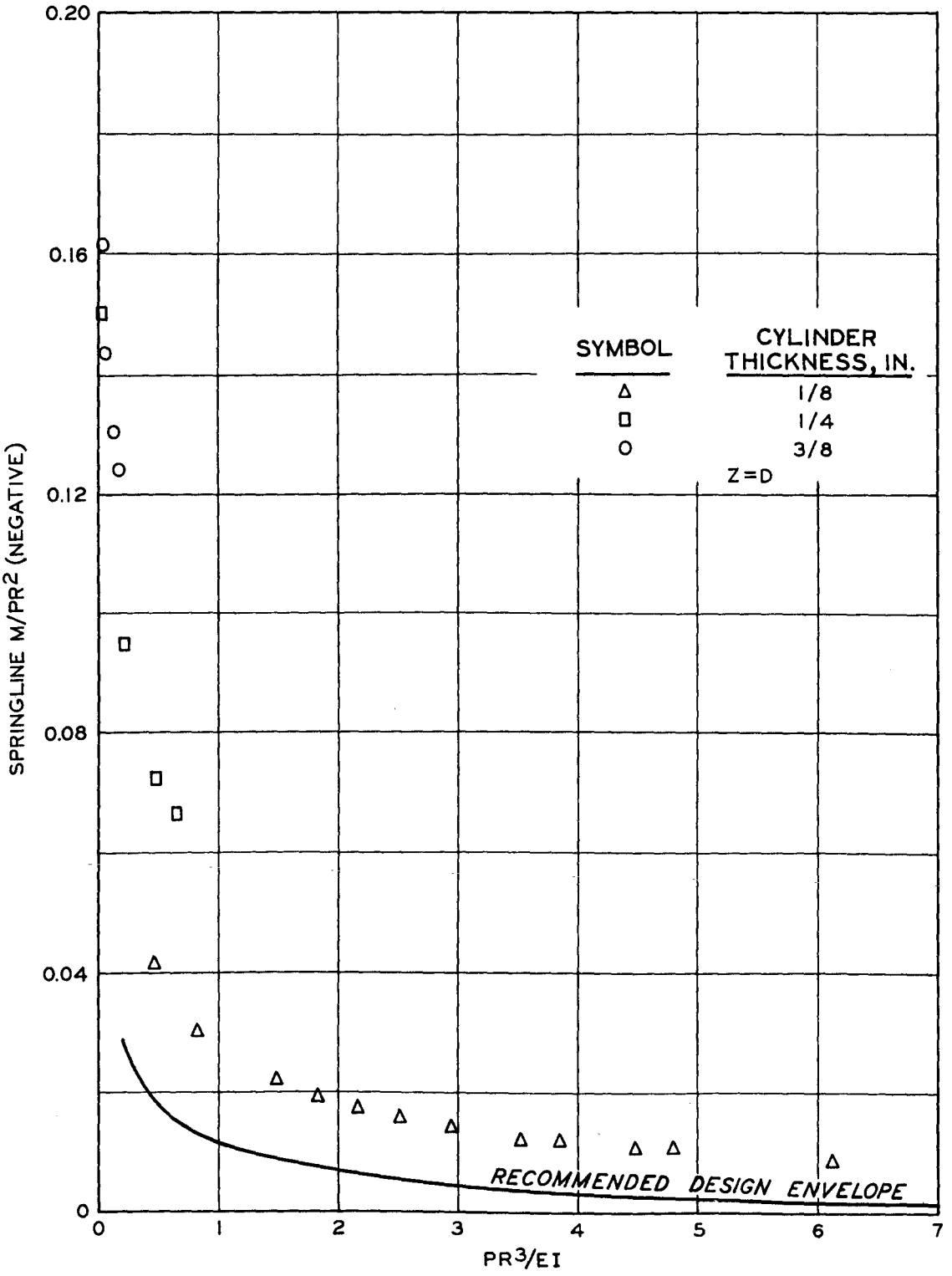

Figure 4.18 (sheet 2 of 3).

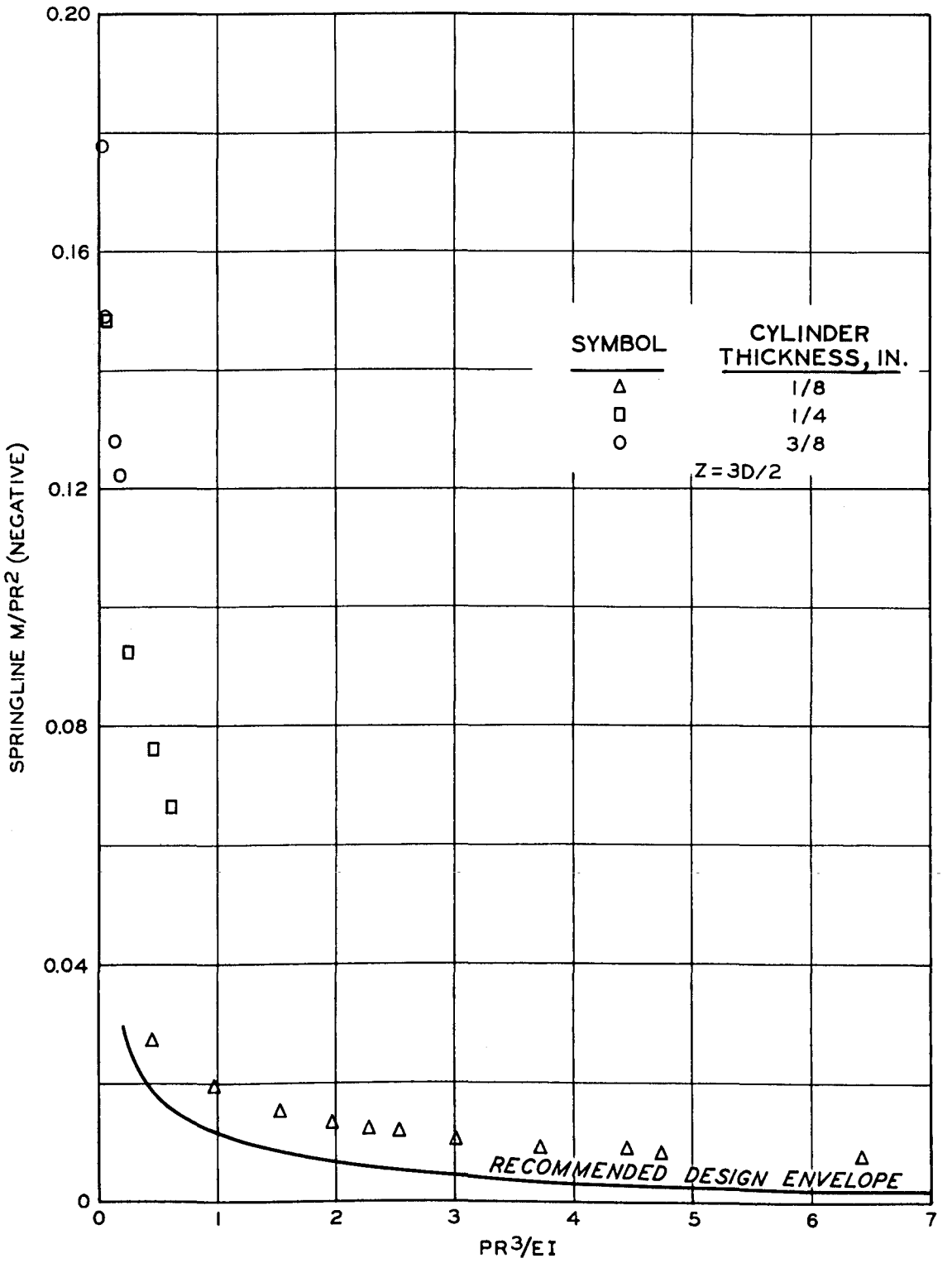

Figure 4.18 (sheet 3 of 3).

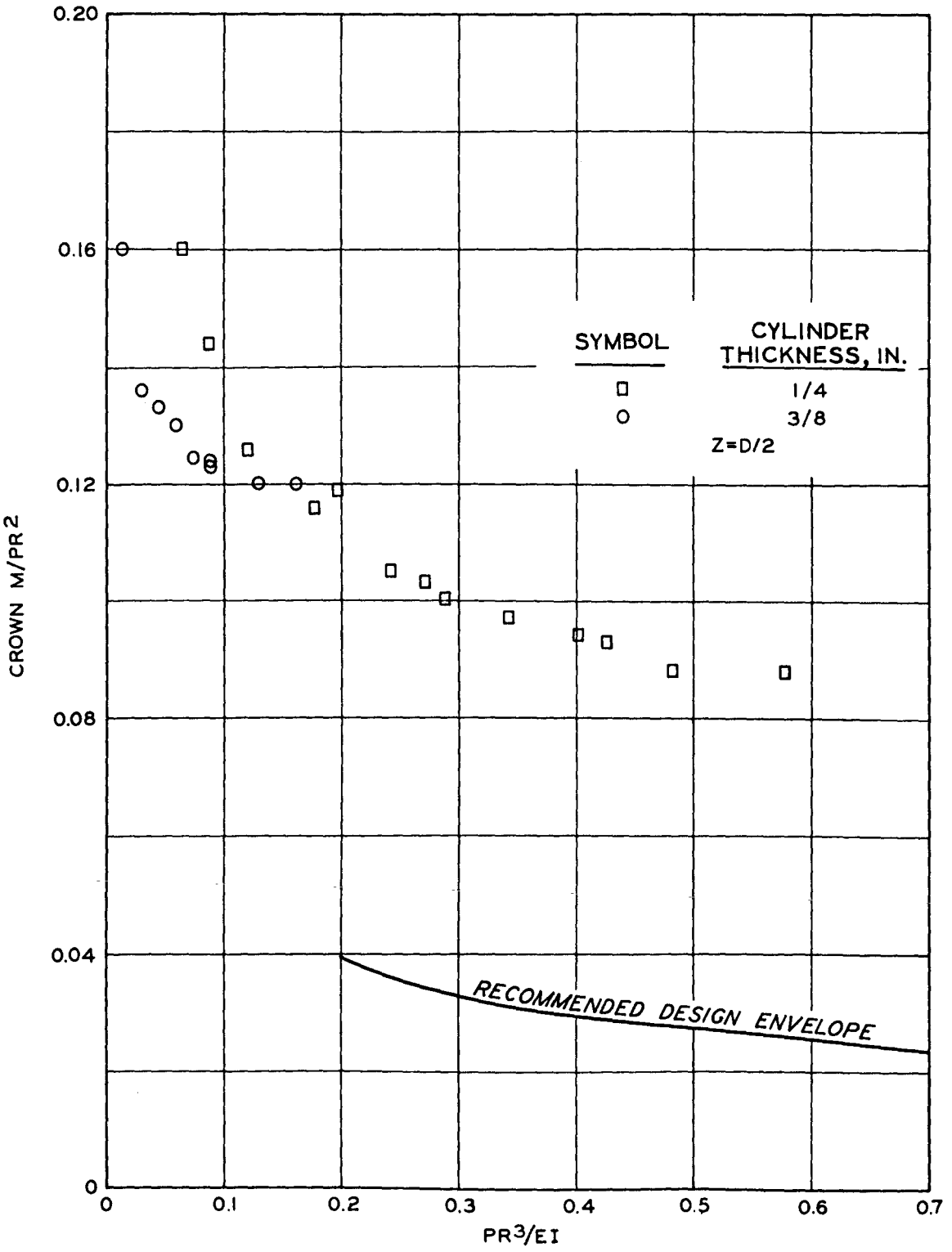

Figure 4.19 Crown normalized moment versus expanded normalized overpressure at Z = D/2, Z = D, and Z = 3D/2 for 1/4- and 3/8-inch-thick cylinders (sheet 1 of 3).

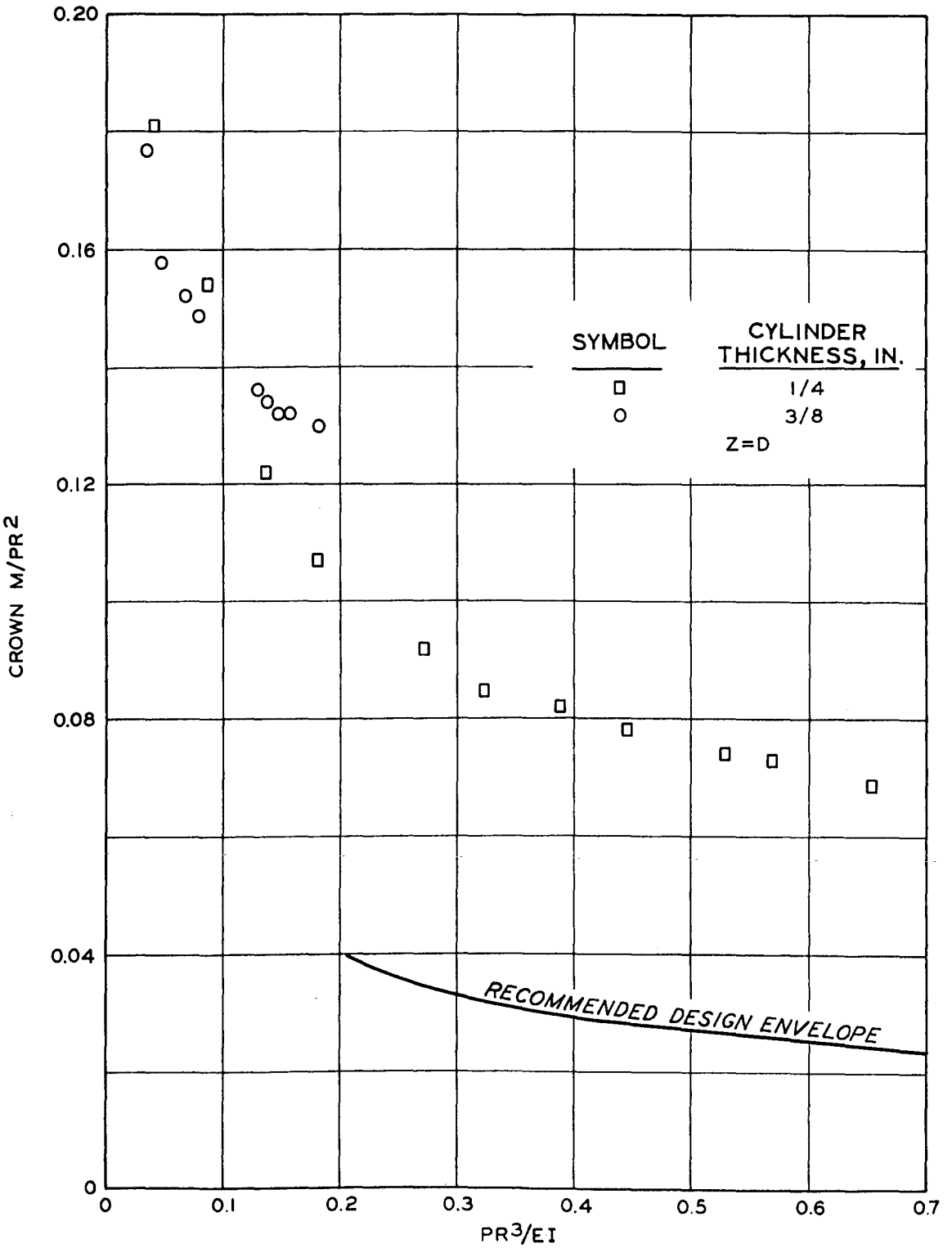

Figure 4.19 (sheet 2 of 3).

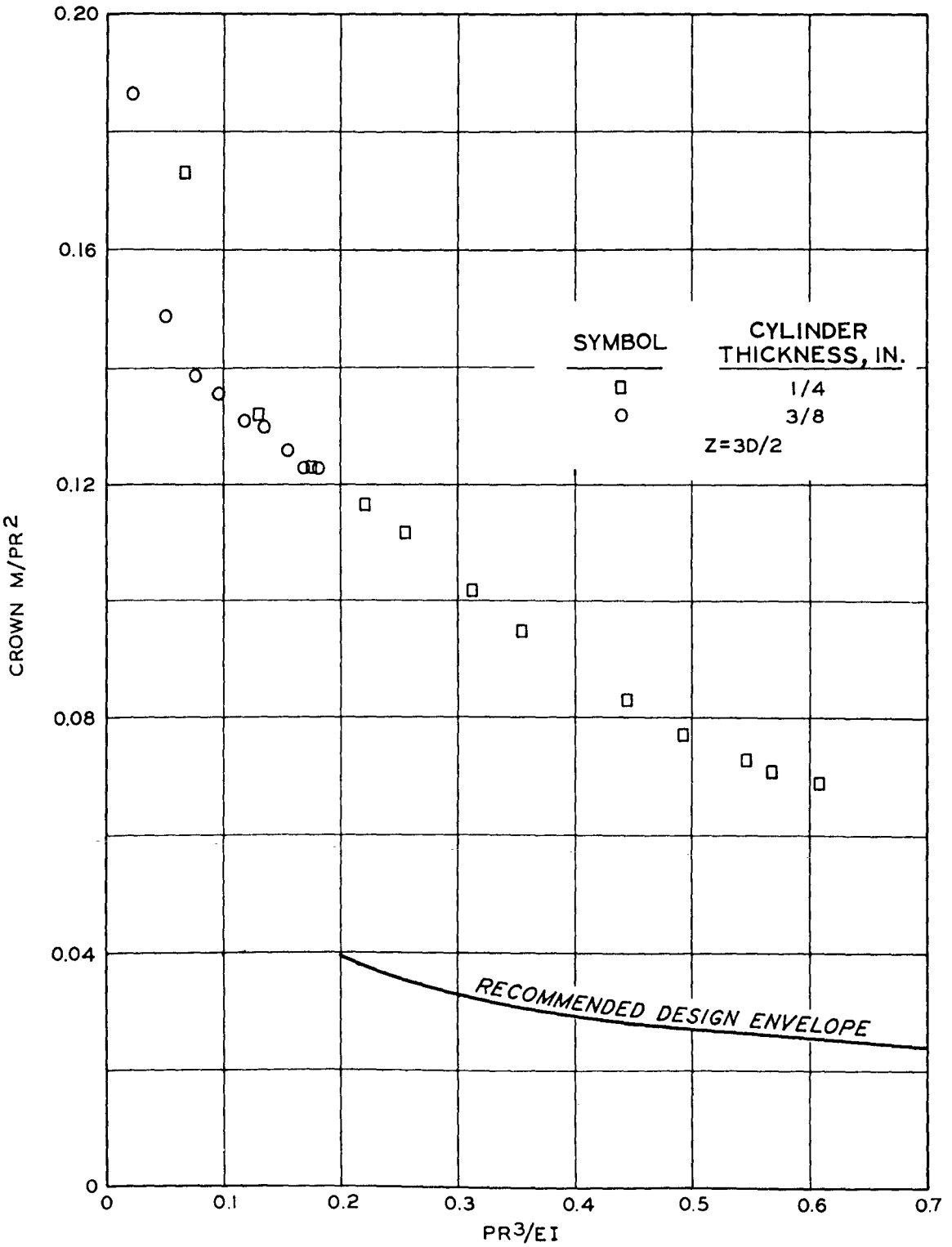

Figure 4.19 (sheet 3 of 3).

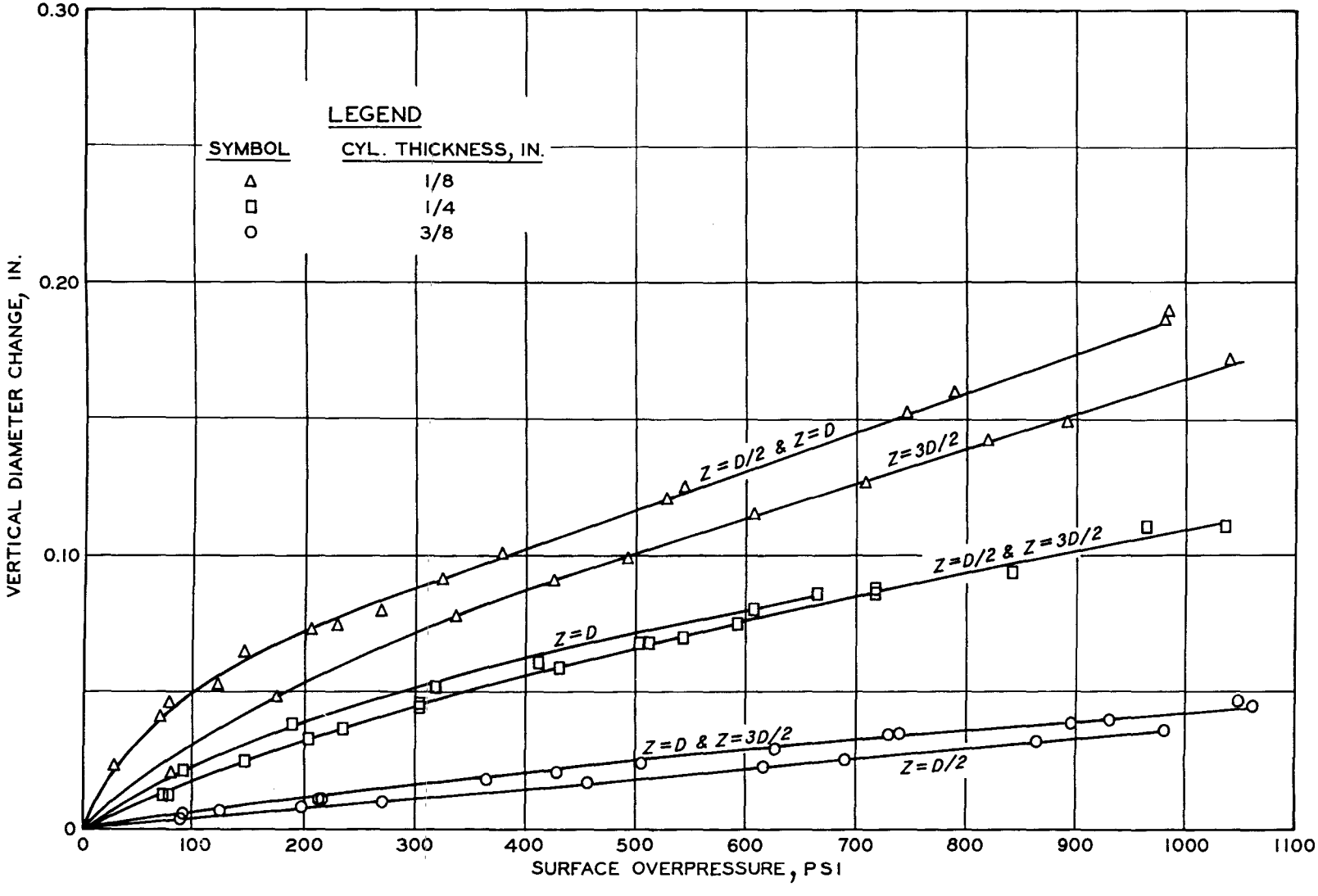

Figure 4.20 Vertical diameter change versus surface overpressure at Z = D/2, Z = D, and Z = 3D/2 for 1/8-, 1/4-, and 3/8-inch-thick cylinders.

CHAPTER 5

CONCLUSIONS AND RECOMMENDATIONS

5.1 CONCLUSIONS

5.1.1 Thrusts. The thrusts developed in the cylinders were generally a linear function of the applied surface overpressure. The maximum and, in general, the minimum thrusts were recorded at the springline and crown, respectively; however, an increase in cylinder stiffness resulted in an increase in the springline thrusts and a decrease in the crown and invert thrusts.

5.1.2 Bending Moments. The absolute values of the normalized crown, springline, and invert bending moments M/PR^2 for the 3/8-inch-thick cylinder were in good agreement with the theoretical reasonable upper-bound values obtained from the analysis of a cylinder subjected to a uniform vertical pressure of magnitude P and a uniformly distributed horizontal pressure of magnitude KP. The bending moments developed in the cylinders were, in general, nonlinear and tended to increase at a decreasing rate with an increase in the applied surface overpressure. For the 1/8-inch-thick cylinder, the crown and invert bending moments were greater than the springline bending moments; however, for the 3/8-inch-thick cylinder, the crown, springline, and invert bending moments were of approximately equal magnitude at the peak surface overpressure of approximately 1,000 psi.

5.1.3 Diameter Change. There was no definite trend observed in the test data to indicate any positive relationship regarding the effect of burial depth and overpressure on vertical diameter change.

5.1.4 Arching Action. Values of the normalized springline thrust T/PR revealed that active soil arching was present during the loading of the 1/8-inch-thick cylinder, whereas passive arching occurred for the 1/4- and 3/8-inch-thick cylinders. The values of the normalized springline thrusts for the 3/8-inch-thick cylinder were in good agreement with the theoretical reasonable upper-bound value for the normalized springline thrust in a virtually rigid cylinder, i.e. 1.4. The

average of the normalized crown and invert thrusts also displayed evidence of the active and passive soil arching and the influence of cylinder stiffness.

5.1.5 Structural Stiffness. Based on the results of this experimental program, it is concluded that cylinder stiffness EI/R^3 is the single most important parameter affecting the response of horizontally oriented, stiff cylindrical structures buried in a dense sand and subjected to static surface overpressures. Thus, in formulating and evaluating design criteria and procedures for structures of the previously described type, proper cognizance should be rendered cylinder stiffness in order to produce safe, serviceable, and economical structures.

5.1.6 Depth of Burial. Test results indicated that, for the cylinder stiffnesses tested, the influence of burial depth was almost insignificant.

5.1.7 Analytical Predictions. Based on the almost constant difference in crown and springline normalized moments throughout the entire range of PR^3/EI values, it is concluded that the general shape of the pressure distribution around the cylinders does not radically change with increasing surface overpressure. From this reasoning, it appears that the validity of analytically predicted cylinder response will greatly depend on the choice of the initial interface pressure distribution together with an appropriate earth pressure coefficient.

5.2 RECOMMENDATIONS

The initial experimental program to investigate the response of stiff steel cylinders buried in a dense dry sand should be continued, and tests should be conducted to determine the dynamic response of these cylinders. In addition, the ultimate strength and mode of failure for these cylinders should be investigated in the WES 6,000-psi-capacity test chamber. This would provide normalized moment data in the region $PR^3/EI > 1$ for the 1/4- and 3/8-inch-thick cylinders. These tests, coordinated with analytical finite element studies currently in

progress at WES, could provide valuable insight into the behavior of stiff steel cylindrical structures.

In order to fully understand the static and dynamic behavior of shallow buried, horizontally oriented, reinforced concrete cylindrical structures in a soil medium, large-diameter reinforced concrete cylinders with stiffnesses similar to those utilized in this test program should be tested. Tests such as this would indicate whether a change in the cylinder material would influence the results. The stiffness of a reinforced concrete cylinder changes as the loading increases because the reinforced concrete is subjected to tensile stress cracks, thus allowing the reinforcement to assume the load. This reduction in the initial stiffness of the reinforced concrete cylinder consequently reduces the thrusts and bending moments developed in the cylinder. In addition, it would be desirable to test some reinforced concrete cylinders to failure to determine the ultimate strength of the cylinders and the mode of failure.

Analytical investigations using finite element methods should be continued in order to develop the capability of predicting the response of reinforced concrete cylinders for those cases for which experimental data are not available. The analytical investigators should consider the nonlinear behavior of both the cylinder material and the soil medium and the static and dynamic loading environments.

APPENDIX A

PROPERTIES OF THE STEEL MECHANICAL TUBING

The cylindrical test specimens used in this study were fabricated from commercially available cold-drawn, low-carbon, seamless, steel mechanical tubing having a 6-inch outside diameter and wall thicknesses of 1/8, 1/4, and 3/8 inch.

To determine the stress-strain properties of the mechanical tubing, longitudinal tension test specimens were cut from a representative section of each of the different-sized tubings. All tension test specimens were proportioned in accordance with ASTM Designation: A 370-617, Supplement II. Each tension test specimen was 9.5 inches long and 1 inch wide at the grips. The widths and gage lengths of the reduced sections of the test specimens were 3/4 and 2-1/2 inches, respectively. Prior to testing, each specimen was instrumented with two strain gages positioned directly opposite each other on opposite faces of the specimens. Completed test specimens of each thickness are shown in Figure A.1. The specimens were tested in a constant-strain-rate device at an average crosshead speed of 0.025 in/min. The test results were recorded on an X-Y plotter, which recorded load and strain simultaneously.

The individual stress-strain curves were then used to construct the average stress-strain curve plotted in Figure A.2. The tension tests did not reveal any significant variation in stress-strain characteristics for the various thicknesses of the mechanical tubing. The modulus of elasticity for the mechanical tubing was 30.0×10^6 psi ± 4 percent. The proportional limit was 47,000 psi ± 5 percent, and the yield strength, as determined by use of the 0.2 percent offset method, was 79,000 psi ± 5 percent.

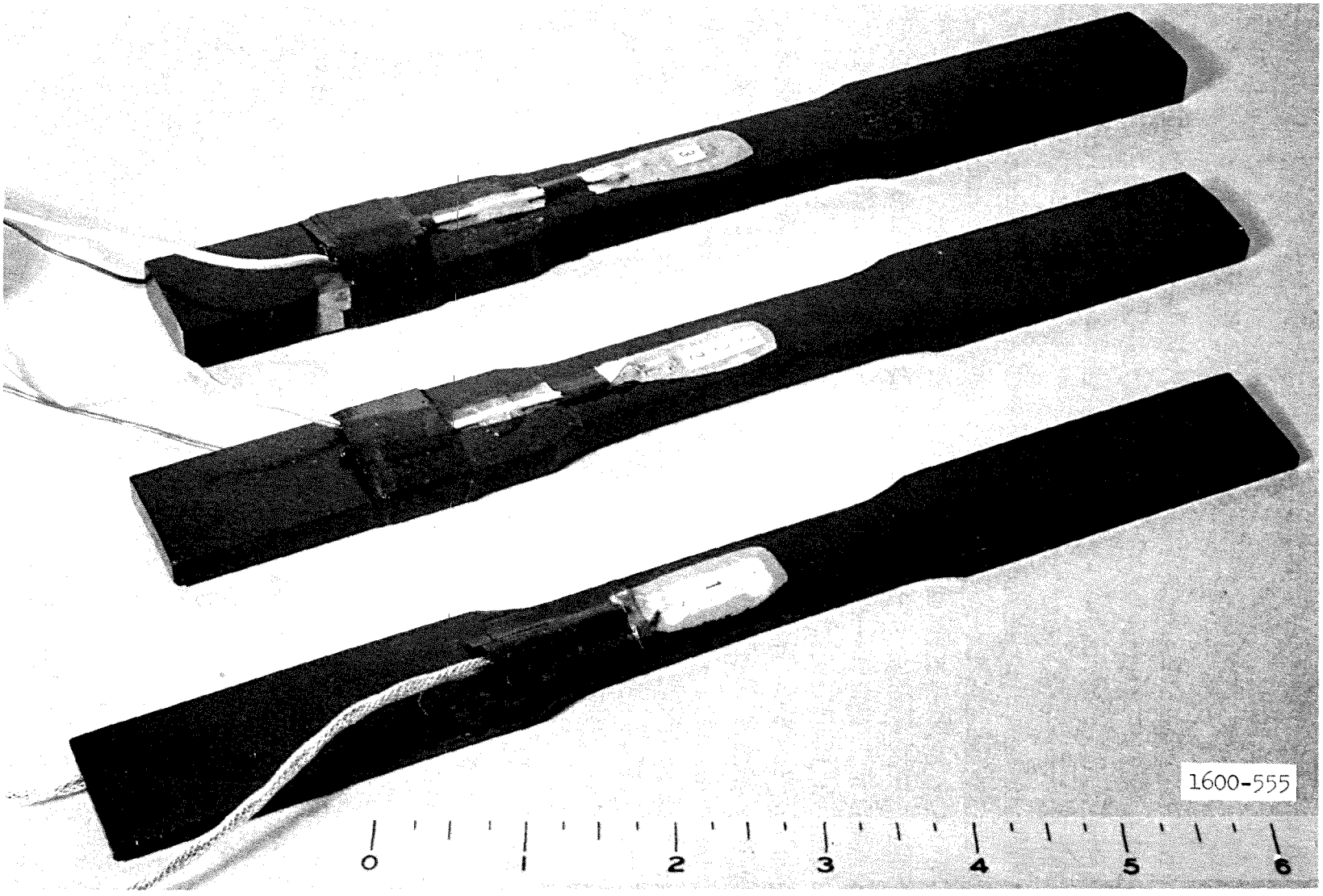

Figure A.1 Typical tension tests specimens.

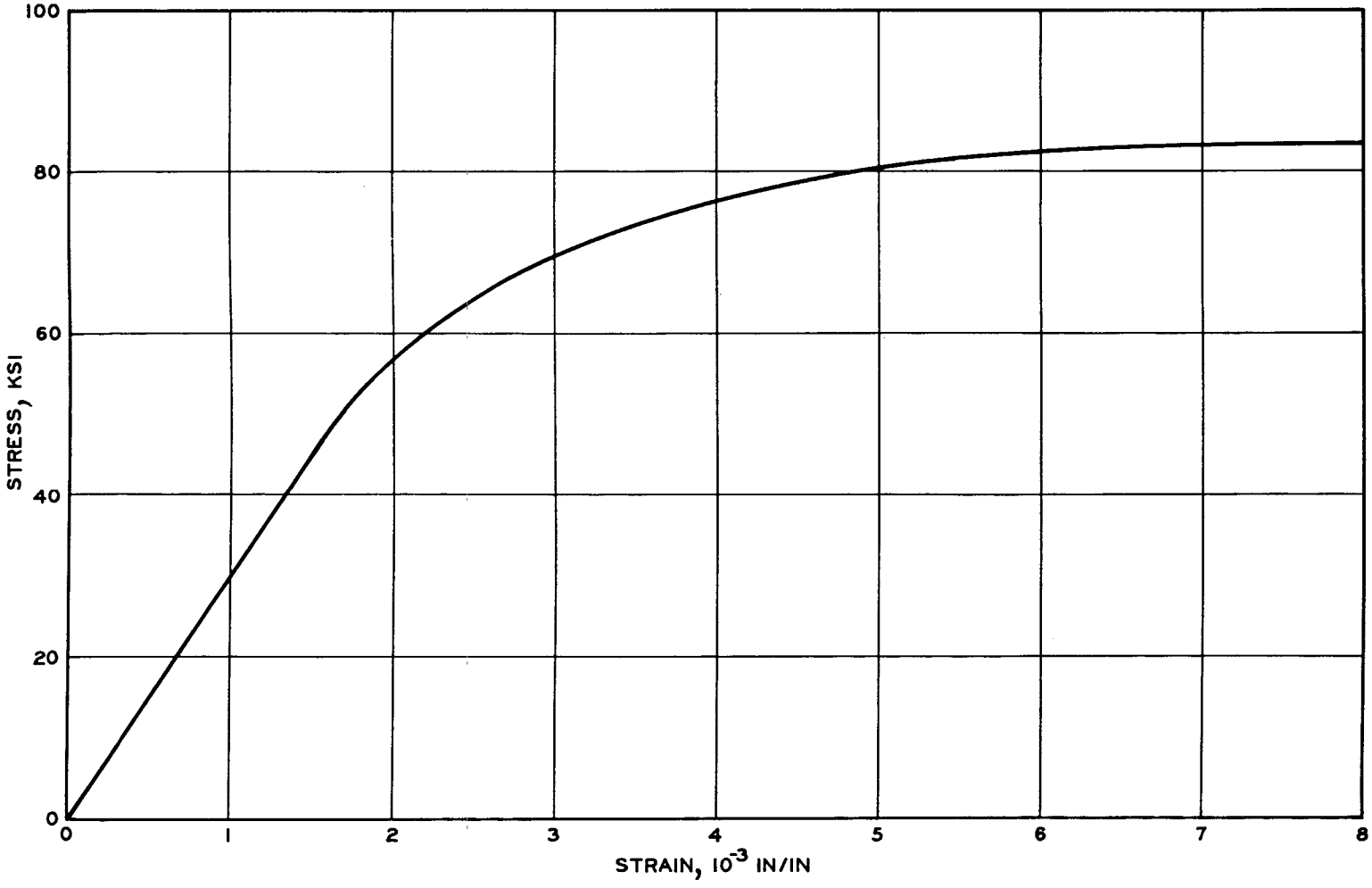

Figure A.2 Average stress-strain curve.

APPENDIX B

SOIL PROPERTIES

Throughout this investigation, only dense air-dry Cook's Bayou No. 1 sand was utilized. Cook's Bayou No. 1 sand is commonly used in experimental programs at the U. S. Army Engineer Waterways Experiment Station because it can be placed at high relative densities with comparative ease and because the test results are reproducible.

A typical grain-size distribution curve for Cook's Bayou No. 1 sand is shown in Figure B.1a, and the angle of internal friction (from the consolidated-drained shear test) versus initial dry unit weight is shown in Figure B.1b. In general, the sand is a uniform fine sand with a coefficient of uniformity C_u of 1.60. The angle of internal friction increases from 34.6 to 42.0 degrees as the dry unit weight ranges between 98.5 and 109 pcf. Laboratory tests also indicated that the minimum and maximum dry densities for this sand were 93.3 and 110.8 pcf, respectively, and that the specific gravity of the sand was 2.65.

Static one-dimensional compression tests were conducted by the United Research Services Corporation (Reference 10) to determine the stress-strain characteristics of Cook's Bayou sand. The results of these tests are presented in Figure B.2. The stress-strain curves are of the stiffening type, which display an increase in tangent modulus with an increase in the stress level. Unfortunately, the stress-strain data are not available for stress levels in excess of 500 psi.

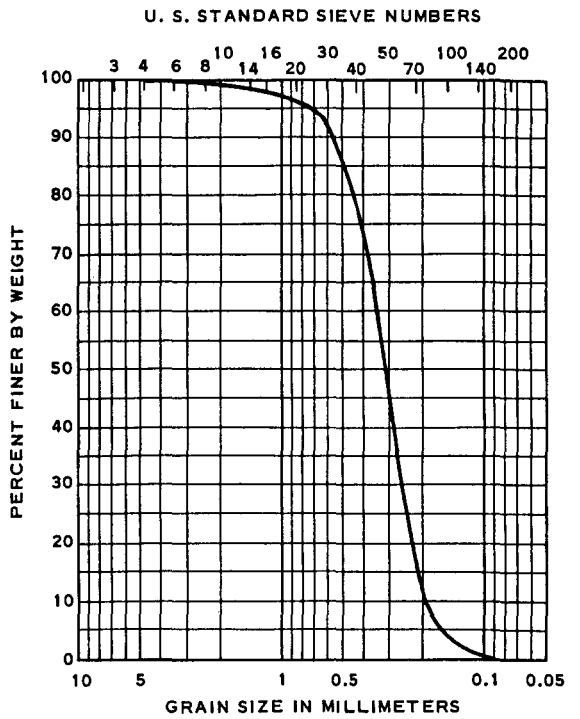

a. GRAIN-SIZE DISTRIBUTION CURVE

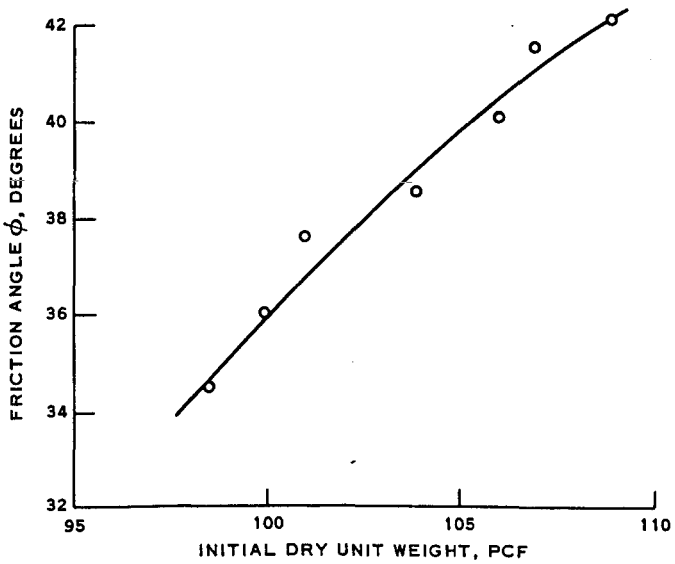

b. CONSOLIDATED-DRAINED SHEAR TEST RESULTS

Figure B.1 Gradation and angle of internal friction curves for Cook's Bayou sand.

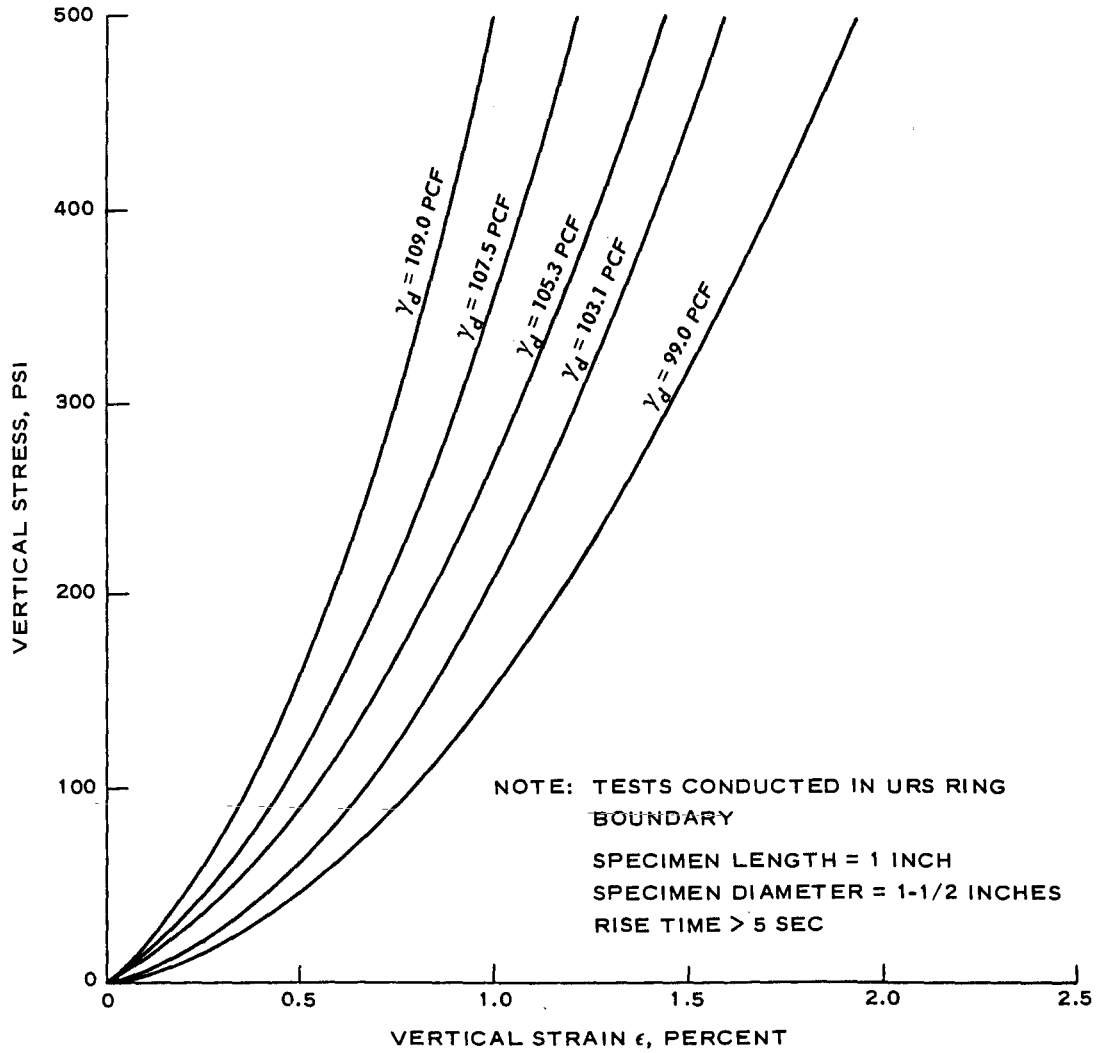

Figure B.2 Static one-dimensional compression test results for Cook's Bayou sand.

REFERENCES

1. G. E. Albritton; "Behavior of Flexible Cylinders Buried in Sand Under Static and Dynamic Loading"; Technical Report No. 1-821, April 1968; U. S. Army Engineer Waterways Experiment Station, CE, Vicksburg, Mississippi; Unclassified.

2. A. F. Dorris; "Response of Horizontally Oriented Buried Cylinders to Static and Dynamic Loading"; Technical Report No. 1-682, July 1965; U. S. Army Engineer Waterways Experiment Station, CE, Vicksburg, Mississippi; Unclassified.

3. K. Hoeg; "Pressure Distribution on Underground Structural Cylinders"; Technical Report No. AFWL-TR-65-98, April 1966; Air Force Weapons Laboratory, Kirtland Air Force Base, New Mexico; prepared by Massachusetts Institute of Technology, Cambridge, Massachusetts, under Contract No. AF 29(601)-6368; Unclassified.

4. A. J. Hendron, Jr., and others; "Design of Cylindrical Reinforced Concrete Tunnel Liners to Resist Air Overpressures"; Contract Report 68.010, June 1968; Naval Civil Engineering Laboratory, Port Hueneme, California; prepared by N. M. Newmark Consulting Engineering Services, Urbana, Illinois, under Contract No. NBy-62218; Unclassified.

5. A. J. Hendron, Jr.; "The Behavior of Sand in One-Dimensional Compression"; Ph. D. dissertation, 1963; Department of Civil Engineering, University of Illinois, Urbana, Illinois; Unclassified.

6. G. E. Albritton; "Description, Proof Test, and Evaluation of Blast Load Generator Facility"; Technical Report No. 1-707, December 1965; U. S. Army Engineer Waterways Experiment Station, CE, Vicksburg, Mississippi; Unclassified.

7. Boynton Associates, La Canada, California; "Operation Manual for 250 psi 4-Foot Diameter Dynamic Load Generator"; Contract Report No. 1-97, November 1960; prepared for U. S. Army Engineer Waterways Experiment Station, CE, Vicksburg, Mississippi, under Contract No. DA-22-079-CIVENG-61-8; Unclassified.

8. J. K. Ingram; "Procedure for Assembling SE-Type Stress Gages"; Instruction Report No. 8, March 1967; U. S. Army Engineer Waterways Experiment Station, CE, Vicksburg, Mississippi; Unclassified.

9. P. F. Hadala; "Sidewall Friction Reduction in the Small Blast Load Generator - Feasibility Study"; Technical Report (in preparation); U. S. Army Engineer Waterways Experiment Station, CE, Vicksburg, Mississippi; Unclassified.

10. W. L. Drubin; "Study of the Dynamic Stress-Strain and Wave Propagation Characteristics of Soils; Measurements of Stress-Strain, Peak Particle Velocity, and Wave-Propagation Velocity in Three Sands"; Contract Report No. 3-91, Report 3, February 1965; U. S. Army Engineer Waterways Experiment Station, CE, Vicksburg, Mississippi; Unclassified.

DISTRIBUTION LIST FOR TECHNICAL REPORT N-73-1

Address	No. of Copies
HQDA (DAEN-CWE) Washington, D. C. 20314	1
HQDA (DAEN-MEZ-A) Washington, D. C 20314	1
HQDA (DAEN-ZN) Washington, D. C. 20314	1
HQDA (DAEN-MCZ-S/COL J. S. C. Smith) Washington, D. C. 20314	1
HQDA (DAEN-MER-D) Washington, D. C. 20314	1
HQDA (DAEN-ASI/Mrs. Zenich) Washington, D. C. 20314	2
HQDA (DAEN-MCE) Washington, D. C. 20314	1
HQDA (DAEN-MCE-D) Washington, D. C. 20314	1
HQDA (DAEN-CWZ-R) Washington, D. C. 20314	1
Division Engineer U. S. Army Engineer Div., Missouri River ATTN: Office of Administrative Services (Library) P. O. Box 103, Downtown Station Omaha, Nebr. 68101	3
Division Engineer U. S. Army Engineer Div., Ohio River Lab Sec, Found. & Mats, Br., Engrg Div. ATTN: ORDED-FL P. O. Box 1159 Cincinnati, Ohio 45201	1
Defense Documentation Center ATTN: Mr. Myer Kahn Cameron Station Alexandria, Va. 22314	12
Director U. S. Army Coastal Engineering Research Center ATTN: Mr. T. Saville, Jr. 5201 Little Falls Road, N. W. Washington, D. C. 20016	1

Address	No. of Copies
Commander/Director U. S. Army Engineer Cold Regions Research and Engineering Laboratory ATTN: Dr. D. Freitag P. O. Box 282 Hanover, N. H. 03755	1
Commander, U. S. Army Mobility Equipment Research and Development Center ATTN: Technical Library Bldg 314 Fort Belvoir, Va. 22060	1
Commander The Engineer Center ATTN: Assistant Commandant Engineer School Fort Belvoir, Va. 22060	1
Director Explosive Excavation Research Laboratory U. S. Army Engineer Waterways Experiment Station P. O. Box 808 Livermore, Calif. 94550	1
Director Explosive Excavation Research Laboratory U. S. Army Engineer Waterways Experiment Station ATTN: Technical Information Division P. O. Box 808 Livermore, Calif. 94550	1
Director U. S. Army Construction Engineering Research Laboratory ATTN: Library P. O. Box 4005 Champaign, Ill. 61820	1
Commander U. S. Army Missile Command Huntsville, Ala. 35809	1
138th Engineer Group (Construction) Department of the Army ATTN: ALBFEN-O Fort Riley, Kans. 66442	1
Commandant U. S. Army Command & General Staff College ATTN: Archives Fort Leavenworth, Kans. 66027	1

Address	No. of Copies
Commander U. S. Army Nuclear Defense Laboratory ATTN: Technical Library Edgewood Arsenal, Md. 21010	1
Director U. S. Army Ballistic Research Laboratories Aberdeen Proving Ground, Md. 21005	4
Commander U. S. Army Electronics Command ATTN: AMSEL-GG-DD Fort Monmouth, N. J. 07703	1
Commander Picatinny Arsenal ATTN: ORDBB-TK Dover, N. J. 07801	1
Commander U. S. Army Munition Command Dover, N. J. 07801	1
Superintendent U. S. Military Academy ATTN: Library West Point, N. Y. 10996	2
Commandant Army War College ATTN: Library Carlisle Barracks, Pa. 17013	1
President U. S. Army Air Defense Board Fort Bliss, Tex. 79916	1
Commandant U. S. Army Air Defense School Fort Bliss, Tex. 79916	1
Commander Eustis Directorate, U. S. Army Air Mobility Research and Development Laboratory ATTN: VDLEU-ADSP Fort Eustis, Va. 23604	1
Commander U. S. Continental Army Command Fort Monroe, Va. 23351	1

Address	No. of Copies
Commander Air Force Weapons Laboratory ATTN: Mr. R. W. Henney Kirtland Air Force Base, N. Mex. 87117	1
Sandia Laboratories ATTN: Dr. M. L. Merritt P. O. Box 5800 Kirtland Air Force Base East, N. Mex. 87115	1
Commander Field Command, Defense Nuclear Agency ATTN: FCTD-T Kirtland Air Force Base, N. Mex. 87115	2
Commander Air Force Weapons Laboratory ATTN: DEV/MAJ George V. Bulin Kirtland Air Force Base, N. Mex. 87117	1
Commander Air Force Weapons Laboratory ATTN: Library Kirtland Air Force Base, N. Mex. 87117	2
Commander Air Force Flight Dynamics Laboratory ATTN: Mr. Frank Janik, Jr. Wright-Patterson Air Force Base, Ohio 45433	1
Air Force Institute of Technology ATTN: AFIT-L Bldg 640 Wright-Patterson Air Force Base, Ohio 45433	1
Commander Air Force Logistics Command Wright-Patterson Air Force Base, Ohio 45433	2
Langley Research Center ATTN: Mr. Philip Donely NASA, Langley Field Hampton, Va. 23365	1
Air Force Systems Command Andrews Air Force Base ATTN: DEE Washington, D. C. 20331	1
Commandant Armed Forces Staff College ATTN: Library Norfolk, Va. 23511	1

Address	No. of Copies
Chief of Research and Development Department of the Army ATTN: DARD-ARE Washington, D. C. 20310	1
Chief of Research and Development Department of the Army ATTN: CRDNCB Washington, D. C. 20310	1
Commandant The Industrial College of the Armed Forces Fort McNair Washington, D. C. 20310	1
Defense Civil Preparedness Agency ATTN: Mr. George Sisson (RE-SR) Washington, D. C. 20301	1
Commander U. S. Army Materiel Command ATTN: AMCRD-DE-N Washington, D. C. 20310	2
Chief of Research and Development Department of the Army ATTN: Director of Army Technical Information Washington, D. C. 20310	3A
Commander U. S. Army Combat Development Command Institute of Nuclear Studies Fort Bliss, Tex. 79916	1
Commanding Officer and Director U. S. Naval Electronics Laboratory San Diego, Calif. 92152	1
Commander U. S. Naval Ordnance Test Station China Lake, Calif. 93555	1
Superintendent U. S. Naval Postgraduate School Monterey, Calif. 93940	1
Commanding Officer U. S. Naval Civil Engineer Corps Officer School U. S. Naval Construction Battalion Center Port Hueneme, Calif. 93041	1

Address	No. of Copies
Commanding Officer and Director U. S. Naval Civil Engineering Laboratory ATTN: Code L31 Port Hueneme, Calif. 93041	2
Commanding Officer Nuclear Weapons Training Center, Pacific U. S. Naval Station, North Island San Diego, Calif. 92136	2
Commanding Officer and Director Naval Ship Research and Development Center Carderock, Md. 20007	1
Commander U. S. Naval Oceanographic Office Suitland, Md. 20023	1
Commander U. S. Naval Ordnance Laboratory ATTN: 243 Silver Spring, Md. 20910	1
Commander U. S. Naval Ordnance Laboratory ATTN: 240 Silver Spring, Md. 20910	1
Commander U. S. Naval Ordnance Laboratory ATTN: 241 Silver Spring, Md. 20910	1
Commanding Officer U. S. Naval Weapons Evaluation Facility ATTN: Code WEVS, Kirtland Air Force Base Albuquerque, N. Mex. 87117	1
Commanding Officer U. S. Naval Damage Control Training Center, Naval Base ATTN: ABC Defense Course Philadelphia, Pa. 19112	1
President U. S. Naval War College Newport, R. I. 02840	1
Underwater Explosions Research Division Naval Ship Research and Development Center Norfolk Naval Shipyard Portsmouth, Va. 23709	1

Address	No. of Copies
Commanding Officer U. S. Naval Weapons Laboratory ATTN: MAL Dahlgren, Va. 22448	1
Commanding Officer Nuclear Weapons Training Center ATTN: Nuclear Warfare Department Atlantic Naval Base Norfolk, Va. 23511	1
Commander-in-Chief U. S. Atlantic Fleet, U. S. Naval Base Norfolk, Va. 23511	1
Commanding General Marine Corps Development & Education Command ATTN: Director, Development Center Quantico, Va. 22134	2
Chief of Naval Operations Navy Department ATTN: OP-75 Washington, D. C. 20350	2
Chief of Naval Operations Navy Department ATTN: OP-03EG Washington, D. C. 20350	1
Chief of Naval Research Navy Department ATTN: Code 418 Washington, D. C. 20390	1
Commandant of the Marine Corps ATTN: Code AQ4E Washington, D. C. 20380	2
Commander Naval Facilities Engineering Command ATTN: NFAC-04 Navy Department Washington, D. C. 20390	1
Commander Naval Facilities Engineering Command ATTN: NFAC-03 Navy Department Washington, D. C. 20390	1

Address	No. of Copies
Director U. S. Naval Research Navy Department Washington, D. C, 20390	1
Special Projects Navy Department ATTN: SP-272 Washington, D. C. 20360	1
Commander Naval Ordnance Systems Command Navy Department Washington, D. C. 20360	1
Commander Naval Ship Engineering Center ATTN: Code 6115 Navy Department Washington, D. C. 20360	1
Director Air University Library Maxwell Air Force Base, Ala. 36112	2
Space and Missile Systems Organization ATTN: MMHH/MAJ T. J. Aneffi Norton Air Force Base, Calif. 92409	1
Director, USAF Project RAND Via: U. S. Air Force Liaison Officer The Rand Corporation ATTN: Library 1700 Main St., Santa Monica, Calif. 90406	1
Dr. Olen A. Nance South Lakewood Dr., Baton Rouge, La. 70810	1
Commander Tactical Air Command ATTN: Document Security Branch Langley Air Force Base, Nebr. 68113	1
Commander Strategic Air Command ATTN: OAWS Offutt Air Force Base, Nebr. 68113	1
Air Force Technical Applications Center Department of the Air Force Washington, D. C. 20333	1

Address	No. of Copies
Research and Development Command Headquarters, USAF ATTN: Combat Components Div. Washington, D. C. 20330	1
Headquarters, USAF ATTN: AFRSTG Washington, D. C. 20330	1
Director of Civil Engineering Headquarters, USAF ATTN: AFOCE Washington, D. C. 20330	1
Commander-in-Chief, Pacific FPO San Francisco 94129	1
U. S. Documents Officer Office of the United States National Military Representative-SHAPE APO New York 09055	1
U. S. Department of the Interior U. S. Geological Survey ATTN: Mr. Harold W. Olsen 345 Middlefield Rd. Menlo Park, Calif. 94025	1
Manager Albuquerque Operations Office U. S. Atomic Energy Commission P. O. Box 5400 Albuquerque, N. Mex. 87115	1
National Aeronautics & Space Administration Man-Spacecraft Center Space Technology Center Box 1537 Houston, Tex. 77001	1
Director Advanced Research Projects Agency ATTN: NTDO Washington, D. C. 20301	1
Assistant to the Secretary of Defense (Atomic Energy) Washington, D. C. 20301	1
Defense Intelligence Agency ATTN: DI-7B Washington, D. C. 20301	1

Address	No. of Copies
Administrator National Aeronautics & Space Administration 400 Maryland Ave., S. W. Washington, D. C. 20546	1
National Military Command Systems Support Center ATTN: Technical Library Pentagon BE 685 Washington, D. C. 20301	1
Commandant National War College ATTN: Class Rec Library Washington, D. C. 20310	1
U. S. Atomic Energy Commission ATTN: Chief, Classified Technical Library Technical Information Service Washington, D. C. 20545	1
Director Weapons Systems Evaluation Group Washington, D. C. 20305	1
Director Defense Nuclear Agency ATTN: SPSS Washington, D. C. 20305	5
Director of Defense Research and Engineering ATTN: Technical Library Washington, D. C. 20301	1
Director of Defense Research and Engineering ATTN: Mr. Frank J. Thomas Washington, D. C. 20301	1
Bureau of Public Roads, Department of Commerce, Federal Highway Administration ATTN: Mr. F. J. Tamanini, Chief, Structures and Applied Mechanics Br. Washington, D. C. 20591	1
Prof. Sandor Popovics, Northern Arizona University P. O. Box 15600 Flagstaff, Ariz. 86001	1
Dr. Donald A. DaDeppo, The University of Arizona Department of Civil Engineering Tucson, Ariz. 85721	1

Address	No. of Copies
Dr. George Howard, College of Engineering, University of Arizona Tucson, Ariz. 85721	1
University of Colorado, School of Architecture ATTN: Prof. G. K. Vetter Boulder, Colo. 80304	1
University of Detroit, Department of Civil Engineering 4001 West McNichols Rd. ATTN: Prof. Warren J. Baker Detroit, Mich. 48221	1
University of Florida, Department of Mechanical Engineering ATTN: Prof. John A. Samuel Gainesville, Fla. 32601	1
University of Illinois ATTN: Prof. A. H. S. Ang Urbana Campus Urbana, Ill. 61801	1
University of Illinois, Urbana Campus ATTN: Prof. G. K. Sinnamon Urbana, Ill. 61801	1
University of Illinois, Urbana Campus Department of Civil Engineering ATTN: Prof. W. J. Hall Urbana, Ill. 61801	1
University of Illinois, Urbana Campus Department of Civil Engineering ATTN: Prof. A. J. Hendron, Jr. Urbana, Ill. 61801	1
Dr. Nathan M. Newmark, Head, Department of Civil Engineering University of Illinois Urbana, Ill. 61801	1
Prof. Mete A. Sozen, Department of Civil Engineering 3112 Civil Engineering Bldg University of Illinois Urbana, Ill. 61801	1
Iowa State University of Science and Technology ATTN: Prof. Glen Murphy Ames, Iowa 50010	2

Address	No. of Copies
Lehigh University, Materials Research Center ATTN: Dr. J. F. Libsch Bethlehem, Pa. 18015	1
Lehigh University, Department of Civil Engineering ATTN: Dr. D. A. Van Horn Bethlehem, Pa. 18015	1
Massachusetts Institute of Technology, Div. of Sponsored Research ATTN: Dr. R. V. Whitman 77 Massachusetts Ave. Cambridge, Mass. 02139	1
Massachusetts Institute of Technology, Div. of Sponsored Research ATTN: Dr. R. J. Hansen 77 Massachusetts Ave. Cambridge, Mass. 02139	1
University of Massachusetts, Department of Civil Engineering ATTN: Dr. M. P. White Amherst, Mass. 01002	1
Prof. F. E. Richart, Jr. (Consultant) Department of Civil Engineering University of Michigan 304 West Engineering Ann Arbor, Mich. 48104	1
Eric H. Wang, Civil Engr, Research Facility University of New Mexico Box 188, University Station Albuquerque, N. Mex. 87106	2
Nova Scotia Technical College ATTN: Dr. G. G. Meyerhof School of Graduate Studies Halifax, Nova Scotia, Canada	1
Pennsylvania State University ATTN: Prof. Richard Kummer 101 Eng. A University Park, Pa. 16802	1
Pennsylvania State University ATTN: Prof. G. Albright Head, Department of Architectural Engineering University Park, Pa. 16802	1

Address	No. of Copies
Purdue University ATTN: Prof. M. B. Scott School of Civil Engineering Civil Engineering Bldg Lafayette, Ind. 47907	1
Rensselaer Polytechnic Institute ATTN: Dr. Clayton Oliver Dohrenwend, Security Officer Mason House Troy, N. Y. 12180	1
Rice University ATTN: Prof. A. S. Veletsos Department of Civil Engineering Houston, Tex. 77001	1
San Jose State College Department of Civil Engineering ATTN: Prof. J. E. Roberts San Jose, Calif. 95100	1
Balcones Research Center ATTN: Dr. J. Neils Thompson University of Texas Austin, Tex. 78712	1
Utah State University ATTN: Prof. R. K. Watkins Department of Mechanical Engineering Logan, Utah 84321	1
University of Washington ATTN: Dr. Arnold Arons Department of Physics Seattle, Wash. 98105	1
University of Washington ATTN: Prof. William Miller Department of Civil Engineering 307 More Hall Seattle, Wash. 98105	1
University of Washington ATTN: Mr. C. H. Norris Department of Civil Engineering Seattle, Wash. 98105	1
Nuclear Defense Design Center, School of Engineering and Applied Science The George Washington University Washington, D. C. 20006	1

Address	No. of Copies
Worcester Polytechnic Institute ATTN: Dr. Carl Koontz Department of Civil Engineering Worcester, Mass. 01609	1
Aerospace Corporation ATTN: Dr. M. B. Watson P. O. Box 95085 Los Angeles, Calif. 90045	1
Agbabian Associates Engineering Consultants 250 North Nash St. El Segundo, Calif. 90245	1
Applied Theory Incorporated ATTN: Dr. John G. Trulio 1010 Westwood Blvd. Los Angeles, Calif. 90024	1
AVCO Corporation ATTN: Mr. R. E. Cooper Research and Advanced Development Div. 201 Lowell St. Wilmington, Mass. 01887	1
Battelle Memorial Institute ATTN: Dr. P. N. Lamori 505 King Ave. Columbus, Ohio 43201	1
Bell Telephone Laboratories ATTN: Mr. R. W. Mayo Whippany Rd. Whippany, N. J. 07981	1
The Boeing Company ATTN: Technical Library P. O. Box 3707 Seattle, Wash. 98124	1
R&D Associates ATTN: Dr. Harold L. Brode P. O. Box 3580 Santa Monica, Calif. 90403	1
Corrugated Metal Pipe Institute ATTN: Mr. W. A. Porter Crestview Plaza, Port Credit Ontario, Canada	1

Address	No. of Copies
Denver Mining Research Center Bldg 20, Denver Federal Center ATTN: Dr. Leonard A. Obert Denver, Colo. 80228	1
Harry Diamond Laboratories, Library ATTN: Mildred H. Weiner Room 207, Bldg 92 Connecticut Ave. & Van Ness St., N. W. Washington, D. C. 20438	1
Edgerton, Germeshausen & Grier, Inc. ATTN: Mr. D. F. Hansen 95 Brookline Ave. Boston, Mass. 02129	1
Engineering Physics Company ATTN: Dr. Vincent J. Cushing 12721 Twinbrook Pkwy Rockville, Md. 20852	1
Engineering Physics Company ATTN: Mr. W. Danek 12721 Twinbrook Pkwy Rockville, Md. 20852	1
General American Transportation Corporation General American Research Div. ATTN: Dr. G. L. Neidhardt 7449 North Natchez Ave. Niles, Ill. 60648	1
General Electric Company, TEMPO ATTN: Mr. Warren Chan (DASIAC) 816 State St. Santa Barbara, Calif. 93101	1
General Electric Company Missile and Space Vehicle Department, Valley Forge Space Technology Center Goddard Blvd. King of Prussia, Pa. 19406	1
General Research Corporation ATTN: Mr. Benjamin Alexander P. O. Box 3587 Santa Barbara, Calif. 93105	1
IIT Research Institute ATTN: Dr. T. Schiffman 10 West 35th St. Chicago, Ill. 60616	1

Address	No. of Copies
Lockheed Missile and Space Company A Div. of Lockheed Aircraft Corp. ATTN: Dr. R. E. Meyerott 111 Lockheed Way Sunnyvale, Calif. 94086	1
Los Alamos Scientific Laboratory ATTN: Report Librarian P. O. Box 1663 Los Alamos, N. Mex. 87544	1
Physics International Company ATTN: Dr. Charles Godfrey 2700 Merced St. San Leandro, Calif. 94577	1
Physics International Company ATTN: Mr. Fred M. Sauer 2700 Merced St. San Leandro, Calif. 94577	1
General Atomic, Div. of General Dynamics Corp. ATTN: Dr. K. D. Pyatt, Jr. P. O. Box 111 10955 John Jay Hopkins Dr. San Diego, Calif. 92112	1
General Research Corporation Document Control Supervisor Westgate Research Park McLean, Va. 22101	1
Dr. John S. Rinehart Senior Research Fellow (R:2) IER/ESSA Boulder, Colo. 80302	1
Southwest Research Institute ATTN: Dr. Robert C. DeHart 8500 Culebra Rd. San Antonio, Tex. 78228	1
URS Corporation ATTN: Mr. Harold G. Mason 1811 Trousdale Dr. Burlingame, Calif. 94010	2
Paul Weidlinger, Consulting Engineer ATTN: Dr. M. L. Baron 110 East 59th St. New York, N. Y. 10022	1

Address	No. of Copies
Dr. Eugene Zwoyer 335-A Jefferson, S. E. Albuquerque, N. Mex. 87108	1
Chief Superintendent Defence Research Establishment, Suffield Ralston, Alberta, Canada	1
Ministry of Defense MEXE Christchurch ATTN: Mr. Bruce T. Boswell Hampshire, England	1
Ministry of Defense MEXE Christchurch ATTN: Dr. Philip S. Bulson Hampshire, England	1
Dr. Wilhelm Sommer IM BWB, 54 Koblenz Am Rhein 2-6, Germany	1

Unclassified
Security Classification

DOCUMENT CONTROL DATA - R & D

(Security classification of title, body of abstract and indexing annotation must be entered when the overall report is classified)

1. ORIGINATING ACTIVITY *(Corporate author)*
U. S. Army Engineer Waterways Experiment Station
Vicksburg, Mississippi

2a. REPORT SECURITY CLASSIFICATION
Unclassified

2b. GROUP

3. REPORT TITLE
BEHAVIOR OF STIFF CYLINDERS BURIED IN SAND UNDER STATIC LOADING

4. DESCRIPTIVE NOTES *(Type of report and inclusive dates)*
Final report

5. AUTHOR(S) *(First name, middle initial, last name)*
Charles D. Norman
James D. Prendergast

6. REPORT DATE	7a. TOTAL NO. OF PAGES	7b. NO. OF REFS
April 1973	112	10

8a. CONTRACT OR GRANT NO.	9a. ORIGINATOR'S REPORT NUMBER(S)
b. PROJECT NO.	Technical Report N-73-1
c. IMED Subtask SC210	9b. OTHER REPORT NO(S) *(Any other numbers that may be assigned this report)*
d.	

10. DISTRIBUTION STATEMENT
Approved for public release; distribution unlimited

11. SUPPLEMENTARY NOTES	12. SPONSORING MILITARY ACTIVITY
	Defense Nuclear Agency Washington, D. C.

13. ABSTRACT

The objective of this investigation was to study experimentally the elastic behavior of horizontally oriented, stiff cylinders buried at shallow depths in dense, dry sand and subjected to static surface overpressures. Static tests were conducted on nine different cylinders in the U. S. Army Engineer Waterways Experiment Station's Small (4-foot-diameter) Blast Load Generator (SBLG). The cylinders were fabricated from steel mechanical tubing having a 6-inch outside diameter and a specially isolated 12-inch-long test section. The nine test specimens comprised three groups of cylinders with wall thicknesses of 1/8, 1/4, and 3/8 inch that corresponded to stiffnesses (EI/R^3) of 170, 1,644, and 5,926 psi, respectively. In order to study the effects of burial depth, the first, second, and third cylinders of each group were tested at depths of 3, 6, and 9 inches, respectively. A total of 14 static tests were conducted, 9 on virgin soil samples and 5 on samples that had been previously loaded. The peak surface overpressure attained for all tests was approximately 1,000 psi. Measurements were made of cylinder hoop strain, vertical diameter change, soil stress, and surface overpressure. The test results indicated that cylinder stiffness significantly affected the overall response of the soil-structure system. Normalized moment (M/PR^2) data obtained from these tests were determined to be much greater than such values for less stiff cylinders. However, the maximum values of the normalized moments from the test data were in close agreement with the analytically predicted upper-bound values for a rigid cylinder. The experimental information for the 1/4- and 3/8-inch-thick cylinders was used to provide data in the low normalized pressure (PR^3/EI) region, for which very little data previously existed. For the range of cylinder stiffnesses tested, normalized thrust values (T/PR) indicated that both active and passive arching occurred and were dependent on cylinder stiffness. A description of the properties of the steel used in fabricating the test cylinders is given in Appendix A, and a description of the confining soil properties is given in Appendix B.

DD FORM 1 NOV 65 1473 REPLACES DD FORM 1473, 1 JAN 64, WHICH IS OBSOLETE FOR ARMY USE.

Unclassified
Security Classification

14. KEY WORDS	LINK A		LINK B		LINK C	
	ROLE	WT	ROLE	WT	ROLE	WT
Buried cylinders						
Sands						
Static loads						